國立交通大學

機械工程學系

碩士論文

以盤狀圓弧刀具創成之曲線齒的

數學模式推導與接觸分析研究

Mathematical Model and Tooth Contact Analysis of Gears

with Curvilinear-Teeth

Generated by a Disk-Type Circular-Arc Cutter

研究生：吳一正

指導教授：徐瑞坤　曾錦煥

共同指導教授：蔡忠杓

以盤狀圓弧刀具創成之曲線齒的
數學模式推導與接觸分析研究

研究生：吳一正　　　　　　　　　　指導教授：徐瑞坤、蔡忠杓

國立交通大學機械工程學系

摘要

圓弧型曲線齒齒輪（circular-arc curvilinear-tooth gear）係指一種由圓弧型盤狀刀具所創成，具有曲線型齒線及圓弧型齒形特徵的齒輪。

不同於以往傳統正齒輪與螺旋齒輪的線接觸型的傳動運轉方式，具曲線型齒線特徵的齒輪組是以點接觸的接觸型態來傳輸動力。點接觸的接觸型態不僅能使齒輪組避免齒緣的接觸及降低由軸向組裝誤差所引起的運動誤差和振動噪音，更可增強齒輪的接觸強度。除此之外，具有曲線型齒線之齒輪在運轉時亦不會產生軸向的推力。

具圓弧型齒形的螺旋齒輪因為具有較一般傳統螺旋齒輪為高的負載能力及更佳的潤滑效果等特性，故常被使用於需傳輸高負載的情況，但是圓弧型螺旋齒輪對於中心距離的組裝誤差是十分敏感的。

本研究係將漸開線型曲線齒齒輪的齒形改以圓弧型外形之齒刀來創成齒輪，亦即應用一把虛擬的圓弧型齒刀依循一曲線路徑而創成出該齒輪之齒面，並根據齒輪原理建立圓弧型曲線齒齒輪之齒面數學模式，同時也以轉位修正的方式來避免齒形過切的情況發生，亦利用齒輪接觸分析技術來探討具有裝配偏差時，齒輪組運動誤差、接觸比及接觸齒印。

Mathematical Model and Tooth Contact Analysis of Gears with Curvilinear-Teeth Generated by a Disk-Type Circular-Arc Cutter

Student: Yi-Zheng Wu   Advisor: Ray-Quan Hsu, Chung-Biau Tsay

Department of Mechanical Engineering

National Chiao Tung University

Abstract

The circular-arc curvilinear-tooth gear, which has curvilinear trace with circular-arc profile, is generated by a circular-arc disk-type cutter.

Gears with curvilinear traces ensure that the gear pair is operated in a point contact condition, which is different from the line contact type of a helical gear pair or spur gear pair. The point contact condition can not only avoid the tooth edge contact, decreases the kinematical errors and vibro-acoustic due to axial misalignments, but also increases the bearing strength of the contact gears. Moreover, a gear pair with curvilinear-tooth traces operates without axial thrust force.

The helical gears with circular-arc profile are used for transmitting with high load circumstance, because their loading capacity and lubricity are better than those of conventional helical gears. However, the circular-arc helical gear pair is quite sensitive to the central distance assembly errors.

This study adopts the rack cutter with circular-arc profile to modify the profile of involute-type curvilinear-tooth gear pair. The gear surface is generated by an imaginary circular-arc rack cutter with a curvilinear trace. According to theory of gearing, a mathematical model of the gears with circular-arc profile and curvilinear-tooth trace is developed. The undercutting of the gears can be avoided by a positive profile-shifted modification during the gear set generation process. The tooth contact analysis technique is utilized to the investigation on kinematical errors, contact ratios and contact patterns of the gear set under axial misalignments.

Acknowledgement (誌謝)

我很幸運！能夠進入地球上最棒的實驗室－最佳化設計實驗室,在這邊渡過了碩士班的時光,能跟隨最慈祥的　曾錦煥教授做學問。在實驗室學習與生活的這兩年中,我成長了許多,除了碩士班應有的訓練外,亦習得許多做人處事的大道理,聽起來像是老生常談,實驗室的伙伴們一定能對我所說的一言一句感同深受。

最難忘的還是曾老師的咳嗽聲,輕撫著他視為孩子們的學生,與大家探討學術上的問題,大家將老師圍成一圈,聽著老師說著成功的道理及做事的方法。實驗室的孩子都是這樣成長茁壯,出了實驗室的大門,我們都能抬起胸膛,大聲的告訴大家：我和別人不一樣。這一切都要感謝　曾錦煥老師。雖然已無法當著您的面,致上學生最誠摯的感謝之意,但學生已不知在心中默唸了數百次,希望您都能聽見。

這篇論文的完成,除了最敬愛的曾老師外,也謝謝蔡忠杓教授在學生碩士班二年級這一年來的細心指導及對論文寫作不厭其煩的指正,蔡老師在研究學問及為人處世所展現的細心、執著和堅毅,都是學生十分佩服的。您的諄諄教誨,學生將永遠銘記於心。

感謝在碩士班二年級指導我們的徐瑞坤教授,徐老師將我們當成自己的學生般,隨時不忘關心、照顧我們,並給予學生論文許多寶貴的建議,謝謝徐老師。

感謝求學生涯中一直默默支持我的父母,因為有你們在背後的鼓勵,給我一個穩定無虞的良好學習環境,讓我能更專心地面對研究所生活的挑戰；如今,順利完成了碩士學位,這些成就都將歸功於我親愛的父母,謝謝你們。

在應用最佳化實驗室的這短短兩年中,留下了許多難忘的回憶。謝謝林聰穎老師、羅接興老師及嘉宏、明達、炫慧、陽光‧‧‧等學長姊們給我了許多學業及生活上的援助。謝謝美惠及筑妃同學,和優秀的你們一同學習讓我不敢怠慢。謝謝培峰、翊猷及岳

iv

良學弟所給予的許多幫忙，讓我能有更多的時間完成這篇論文。也謝謝齒輪實驗室的學長、學弟，給了我許多論文上的建議及課業上的幫助。感謝實驗室的每位伙伴，我永遠不會忘記大家互相扶持，攜手走過的每一天。感謝你們的包容與協助，讓我能順利、充實、快樂的渡過這段時光。有你們真好！

感謝論文的口試委員：清華大學宋震國教授及中正大學馮展華教授，百忙中不辭辛勞的撥冗參加學生的碩士論文口試，並對學生的論文提出了寶貴的建議及修正，讓學生的論文更加充實且完整，謝謝你們。

這兩年的研究生活中，因為有你們的存在，讓我能一路走過從所未經歷過的挫折及難關。祝福這些長輩及朋友們能永遠平安、順利。

Table of Contents

List of Figures

List of Tables

Nomenclature

a   semi-major length of contact ellipse, as shown in Fig. 6-6

b   semi-minor length of contact ellipse, as shown in Fig. 6-6

A initial point of circular-arc rack cutter Σ_j ($j = $ p, g), as shown in Fig. 3-6

B end point of circular-arc rack cutter Σ_j ($j = $ p, g), as shown in Fig. 3-6

$C^{(j)}$ center of the circular-arc trace of rack cutter Σ_j ($j = $ p, g), as shown in Fig. 3-7

C ideal center distance of gear pair, $C = r_1 + r_2$

ΔC center distance variation (in mm)

C' center distance of gear pair with variation ΔC, $C' = C + \Delta C$

d_i perpendicular distance of tooth surface Σ_j to common tangent plane T ($j = $ p, g) (in mm), as shown in Fig. 6-1

$l_c^{(i)}$ parameter of defining location of singular point on rack cutter Σ_j ($j = $ p, g)

$\mathbf{L}_{ij}$ 3×3 vector transformation matrix transforming from coordinate system S_j to S_i

m_c contact ratio, defined in Eq.(5.20)

$\mathbf{M}_{ij}$ 4×4 homogeneous coordinate transformation matrix transforming from coordinate system S_j to S_i

M normal module

$\mathbf{n}$ unit normal vector

$\mathbf{n}_i^{(j)}$ unit normal vector of surface Σ_j (j =p, g, 1, 2) represented in coordinate system S_i

     (i = c, f)

$\mathbf{N}_c^{(g)}$ normal vector of surface Σ_C represented in coordinate system S_g

$O_R^{(i)}$ center of the circular arc $\widehat{MN}$ of rack cutter Σ_j (j =p, g), as shown in Fig. 3-6

(r, θ_T) polar coordinate system on common tangent plane T, as shown in Fig. 6-1(a)

r_i radius of operating pitch cylinder of the gear blank i (i =1, 2) (in mm)

$R^{(j)}$ radius of circular-arc of the rack cutter Σ_j (j =p, g)

$\mathbf{R}_i^{(j)}$ position vector of surface j represent in coordinate system S_i

R_{ab} radius of the disk-type circular-arc cutter

S^G tooth thickness measured along the pitch circle

$S_i\left(X_i, Y_i, Z_i\right)$ coordinate system i (i = 1, 2, f, h, m, n, T, v,)

$S_c^{(j)}\left(X_c^{(j)}, Y_c^{(j)}, Z_c^{(j)}\right)$ coordinate system i attached to rack cutter Σ_j (j = p, g)

$S_r^{(j)}\left(X_r^{(j)}, Y_r^{(j)}, Z_r^{(j)}\right)$ coordinate system r attached to rack cutter Σ_j (j = p, g)

$T^{(i)}$ teeth number of rack cuter Σ_j (j = p, g)

$\mathbf{V}^{(12)}$ relative velocity of body 1 and body 2

$\mathbf{V}_k^{(ij)}$ relative velocity of body i to body j represented in coordinate system S_k

$\mathbf{V}_i^{(j)}$ velocity of surface Σ_j (j = p, g, 1, 2) represented in coordinate system S_i

$\mathbf{V}_r^{(i)}$ tangent velocity of contact point on body i (i = g, 1)

$\mathbf{V}_{tr}^{(i)}$ relative velocity of contact point on body i (i = g, 1)

x coefficient of cutter shifting

W face width (in mm)

Σ_j surface of rack cutter j (j = p, g)

Σ_i surface of gear i (i = 1, 2)

α normal pressure angle of rack cutter

α_{ptip} instance normal pressure angle on the tip of rack cutter Σ_p , shown in Fig. 4-6

α_{gtip} instance normal pressure angle on the tip of rack cutter Σ_g , shown in Fig. 4-6

ε transformed angle of coordinate system (in degree)

δ transformed angle of coordinate system (in degree)

δ_{bl} backlash of the gear

ϕ_{1E} rotation angle of final meshing position of the gear
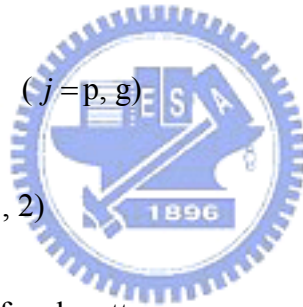
ϕ_{1S} rotation angle of initial meshing position of the gear

ϕ_i rotation angle of gear blank i (i =1, 2) (in degree)

ϕ_i' rotation angle of gear gear i when meshing with each other (i =1, 2) (in degree)

$\Delta\phi_2'$ transmission error (in arc-sec.)

$\gamma^{(j)}$ trace parameter of circular-arc rack cutter j (j =p, g)

$\gamma_{\max}^{(j)}$ maximum value of $\gamma^{(j)}$ which corresponds to the final position of working part of

disk-type rack cutter Σ_j (j =p, g)

$\gamma_{\min}^{(j)}$ minimum value of $\gamma^{(j)}$ which corresponds to the initial position of working part of

disk-type rack cutter Σ_j (j =p, g)

$\Delta\gamma_h$ horizontal axial misalignment (in degree), as shown in Fig. 5-1

$\Delta\gamma_v$ vertical axial misalignment (in degree), as shown in Fig. 5-1

$\theta^{(j)}$ parameter of the circular-arc-lined cutting blade surface of Σ_j (j =p, g)

$\theta_{\max}^{(j)}$ maximum value of $\theta^{(j)}$ which corresponds to the final position of working part of

circular-arc normal section for rack cutter Σ_j (j =p, g)

$\theta_{\min}^{(j)}$ minimum value of $\theta^{(j)}$ which corresponds to the initial position of working part of

circular-arc normal section for rack cutter Σ_j (j =p, g)
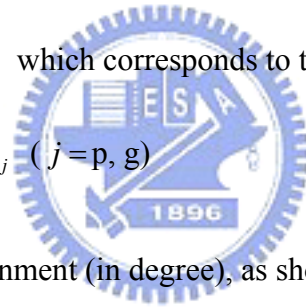
$\theta_{uc}^{(j)}$ value of the $\theta^{(j)}$ where singular point is appeared on rack cutter Σ_j (j = p, g)

ω_t rotational speed of the disk-type circular-arc cutter, as shown in Fig. 3-1

ω_1 rotational speed of gear blank i (i = 1, 2)

Δ_1 equality equation for tooth undercutting, defined in Eq.(4.9) and Eq.(4.17)

Δ_2 equality equation for tooth undercutting, defined in Eq.(4.10) and Eq.(4.18)

Δ_3 equality equation for tooth undercutting, defined in Eq.(4.11) and Eq.(4.19)

Δ_4 equality equation for tooth undercutting, defined in Eq.(4.12) and Eq.(4.20)

ΔR difference between $R^{(g)}$ and $R^{(p)}$

FEA   finite element analysis

KE   kinematical errors

TCA   tooth contact analysis

CHAPTER 1

Introduction

1.1 Background

Gears play a very important role in transmissions. One of the first documented uses of gears can be traced back to more than forty centuries ago when the Egyptians used gear transmissions in their camel-driven watering facilities. Today, gears are widely used in industry for power transmissions because of their high efficiency. Gear transmissions are used in a wide variety of products, such as printer mechanism, mechanical watches, power plants, vehicle transmissions, etc.
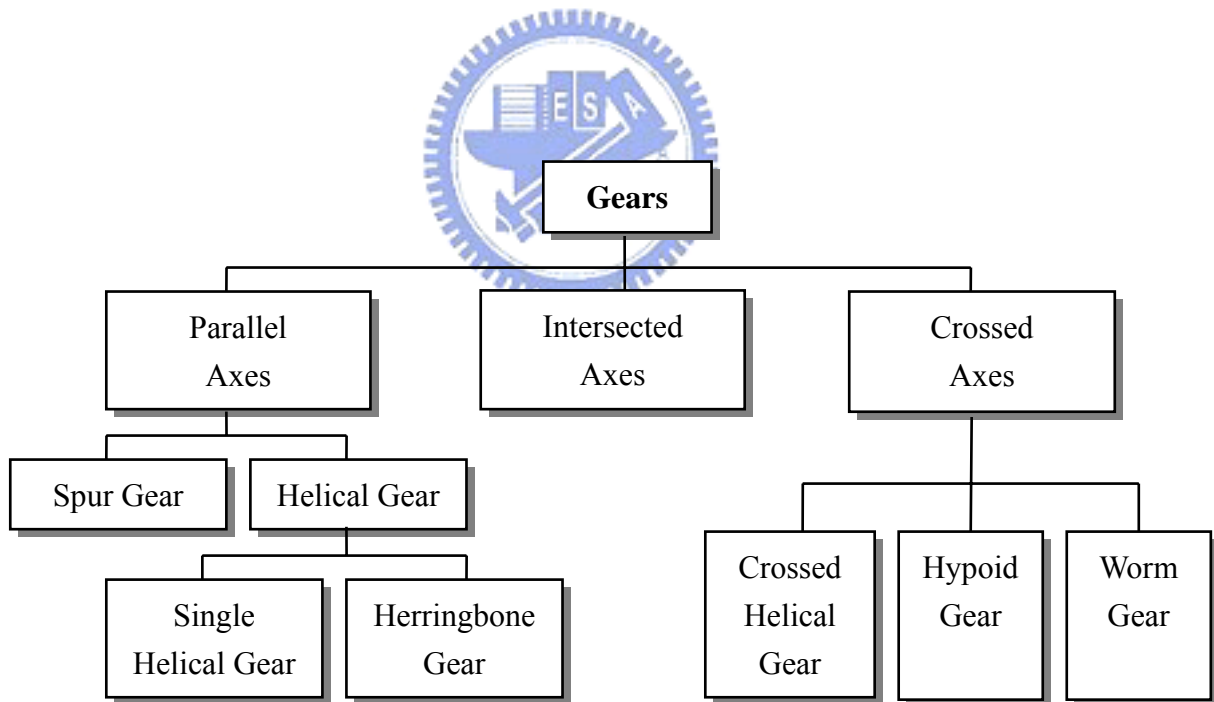
Fig. 1-1 Classification of gears

There are a lot of kinds of gears, such as spur gear, bevel gear, helical gear, worm gear and so on, which are used in many different ways. Gears are used to transmit the power between two shafts, and their classifications, are shown in Fig. 1-1, which are sorted by the axis relations. The classifications of the gears are parallel axes, intersecting axes, and crossed axes [1].

Cylindrical gears, such as spur gear, helical gear and herringbone gear, are widely used to transmit powers between parallel shafts and the shafts are rotated in opposite directions. The tooth traces of the spur gear are parallel to the rotational axis as shown in Fig. 1-2(a). The advantages of spur gears are easy to manufacture and inexpensive, but the spur gear pair tends to be noisy at high speed and is sensitive to the axial misalignments. Step gear has two or more spur gears fastened together and each gear is advanced relative to the adjacent one by a small amount of screw motion. Helical gear can be viewed as a stepped gear with an infinite number of steps. The tooth trace of the helical gear is shown in Fig. 1-2(b). The major advantage of helical gears is that they are engaged with a gradual contact between the teeth compared with spur gear, which make contact across the entire face at once during operation. This gradual contact results in less noisy and longer life cycle of the gear pair during operation.

Whereas the contact force of helical gear pair is not perpendicular to its rotational axis, an axial thrust force is produced to push the gears apart. The herringbone gear made by two opposite directions helical gears are bolted together, has been developed to reduce or eliminate the axial thrust force. The trace of the herringbone gear is shown in Fig. 1-2(c). The advantages of herringbone gear include the advantages of helical gear and also have no axial thrust force during operation because of the balance of thrust force. A herringbone gear is bolted by two helical gears, thus the manufacture cost is higher.

(a) Spur Gear　　　　(b) Helical Gear　　　　(c) Herringbone Gear
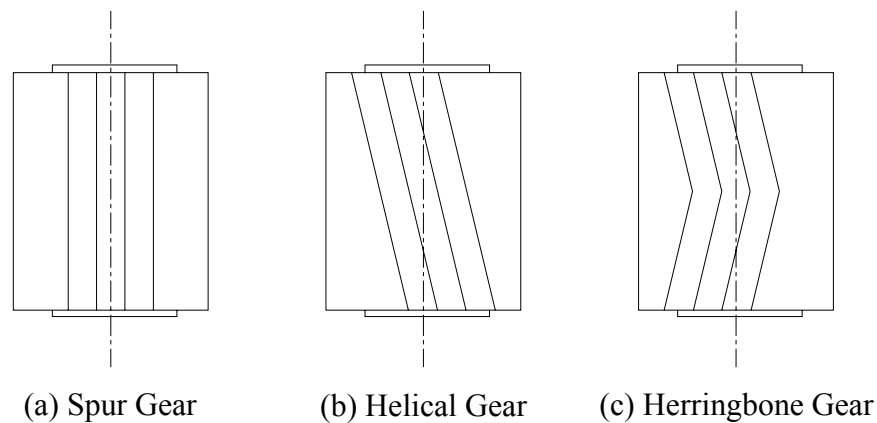
Fig. 1-2 Various types of tooth traces for parallel axis gears

1.2 Literature Reviews

Curvilinear-tooth gear has many excellent performances, such as higher bending strength, lower noise, better lubrication effect, no axial thrust force, etc. It will be introduced in the next chapter. The generation method is first proposed by Liu [2] with a face mill-cutter on a special machine. Tseng and Tsay [3] developed a mathematical model of cylindrical gears with curvilinear shaped teeth by using an imaginary rack cutter and investigated the tooth undercutting of curvilinear-tooth gears. However, in modern gear practice and manufacturing, the gears are usually generated by a hobbing or CNC cutting process. Tseng and Tsay [4] proposed a generating process of using a hob cutter which has a higher cutting efficiency than a rack cutter, the mathematical model for generation, the theoretical analysis on the tooth undercutting and secondary cutting of the gear teeth in the generation process were investigated with numerical examples.

The kinematical errors (KE) induced by gear axial misalignments is an efficient factor to predict the contact behaviors of gear pair, such as the noise, vibration, etc. Tsay [5] applied

TCA (tooth contact analysis) techniques to simulate the meshing conditions for involute helical gears. The TCA technique was also used in cylindrical gears with curvilinear shaped teeth by Tseng and Tsay [6].

The circular-arc tooth gear is a kind of gears with a higher loading compatibility. Circular-arc helical gears have been proposed by Wildhaber [7] in 1926 and Nobikov [8] in 1956. These types of gears became very popular in 1960s because of their low contact stress. Litvin and Tsay [9] investigated the mathematical model and TCA for the circular-arc helical gears by considering the gears were generated by imaginary circular-arc rack cutters.

Recently, Litvin et al. [10][11][12][13] proposed a concept of tooth surface topology that will reduce the KE and localize the bearing contact. The KE can be reduced by imposing a pre-designed parabolic-like KE on the gear tooth surfaces, which may absorb discontinuous KE caused by axial misalignments [10]. Meanwhile, the localization of bearing contact can be achieved by tooth modifications to obtain point contacts instead of line contacts, whether under an ideal or a misaligned meshing condition.
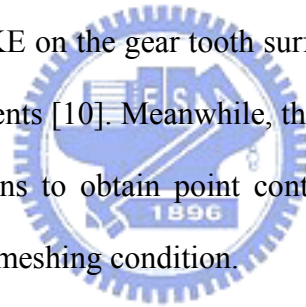
1.3 Motivations

Curvilinear-tooth gear pair can be used to transmit powers between two parallel shafts. It can sustain a higher bending and contacting strength, and can operate quietly and smoothly. Besides, no axial thrust force occurs for the curvilinear-tooth gear pair is during its operation. Tseng [3] also investigated the TCA simulation of the curvilinear-tooth gear.

The gear designers and manufacturers always aspire to design and manufacture a gear with a high loading capacity and low sensitivity to assembly errors. In order to achieve this goal, researchers focus on the development of advanced materials and new methods of heat

treatment or on design of stronger tooth profiles and methods of gear manufacturing. There are many methods to design for a stronger tooth profile, such as adding circular root fillets [14], predicting the power loss for high contact ratio spur gears with nonstandard addendum proportions by using cutter elongation of tool shifting [15], or modifying the straight edge rack cutter into a circular-arc profile [16][17], etc. A gear pair with a higher loading can be designed by a higher contact ratio or a larger contact area of tooth surfaces. A higher contact ratio can reduce the stress by distributing load among neighboring teeth. It is good practice to maintain a gear contact ratio larger than 1.2. With a higher contact ratio, loadings on the gear teeth surface can be dispersed by more contact gear teeth. The contact area on tooth surface can efficiently disperse the contact stress during contact.

It is said that the curvilinear-tooth gear has several advantages and characteristics. In order to obtain a curvilinear-tooth gear set which can endure a higher contacting strength, the profile of the involute curvilinear gear can be considered to be modified. The normal section of the rack cutter is designed as a circular-arc to produce the tooth profile. The tooth which generated by a circular-arc rack cutter is called a circular-arc tooth. Comparing the circular-arc tooth with involute tooth, the minor axis of the contact ellipse of the tooth generated by a circular-arc cutter is larger than that of an involute tooth. It means that there is a larger contact area for the modified curvilinear-tooth gear and this result in a smaller contact stress. In this thesis, two conjugate circular-arc rack cutters are used to generate the curvilinear gear pair respectively with circular-arc teeth to improve the bearing contact of the curvilinear gear.

1.4 Thesis Overviews

In this thesis, a gear with curvilinear teeth generated by a disk-type circular-arc cutter is

briefly proposed. In all, this thesis includes seven chapters, and the contents of each chapter are described as follows:

1. CHAPTER 1 is the introduction of the background, motivations, literature reviews and a brief overview of this thesis.

2. CHAPTER 2 introduces the curvilinear-tooth gear and the circular-arc tooth gear. Advantages and disadvantages of these two gears are briefly discussed.

3. The mathematical model of the circular-arc curvilinear-tooth gear set has been developed in CHAPTER 3. The circular-arc profile on its curvilinear-tooth gear is generated by a disk-type rack cutter with circular-arc normal section geometry. However, the generation method of the circular-arc curvilinear-tooth gear is simulated by a circular-arc profile rack cutter. Equations of the circular-arc curvilinear-tooth gear can be obtained by applying the theory of gearing and the equations of the cutter. Computer graph illustrates the shape of the gear pair, and it also proves the correctness of the developed mathematical model. In addition, the equations of the gear set are the bases for further investigations, such as tooth contact analysis, contact ratio and contact ellipses.

4. CHAPTER 4 includes the study of tooth undercutting of the proposed gear pair. The undercutting points are the singular points on the generated tooth surface. Consequently, it can be derived according the theory of gearing. Some tables and graphs are built up by applying the developed computer programs to give suggestions for the manufactures and designers to prevent the tooth undercutting.

5. The TCA technique is applied to find the KE of the circular-arc curvilinear-tooth gear in CHAPTER 5. Tooth contact simulation model includes the center distance

variation, horizontal axial misalignment and vertical axial misalignment of the gear set. The KE curve are tried to pre-design into a parabolic form in order to prevent the jump of the junction. Several numerical examples are presented to demonstrate the influences of gear design parameters and assembly errors on the KE and contact analysis of the mating gear pair.

6. Contact pattern is an important symbol of gear loading capability. The contact pattern can be simulated based on the developed mathematical model of the gear set. Some numerical examples express the relationships between the design parameters and contact patterns. In this thesis, the contact patterns are evaluated by applying the surface topology method.

7. CHAPTER 7 concludes this thesis by summarizing the major findings of the accomplished work, and also discusses some potential topics for future study.
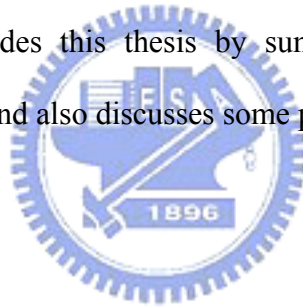
CHAPTER 2

The Curvilinear-Tooth Gear and the Circular-Arc Tooth Gear

2.1 Introduction

The shape of a gear can be described into two ways: one mentioned the profile of the cross section of gear. Fig. 2-1(a) is the involute-shape gear profile of a spur gear shown in Fig. 2-1(b). As everyone knows that most applications of the gear profiles are in the involute shape.

(a)   (b)
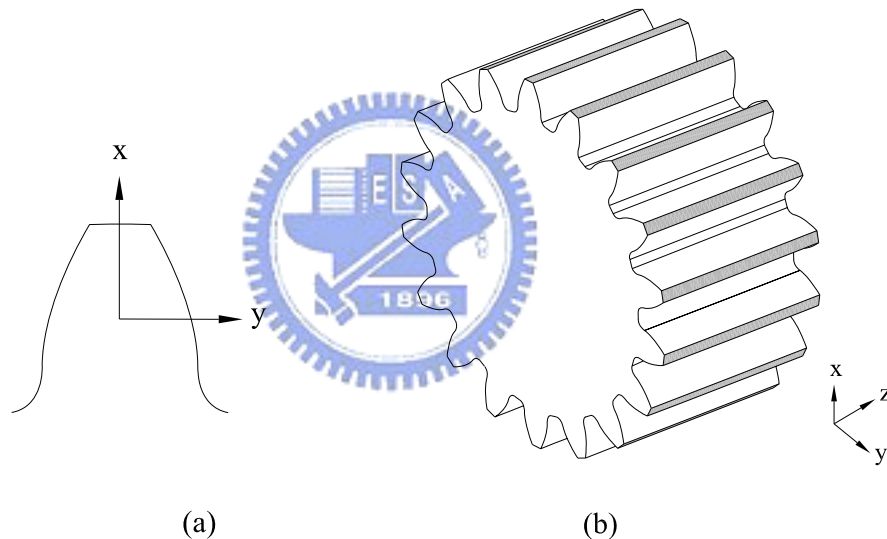
Fig. 2-1 Schema of gear profile and gear tooth trace of a spur gear

The other description for a gear shape is the trace of its tooth, e.g. gears with trace parallel to the rotational axis as marked with shadow zones in Fig. 2-1(b) is called a spur gear. Different profiles and traces of gears have their own characteristics, the usage of gear is according to there characteristics. In this chapter, two kinds of gear types will be introduced.

One is the curvilinear-tooth trace gear and another one is the circular-arc tooth profile gear.

2.2 The Curvilinear-Tooth Gear

Curvilinear-tooth gear is one kind of cylindrical gears as shown in Fig. 2-2, and has circular-arc tooth traces. Since the circular arc tooth trace is symmetrical, thus gear axial thrust force may be eliminated. Besides, the curvilinear-tooth gear has the characteristics as follows [2]:

1. Curvilinear-tooth gears endure a higher bending and contacting strength; thus, the size of transmission gear boxes may be reduced while transmitting the power or torque.

2. The teeth of curvilinear-tooth gear pair engaged simultaneously smoothly with low noise.

3. Lubrication oil is retained within the concave tooth surfaces, therefore there is always an oil film between the two engaged surfaces, resulting in good lubrication qualities.

The spur, helical, and herringbone gear pairs with parallel axes are in line contact. However, the line contact of gear tooth surfaces can be realized only for an ideal contact of the gear drive. In reality, the gear assembly errors of axial misalignments and errors of lead angles result in the so-called edge contact, a specific instantaneous contact caused by curve-to-surface tangency as shown in Fig. 2-3. Therefore, the stress is concentrated at the contact edge. Gear manufacturers always cut gears with tooth crowning to make the line contact become a point contact, and to avoid the edge contact of gears as shown in Fig. 2-4. The point contact of gears will spread over a contact ellipse with loadings. When a gear set

has an axial misalignment without crowning, tooth edge contact will occur and this will induce a serious stress concentration. In this circumstance, the noise and vibration of the gear pair may occur during the gear meshing. The curvilinear-tooth gear also has a characteristic similar to a crowned tooth, as shown in Fig. 2-5. The contact type of the curvilinear-tooth gear is in a point contact situation no matter there is an axial misalignment or not.
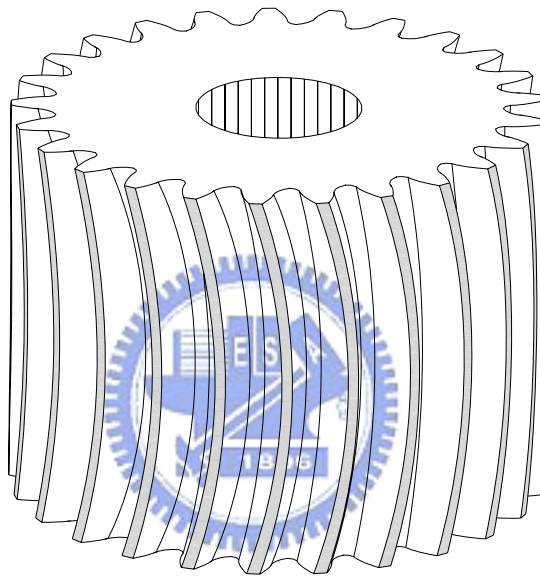
Fig. 2-2 Schema of curvilinear-tooth gear [3]

2.3 The Circular-Arc Tooth Gear

The theory of circular-arc tooth gears is first proposed by Wildhaber [7] in U.S. patent, 1926. Later, Novikov [8], also proposed another patent for helical gears with circular-arc teeth. Therefore, the circular-arc tooth gear is also called the Wildhaber-Novikov (W-N) gear. The profiles of the Wildhaber's and Novikov's are quite similar to each other. It is noted that the circular-arc tooth gears are generated by two imaginary rack cutters, described in two
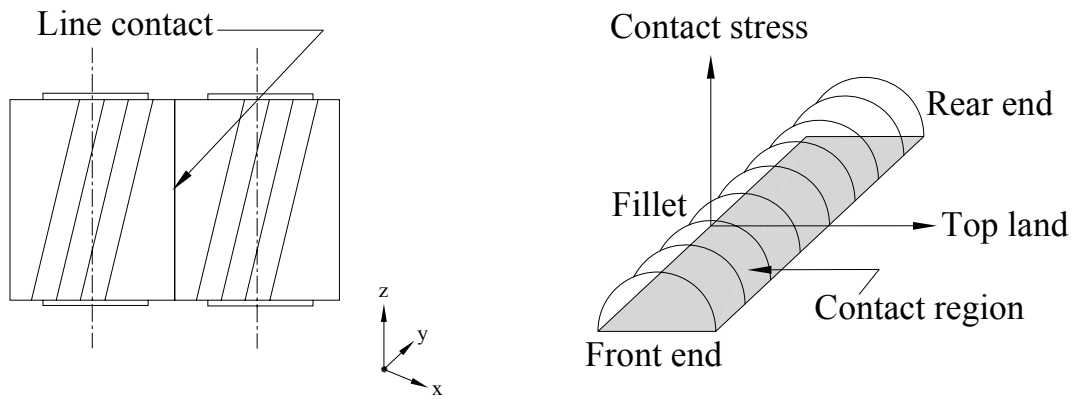
(a) Helical gear pair without axial misalignment
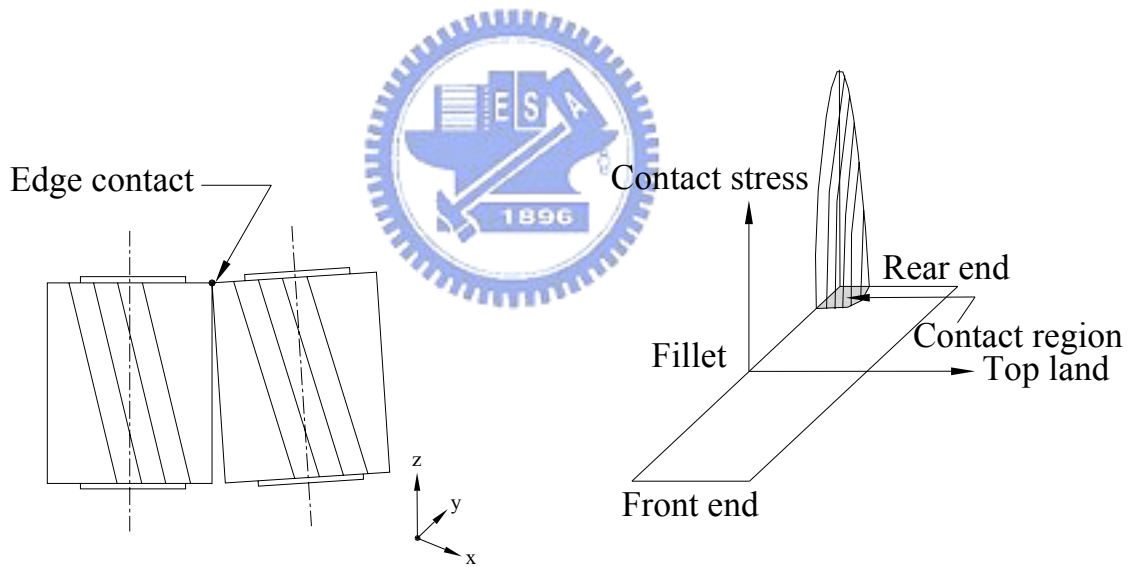
(b) Helical gear pair with axial misalignment

Fig. 2-3 Contact region of a helical gear pair
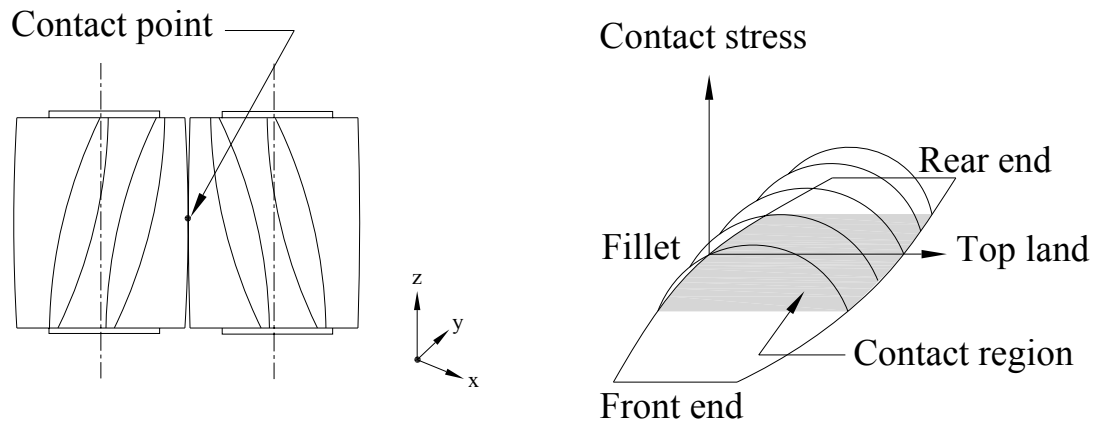
(a) Helical gear with crowning teeth pair without axial misalignment
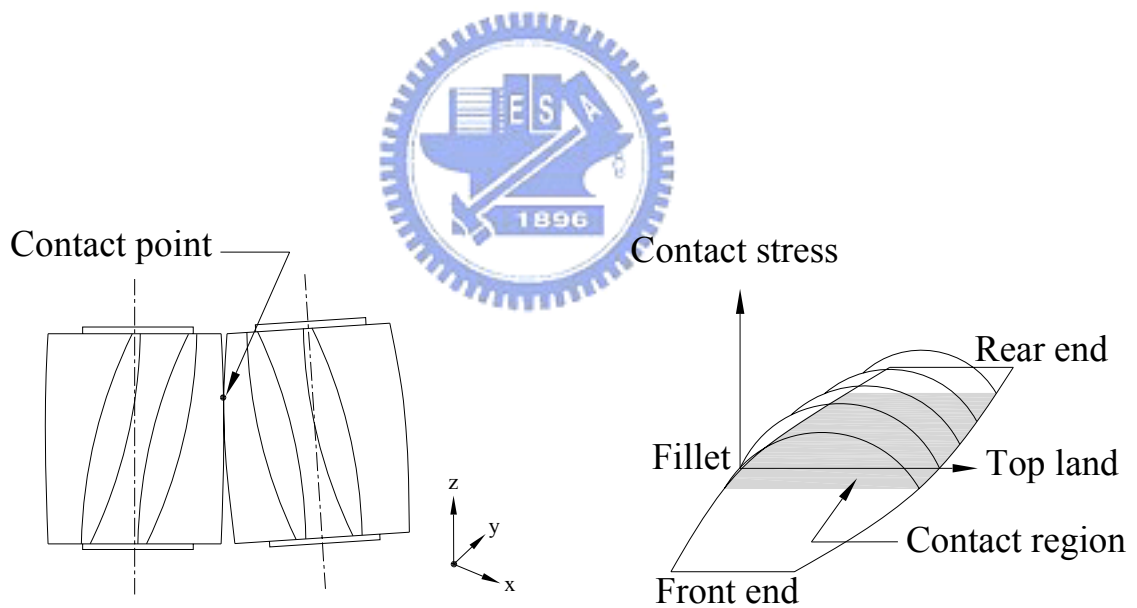
(b) Helical gear with crowning teeth pair with axial misalignment

Fig. 2-4 Contact region of a crowned teeth gear pair
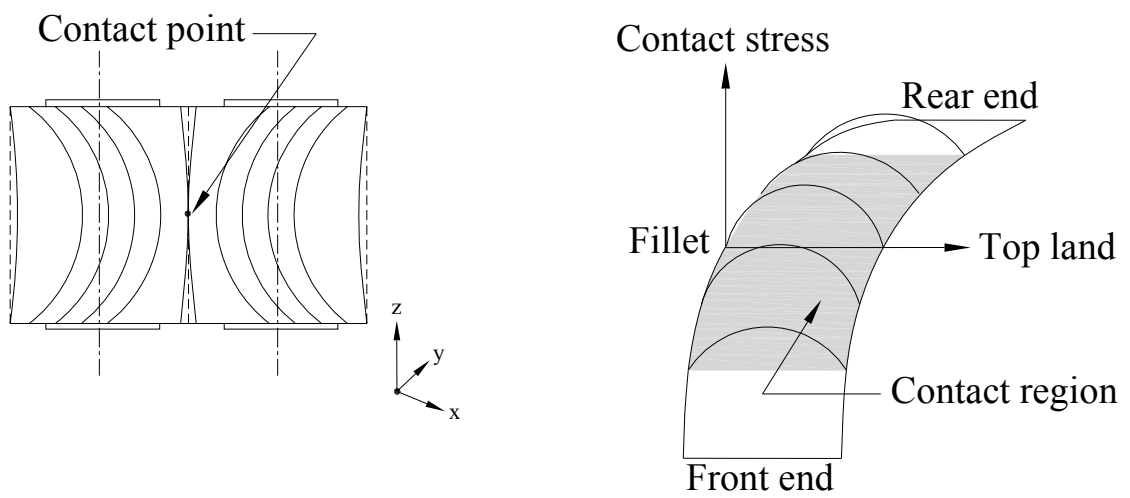
(a) Curvilinear gear pair without axial misalignment
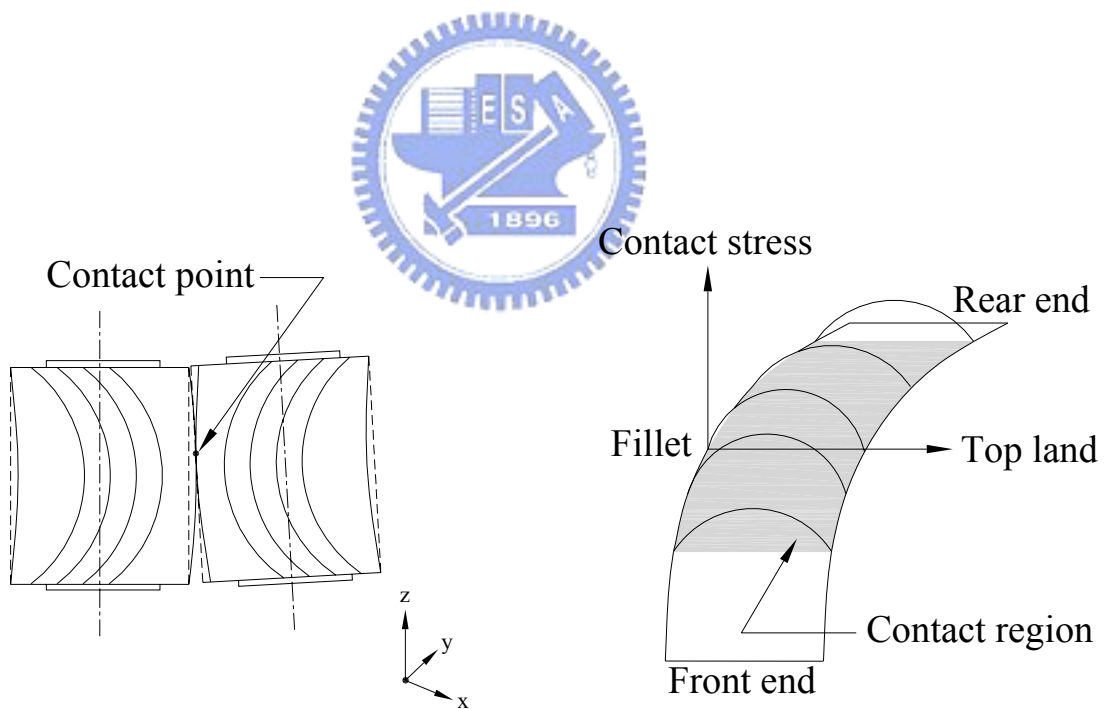
(b) Curvilinear gear pair with axial misalignment

Fig. 2-5 Contact region of a curvilinear-tooth gear pair

circular-arc curves as shown in Fig. 2-6, where the $R^{(p)}$ and $R^{(g)}$ are the radii of the two cutters, where $O_R^{(p)}$ and $O_R^{(g)}$ are the center of these circular-arc. In order to generate a pair of conjugate gear surfaces, the rack cutters can be considers as two separate rack cutters which may be imagine as a mold and its corresponding cast express in Fig. 2-7. One of these rack cutters generates the pinion and the other generates gear.
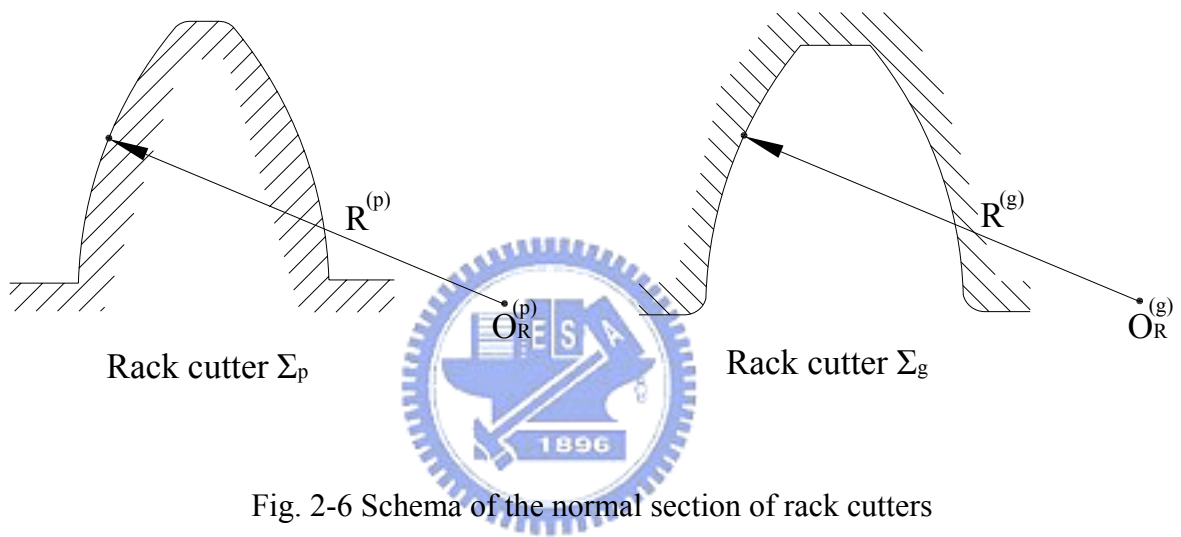
Fig. 2-6 Schema of the normal section of rack cutters
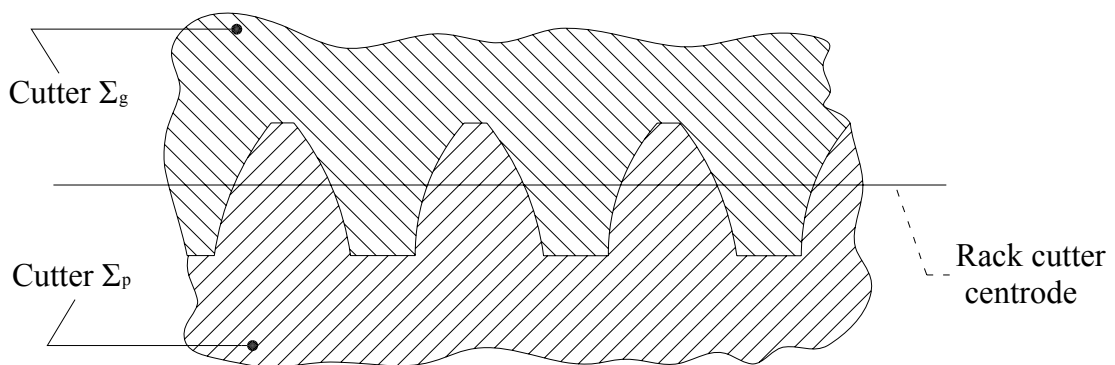
Fig. 2-7 Imaginary of the separating rack cutters

Since the normal section of each rack cutter has circular-arc edges, thus the tool needs a higher precision requirement. However, the technology is brilliant enough to produce high precision circular-arc cutter now.

It is known that a circular-arc gear has the following two major advantages:

1. Reducing the contacting stress. Theoretically, the gear surfaces are contact when two gears are meshed with each other. However, the contact area spread over a contact ellipse due to elastic deformation under loading. After operating for a period of time, the two meshing surfaces fit each other into a suitable shape for meshing. It is said that the curvatures on the contact point of these two gears tend to equal gradually. The contact surfaces enlarge quickly with the operation loading. Hence, the loading limit is three to five times higher than an involute gear pair [18].

2. Better conditions of lubrication. The sliding velocity of every point on the gear surface are equal in a slight value, it means the wear problem of the circular-arc tooth gear is not serious. Rotation speed of the circular-arc tooth gear is high on the vertical direction of the gear surface, so the oil- membrane can be formed easily. Thus the lubrication of the circular-arc gear pair is ten times better than an involute gear pair [19]. With the better lubrication, the life time of this type of gears becomes longer and abrasion becomes less serious.

The circular-arc gear can provide power transmission with a high loading, and it is widely used in the transmission system of hoists, elevators, mechanisms for mining industry, and many transmission systems with a high load/weight ratio. Although the circular-arc gear tooth surfaces are in point contact at every instant, the contact area is also larger than that of involute gear pair under load with elastic deformation.

Nevertheless, there are also three major disadvantages of the circular-arc gear as below:

1. The profile of the rack cutter is in a circular-arc shape, and it is manufactured by several processes requiring high precision, and the heat treatment process may somewhat cause distortion of the cutter shape. Therefore, the menufacturing cost of this cutter is higher.

2. There are no international standards for the circular-arc gears, e.g.. the radius of circular-arc edge. Hence, the circular-arc gear cannot be exchanged facilely. It means the comparability with the circular-arc gear is not good.

3. The kinematical error occurs if there has error of center distance. However, the variation of center distance takes no effects for involute gear pair.

2.4 Remarks

Gears are used in power transmissions. Therefore, good gears always include two essential factors: high loading capacity and low sensitivity to assembly errors. The goal can be achieved by designing the profile and tooth-trace for the gear pair. Two types of gears are introduced in this chapter, one is the curvilinear-tooth gear which has a curvilinear tooth-trace, and the other one is the circular-arc tooth gear which is generated by two conjugate rack cutters. Both of these two gears benefit to developing the performance of the gear pair.

CHAPTER 3

Mathematical Model of Gears with Curvilinear-Teeth

Generated by a Disk-Type Circular-Arc Cutter

3.1 Introduction

In this chapter, the mathematical model of curvilinear-teeth generated by the disk-type circular-arc cutter will first be developed. Based on the theory of gear [10][20], the surface equation of circular-arc gears with curvilinear-teeth is derived as the envelope of the locus of circular-arc cutter. Hence, an imaginary rack cutter surface with circular-arc normal section will be first established to simulate the generation of the gear tooth.

3.2 Mathematical Model of Circular-Arc Gears with Curvilinear-Teeth

3.2.1 Generation Method

The curvilinear-tooth gear is generated by the cutting machine as shown in Fig. 3-1. Gear teeth are produced by a rotating disk-type cutter. The spindle of the disk-type cutter with radius R_{ab} rotates on the axis $B-B$ with an angular velocity ω_t and translating velocity $\omega_1 r_1$ to the right, where r_1 is the pitch radius of the gear blank and ω_1 is the angular velocity of it. The cutting process of a curvilinear-tooth gear was developed by Liu [2] as steps below:

1. The gear blank rotates with an angular velocity ω_1 in clockwise. At this moment, the disk-type cutter rotates with an angular velocity ω_t in counterclockwise and translates with a velocity $r_1 \omega_1$ to right. A curvilinear-tooth space may be generated on the gear blank by this process.

17
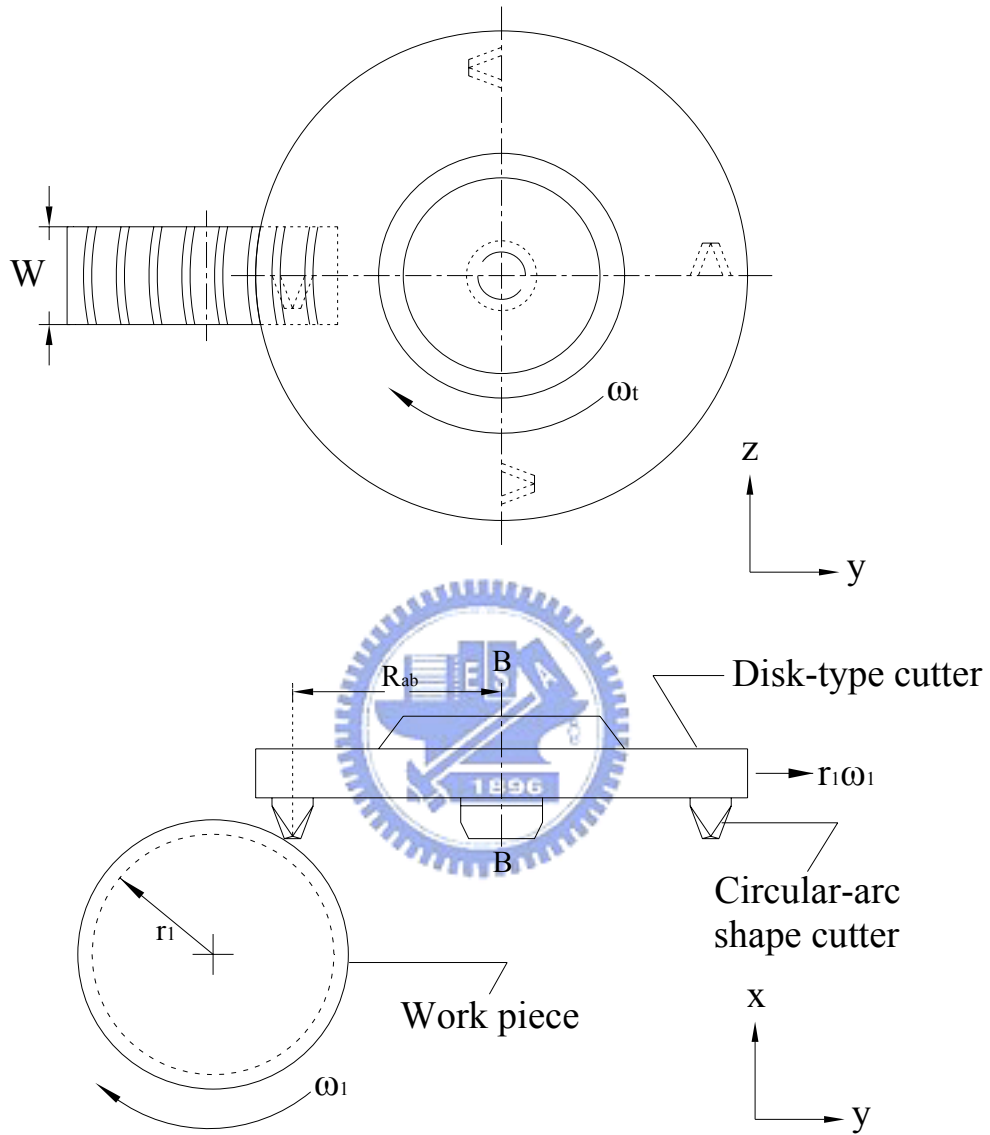
Fig. 3-1 The cutting process of a curvilinear-tooth gear with a disk-type tool [2]

2. After generating the tooth space of the gear, the gear blank stop rotating and then spin to the next working position with considering adjustment for the backlash δ_{bl}.

3. In order to cut the other tooth space, the disk-type cutter rotates with an angular velocity ω_t in clockwise and translates with a velocity $r_1\omega_1$ to left, the gear blank rotates in the counterclockwise with angular velocity ω_1 in the mean time (contrary to the Fig. 3-1), then the other tooth space is generated by this process. In order to prevent the interfering, the radius of the disk-type cutter used to generate the different side of the tooth surface should be modified. In this thesis, the difference between the different side of the gear tooth is defined as S^G.

4. Generating cycle is repeated and this sequence is continued until all the spaces and teeth are formed.
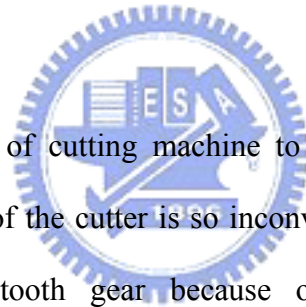
Obviously, the structure of cutting machine to produce the curvilinear-tooth gear is complex, and the assembling of the cutter is so inconvenient. Adjusting and grinding is also arduous for the curvilinear-tooth gear because of its special trace. Therefore, the manufacturing cost of curvilinear-tooth gears is higher than that of spur gears or helical gears. In this thesis, the cutting machine is adopted and the straight line cutter shape is replaced by the circular-arc cutter shape. Gears made by this process are called the curvilinear-tooth gears generated by a disk-type circular-arc cutter.

Although the gear is generated by a disk-type cutter, however it can be considered that the gear is generated by an imaginary rack cutter as shown in Fig. 3-2. The surfaces of the two cutters are labeled as Σ_g and Σ_p, and we may imagine that the two surfaces are rigidly connected to each other and are in tangency along the curve $a-a$ as shown in Fig. 3-3. The normal section of each rack cutter is a circular arc. Fig. 3-4 shows the relationships among the

pitch plan of rack cutter and the axode of the two gears. The locus of an instantaneous axis of

rotation represented in a coordinate system that is attached to a movable body is known as the

body axode.
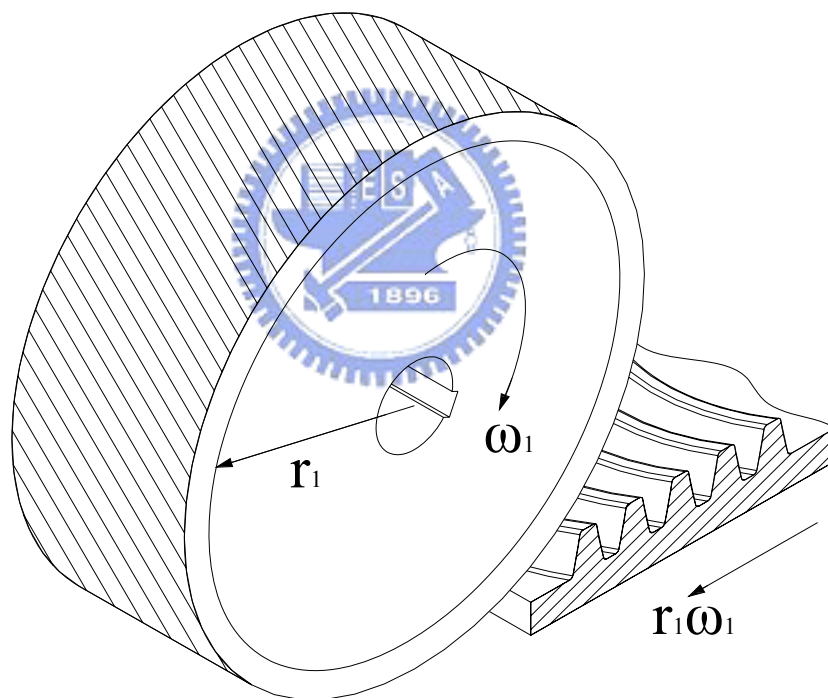
Fig. 3-2 The relationship between imaginary rack cutter and blank
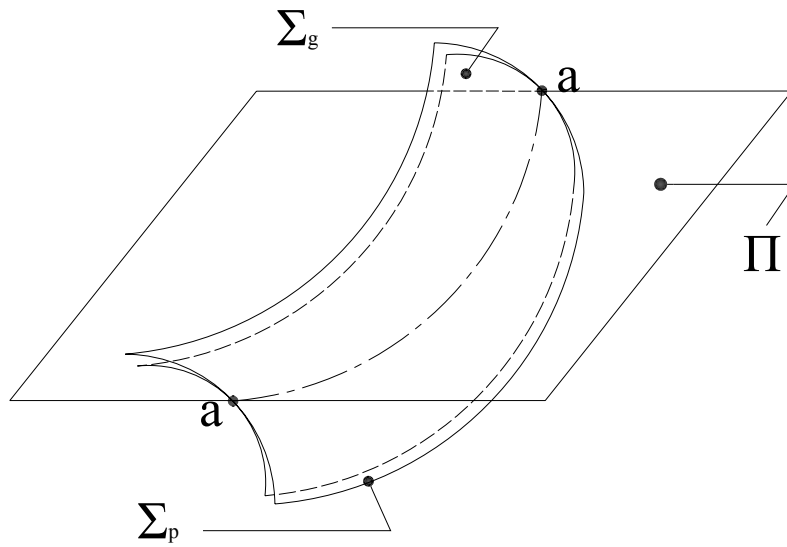
Fig. 3-3 Surfaces of the imaginary cutters Σ_g and Σ_p
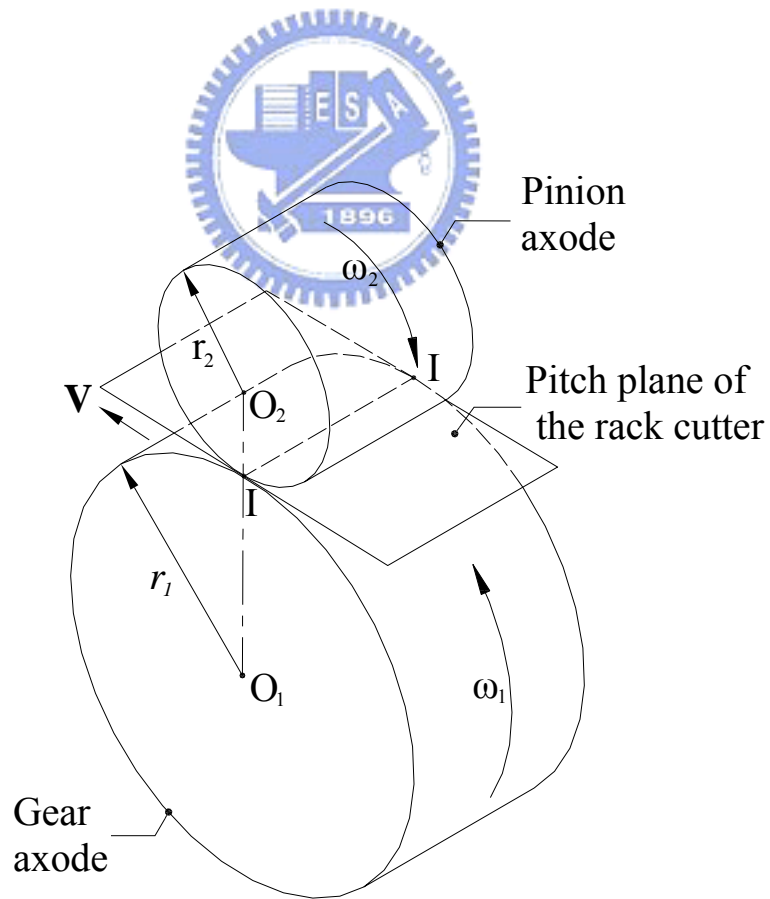
Fig. 3-4 The axodes of the gears

The two gears are rotating with an angular velocity ω_1 and ω_2 in opposite directions about their respective rotation axes. The radii of the two axodes are $r_1 = \dfrac{V}{\omega_1}$, $r_2 = \dfrac{V}{\omega_2}$. The tangent line $I-I$ of the two axodes is called the instantaneous axis of rotation. The tangent plane to the axodes is also the pitch plane of the rack cutters. The gear is generated by the cutter Σ_g and the pinion is generated by the cutter Σ_p. Namely, the mathematical model of the gear is generated by the surface Σ_g, and another one is generated by Σ_p. Finally, the mathematical model of the generated gear tooth surface is the combination of the meshing equation and the locus equation of imaginary rack cutter surface. Points on gear surface can be calculated by solving the developed gear mathematical model by using numerical methods.

3.2.2 Equation of the Disk-Type Circular-Arc Cutter

The teeth surfaces of a pair of conjugate circular-arc with curvilinear-teeth gear can be generated by two imaginary circular-arc rack cutters with curvilinear trace. These two rack cutters of Σ_g and Σ_p are shown in Fig. 3-5(a). The normal sections of the cutters are also shown in Fig. 3-5(b). Parameters A and B determine the initial and end points of the circular-arc curve, respectively, as shown in Fig. 3-6. $O_R^{(g)}$ is the center of the circular-arc $\widehat{MN}$ with a radius of $R^{(g)}$; S^G is the tooth thickness measured along the pitch line of the rack cutter; $\theta^{(g)}$ is the design parameter of the rack cutter which determines the point on the circular arc $\widehat{MN}$. The normal section of the circular-arc rack cutter is rigidly attached to coordinate system $S_r^{(g)}(X_r^{(g)}, Y_r^{(g)}, Z_r^{(g)})$ with its origin $O_r^{(g)}$, as shown in Fig. 3-6. The circular-arc curve $\widehat{MN}$ can be represented in coordinate system $S_r^{(g)}(X_r^{(g)}, Y_r^{(g)}, Z_r^{(g)})$ as follows:

$$x_r^{(g)} = -R^{(g)}\left(\sin\alpha - \sin\theta^{(g)} \right),$$

$$y_r^{(g)} = \pm \left\{ R^{(g)} \left(\cos\alpha - \cos\theta^{(g)} \right) - \frac{S^G}{2} \right\}, \tag{3.1}$$

$$z_r^{(g)} = 0 \,,$$

and

$$\theta_{\min}^{(g)} \le \theta^{(g)} \le \theta_{\max}^{(g)} \,, \quad \theta_{\min}^{(g)} = \sin^{-1}\left[\frac{R^{(g)}\sin\alpha - B}{R^{(g)}} \right], \quad \theta_{\max}^{(g)} = \sin^{-1}\left[\frac{R^{(g)}\sin\alpha + A}{R^{(g)}} \right], \tag{3.2}$$

(a)   (b)
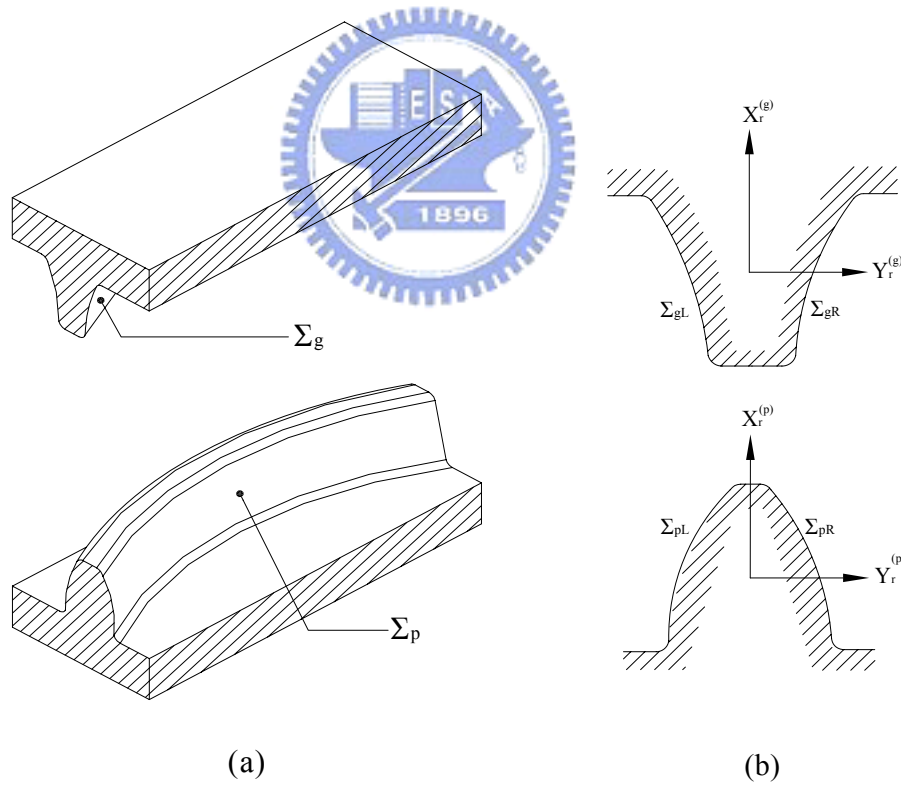
Fig. 3-5 Imaginary circular-arc rack cutters Σ_g and Σ_p
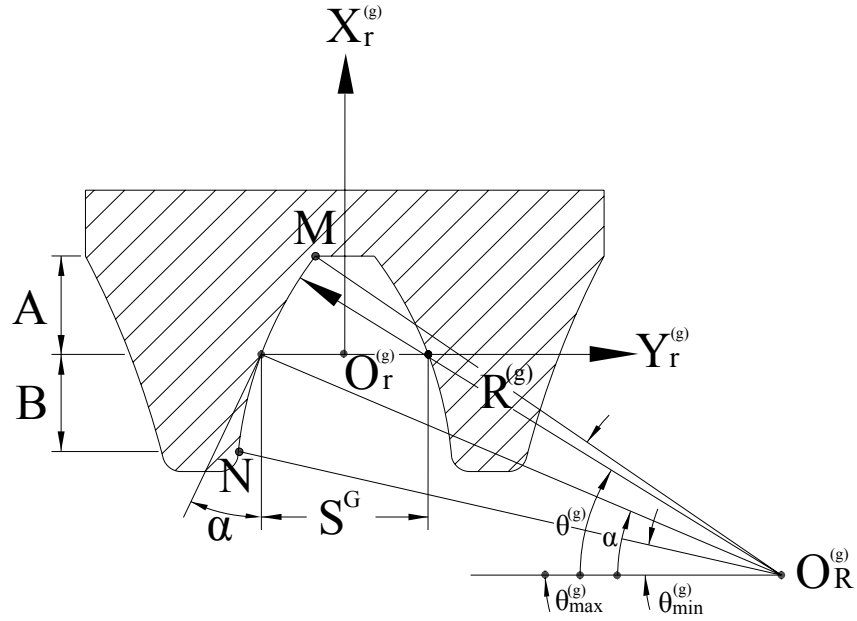
Fig. 3-6 Normal section of the circular-arc rack cutter Σ_g

where $\theta^{(g)}$ is a design parameter of the circular-arc rack cutter, ranging from $\theta_{min}^{(g)}$ to $\theta_{max}^{(g)}$, and α denotes the normal pressure angle defined in Fig. 3-6, and $R^{(g)}$ represents the radius of the circular-arc $\widehat{MN}$. The symbol "$\pm$" represents the different side of the cutter Σ_g, where "$-$" indicates the right side circular-arc rack cutter Σ_{gR} and "$+$" indicates Σ_{gL}.

To form a circular-arc rack cutter with curvilinear-trace, the normal section of the circular-arc (Fig. 3-6) should attach to coordinate system $S_r^{(g)}\left(X_r^{(g)}, Y_r^{(g)}, Z_r^{(g)}\right)$, as shown in Fig. 3-7. It is noted that the circular-arc $\widehat{ab}$ is the cutting path of the disk-type rack cutter. The cutting path of the cutter consequently causes a crowning effect on the generated tooth flank. Coordinate system $S_c^{(g)}\left(X_c^{(g)}, Y_c^{(g)}, Z_c^{(g)}\right)$ is rigidly attached to the middle of transverse section of the imaginary rack cutter. Coordinate system $S_r^{(g)}\left(X_r^{(g)}, Y_r^{(g)}, Z_r^{(g)}\right)$ is attached to

24

coordinate system $S_c^{(g)}\left(X_c^{(g)}, Y_c^{(g)}, Z_c^{(g)}\right)$ with a variable angle $\gamma^{(g)}$. The center of the curvilinear-trace is located at point $C^{(g)}$ with a radius of R_{ab} and W represents the width of the gear pair.

The imaginary rack cutter surface Σ_g represented in coordinate system $S_c^{(g)}\left(X_c^{(g)}, Y_c^{(g)}, Z_c^{(g)}\right)$ can be obtained by applying the following homogeneous coordinate transformation matrix equation as follows:

$$\mathbf{R}_c^{(g)} = \mathbf{M}_{cr}\mathbf{R}_r^{(g)},$$ (3.3)

where $\mathbf{M}_{cr} = \begin{bmatrix} 1 & 0 & 0 & 0 \\ 0 & \cos\gamma^{(g)} & \sin\gamma^{(g)} & R_{ab}(1-\cos\gamma^{(g)}) \\ 0 & -\sin\gamma^{(g)} & \cos\gamma^{(g)} & R_{ab}\sin\gamma^{(g)} \\ 0 & 0 & 0 & 1 \end{bmatrix}$. (3.4)

Matrix $\mathbf{M}_{cr}$ is a homogeneous coordinate transformation matrix transforming from coordinate system $S_r^{(g)}(X_r^{(g)}, Y_r^{(g)}, Z_r^{(g)})$ to $S_c^{(g)}\left(X_c^{(g)}, Y_c^{(g)}, Z_c^{(g)}\right)$. Using the Eq.(3.1), Eq.(3.3), and Eq.(3.4) the mathematical model of the disk-type circular-arc cutter represented in coordinate system $S_c^{(g)}\left(X_c^{(g)}, Y_c^{(g)}, Z_c^{(g)}\right)$ can be obtained as following:

$$\mathbf{R}_c^{(g)} = \begin{bmatrix} x_c^{(g)} \\ y_c^{(g)} \\ z_c^{(g)} \\ 1 \end{bmatrix} = \begin{bmatrix} x_r^{(g)} \\ y_r^{(g)}\cos\gamma^{(g)} + z_r^{(g)}\sin\gamma^{(g)} + R_{ab}(1-\cos\gamma^{(g)}) \\ y_r^{(g)}\sin\gamma^{(g)} + z_r^{(g)}\cos\gamma^{(g)} + R_{ab}\sin\gamma^{(g)} \\ 1 \end{bmatrix},$$ (3.5)

and

$$\gamma_{\min}^{(g)} \le \gamma^{(g)} \le \gamma_{\max}^{(g)}, \quad \gamma_{\min}^{(g)} = -\sin^{-1}\left[\frac{W}{2R_{ab}}\right], \quad \gamma_{\max}^{(g)} = \sin^{-1}\left[\frac{W}{2R_{ab}}\right].$$ (3.6)

Substituting Eq.(3.1) into Eq.(3.5) yields the imaginary rack cutter surface represented in coordinate system $S_r^{(g)}(X_r^{(g)}, Y_r^{(g)}, Z_r^{(g)})$ is as follows:

$$\mathbf{R}_c^{(g)} = \begin{bmatrix} x_c^{(g)} \\ y_c^{(g)} \\ z_c^{(g)} \\ 1 \end{bmatrix} = \begin{bmatrix} -R^{(g)}\left(\sin\alpha - \sin\theta^{(g)}\right) \\ R_{ab}\left(1 - \cos\gamma^{(g)}\right) \pm \cos\gamma^{(g)}\left(-\dfrac{S^G}{2} + R^{(g)}\left(\cos\alpha - \cos\theta^{(g)}\right)\right) \\ \sin\gamma^{(g)}\left(R_{ab} \pm \left(\dfrac{S^G}{2} - R^{(g)}\left(\cos\alpha - \cos\theta^{(g)}\right)\right)\right) \\ 1 \end{bmatrix}. \tag{3.7}$$

The normal cross section of rack cutter Σ_p is shown in Fig. 3-8. Similarly, the mathematical model of the rack cutter surface Σ_p can be established by following the above-mentioned steps:
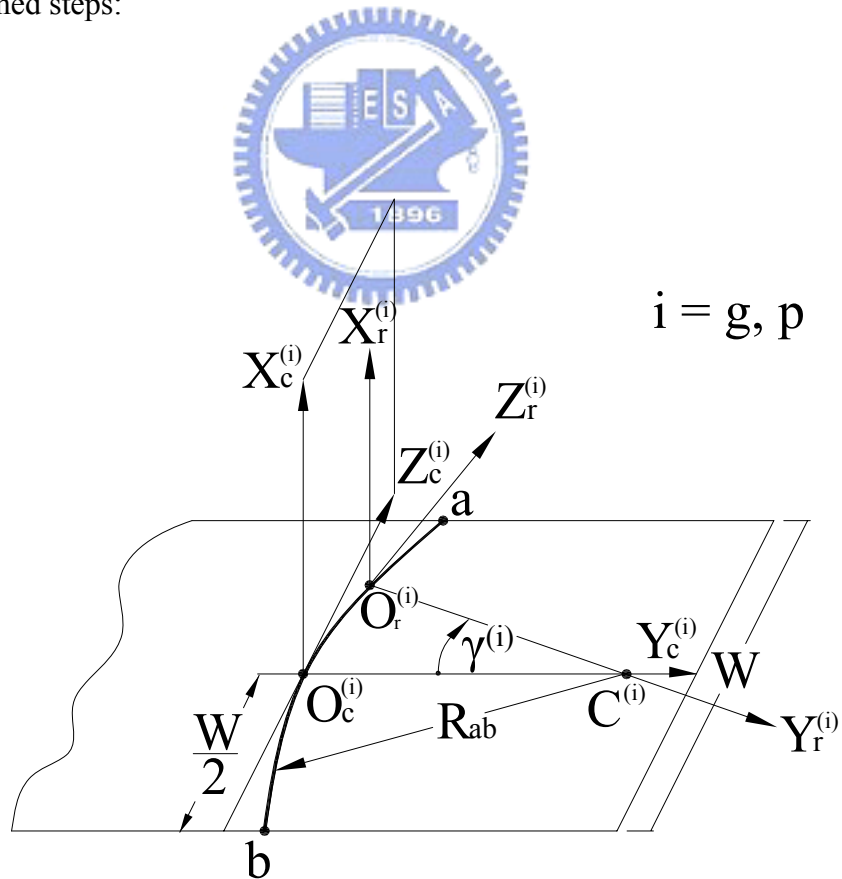
Fig. 3-7 Formation schema of the imaginary rack cutter Σ_p and Σ_g

26
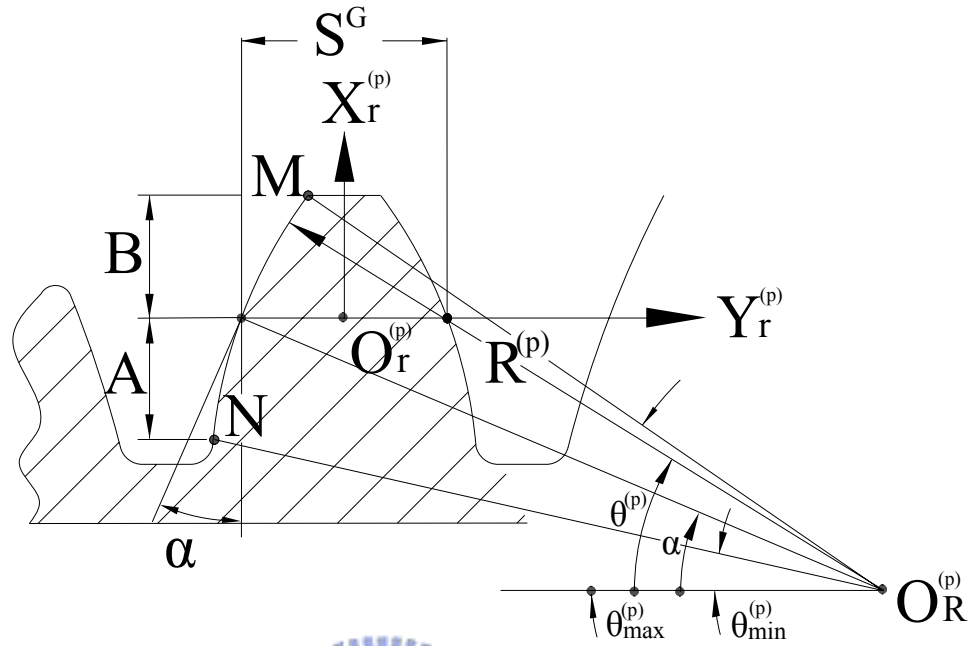
Fig. 3-8 Normal section of the circular-arc rack cutter Σ_p

$$\mathbf{R}_c^{(p)} = \begin{bmatrix} x_c^{(p)} \\ y_c^{(p)} \\ z_c^{(p)} \\ 1 \end{bmatrix} = \begin{bmatrix} -R^{(p)}\left(\sin\alpha - \sin\theta^{(p)}\right) \\ R_{ab}\left(1-\cos\gamma^{(p)}\right) \pm \cos\gamma^{(p)}\left(-\dfrac{S^G}{2} + R^{(p)}\left(\cos\theta^{(p)} - \cos\alpha\right)\right) \\ \sin\gamma^{(p)}\left(R_{ab} \pm \left(\dfrac{S^G}{2} - R^{(p)}\left(\cos\theta^{(p)} - \cos\alpha\right)\right)\right) \\ 1 \end{bmatrix}. \tag{3.8}$$

and the unit normal vector of the generating surface $R_c^{(g)}$ is obtained by:

$$\mathbf{N}_c^{(g)} = \frac{\partial \mathbf{R}_c^{(g)}}{\partial \theta^{(g)}} \times \frac{\partial \mathbf{R}_c^{(g)}}{\partial \gamma^{(g)}}. \tag{3.9}$$

and

27

$$
\mathbf{n}_c^{(g)} = \frac{\mathbf{N}_c^{(g)}}{\left|\mathbf{N}_c^{(g)}\right|}. \tag{3.10}
$$

Eqs.(3.7), (3.9) and (3.10) result in the unit normal vector of the generating surface represented in the coordinate system $S_c^{(g)}\left(X_c^{(g)}, Y_c^{(g)}, Z_c^{(g)}\right)$ as follow:

$$
\mathbf{n}_c^{(g)} = \begin{bmatrix} \mathbf{n}_{Xc}^{(g)} \\ \mathbf{n}_{Yc}^{(g)} \\ \mathbf{n}_{Zc}^{(g)} \end{bmatrix} = \begin{bmatrix} \sin\theta^{(g)} \\ \pm(-\cos\gamma^{(g)}\cos\theta^{(g)}) \\ \pm\sin\gamma^{(g)}\cos\theta^{(g)} \end{bmatrix}, \tag{3.11}
$$

where the upper sign of symbol "±" indicates the left-side of the rack cutter surfaces. Similarly, the unit normal vector of the rack cutter surface Σ_p can be also obtained by following the similar process:

$$
\mathbf{n}_c^{(p)} = \begin{bmatrix} \mathbf{n}_{Xc}^{(p)} \\ \mathbf{n}_{Yc}^{(p)} \\ \mathbf{n}_{Zc}^{(p)} \end{bmatrix} = \begin{bmatrix} \sin\theta^{(p)} \\ \pm(-\cos\gamma^{(p)}\cos\theta^{(p)}) \\ \pm\sin\gamma^{(p)}\cos\theta^{(p)} \end{bmatrix}. \tag{3.12}
$$

The relative velocity of the gear with respect to the rack cutter Σ_g can be obtained by considering the gear generation mechanism as shown in Fig. 3-9. The rack cutter translates to the left tangent to the axode of the gear. Therefore, the velocity of the point on the rack cutter represented in coordinate system $S_f\left(X_f, Y_f, Z_f\right)$ is:

$$
\mathbf{V}_f^{(1)} = \begin{bmatrix} 0 \\ -\omega_1 r_1 \\ 0 \end{bmatrix}, \tag{3.13}
$$

where r_1 is the pitch radius of the gear blank, and ω_1 is the rotation speed of the gear blank during its generation.
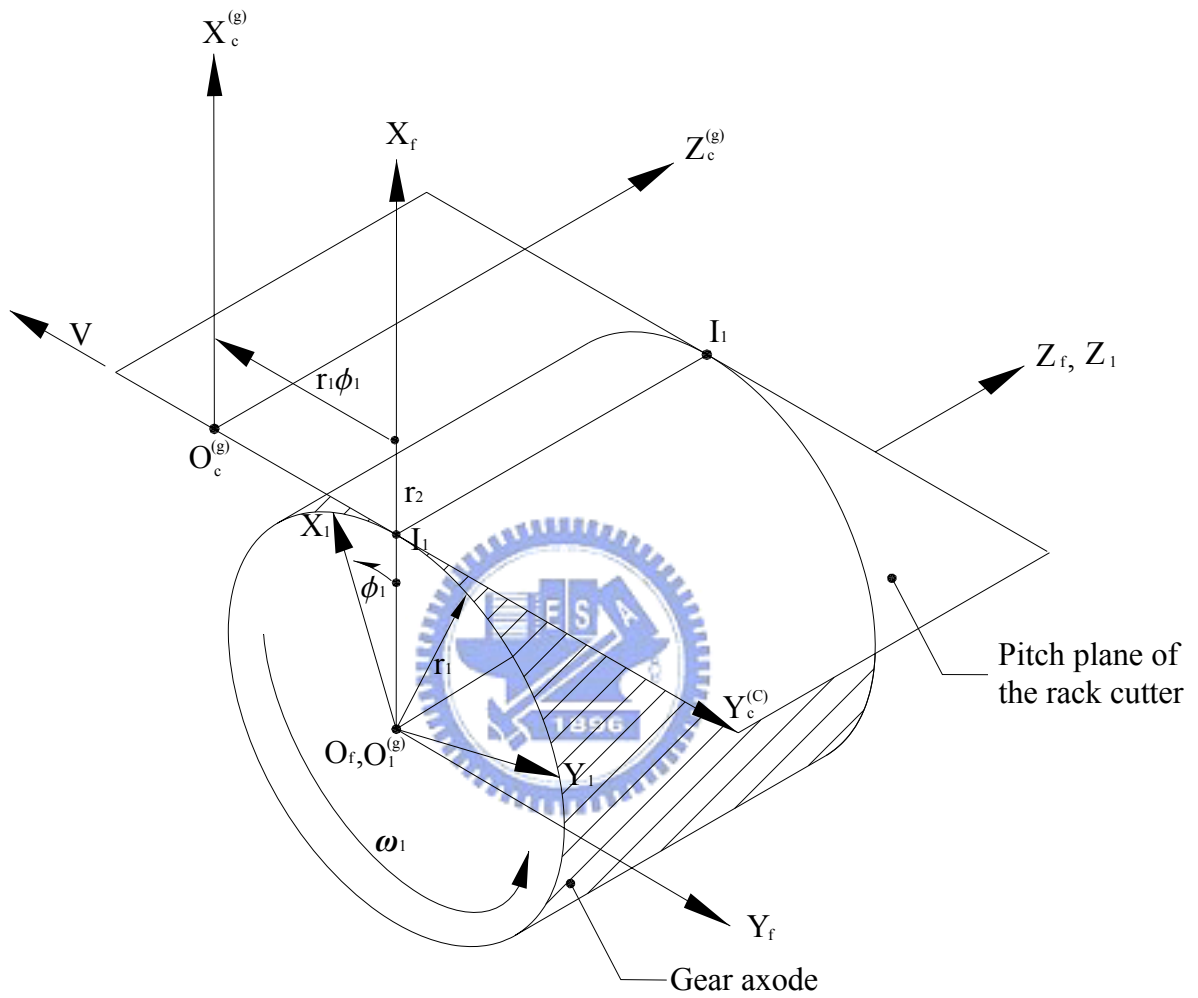
Fig. 3-9 Kinematical relationship between the imaginary rack cutter Σ_g and the gear

The velocity of the point on the rack cutter Σ_g can be expressed in the coordinate system $S_f(X_f, Y_f, Z_f)$ as follow:

$$\mathbf{V}_f^{(g)} = \omega_1 \times R_c^{(g)} + \overline{O_c^{(g)} O_f} \times \omega_1 = \begin{bmatrix} \left(y_c^{(g)} - r_1 \phi_1 \right) \omega_1 \\ -\left(x_c^{(g)} + r_1 \right) \omega_1 \\ 0 \end{bmatrix}. \tag{3.14}$$

The relative velocity of the gear with respect to the left and right side of the cutter Σ_g can be attained by subtracting Eq.(3.13) and Eq.(3.14):

$$\mathbf{V}_f^{(p1)} = \mathbf{V}_f^{(p)} - \mathbf{V}_f^{(1)} = \begin{bmatrix} \left(r_1 \phi_1 - y_c^{(p)} \right) \omega_1 \\ x_c^{(p)} \omega_1 \\ 0 \end{bmatrix}, \tag{3.15}$$

where

$$x_c^{(g)} = -R^{(g)} \left(\sin \alpha - \sin \theta^{(g)} \right), \tag{3.16}$$

$$y_c^{(g)} = R_{ab} \left(1 - \cos \gamma^{(g)} \right) \pm \cos \gamma^{(g)} \left(-\frac{S^G}{2} + R^{(g)} \left(\cos \alpha - \cos \theta^{(g)} \right) \right).$$

Similarly, the relative velocity of the pinion with respect to the left and right sides of the rack cutter Σ_p can also be attained by applying the same steps according to the kinematical relationships shown in Fig. 3-10:

$$\mathbf{V}_f^{(p2)} = \mathbf{V}_f^{(p)} - \mathbf{V}_f^{(2)} = \begin{bmatrix} \left(r_2 \phi_2 - y_c^{(p)} \right) \omega_2 \\ x_c^{(p)} \omega_2 \\ 0 \end{bmatrix}, \tag{3.17}$$

where,

$$x_c^{(p)} = -R^{(p)} \left(\sin \alpha - \sin \theta^{(p)} \right), \tag{3.18}$$

30

$$y_c^{(p)} = R_{ab} \left(1 - \cos \gamma^{(p)}\right) \pm \cos \gamma^{(p)} \left(-\frac{S^G}{2} + R^{(p)} \left(\cos \theta^{(p)} - \cos \alpha\right)\right).$$

Fig. 3-11 illustrates the geometrical relationship between the contact surfaces and tangent point. The contact points on gear surfaces Σ_1, Σ_2 are M_1 and M_2, respectively. T is the tangent plane of these two surfaces. Relative velocity $\mathbf{V}^{(12)}$ is defined in physical terms as the velocity of point M_1 of Σ_1 as seen by an observer at point M_2 of Σ_2. Theoretically, in the generation process, gear and cutter are in pure rolling or sliding on the contact surfaces. It means that these two contact surfaces never embed into each other. Thus, the relative velocity of the gear with respect to the cutter along their common normal direction is equal to zero. Then, it can be said that the relative velocity $\mathbf{V}^{(12)}$ lies on the common tangent surface and perpendicular to the unit normal vector $\mathbf{n}$ at the common tangent point. Therefore, the following equation must be observed:

$$\mathbf{n} \cdot \mathbf{V}^{(12)} = 0. \tag{3.19}$$

Eq.(3.19) is called the "meshing equation". Based on the meshing equation, parameters ϕ_1 and ϕ_2 can be expressed in the following implicit form:

and
$$\begin{aligned} f\left(\theta^{(g)}, \gamma^{(g)}, \phi_1\right) &= 0 \\ f\left(\theta^{(p)}, \gamma^{(p)}, \phi_2\right) &= 0 \end{aligned}, \tag{3.20}$$

where ϕ_1 and ϕ_2 are the rotation angle of the gear and the pinion, respectively.

The meshing equation of the rack cutter Σ_g with the gear can be obtained by solving the equation:

$$\mathbf{n}_f^{(g)} \cdot \mathbf{V}_f^{(g1)} = 0, \tag{3.21}$$
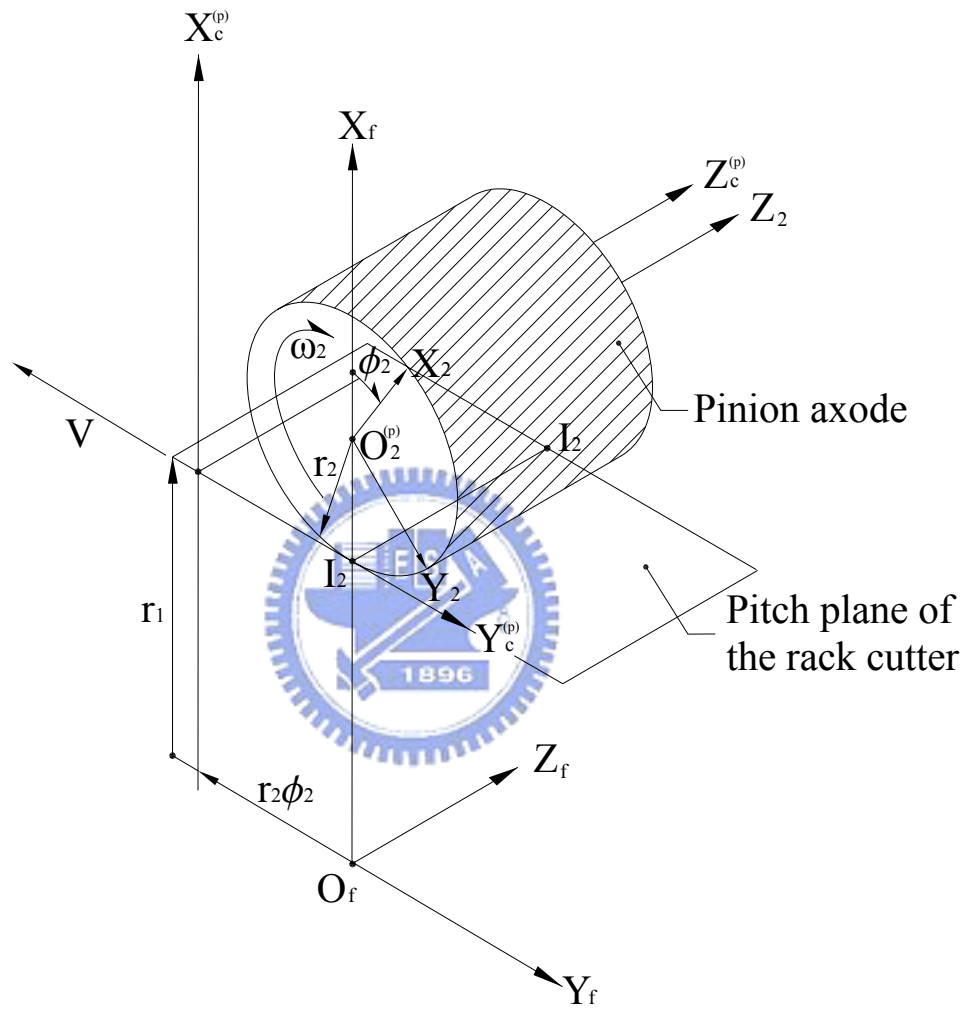
Fig. 3-10 Kinematical relationship between the imaginary rack cutter Σ_p and the pinion
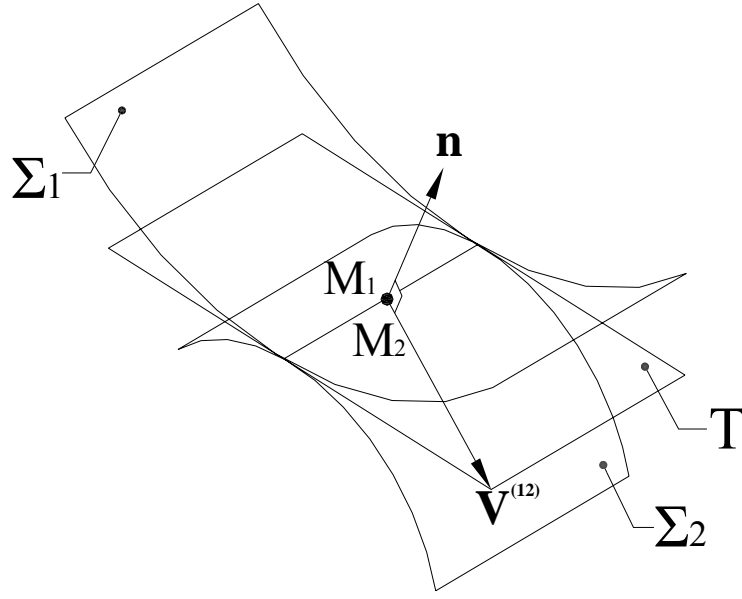
Fig. 3-11 Relationship between two tangent surfaces

substituting Eqs.(3.11) and (3.15) into Eq.(3.21) yields:

$$f\left(\gamma^{(g)},\theta^{(g)},\phi_1\right)=-\frac{R^{(g)}}{4}(\mp 2R_{ab}-S^G+2R^{(g)}\cos\alpha-2R^{(g)}\cos\theta^{(g)})$$
$$\left\{2\cos\gamma^{(g)}\left[r_1(-1+\omega_1)\cos\theta^{(g)}+R^{(g)}\omega_1\sin(\alpha-\theta^{(g)})\right]\right.$$
$$\left.+\sin\theta^{(g)}\left[\mp 2R_{ab}\omega_1\pm 2r_1\phi_1+(\pm 2R_{ab}+S^G)\omega_1\cos\gamma^{(g)}\right]\right\}=0. \qquad (3.22)$$

Similarly, the equation of meshing about the rack cutter Σ_p and the gear can be obtained by the same step:

$$f\left(\gamma^{(p)},\theta^{(p)},\phi_2\right)=-\frac{R^{(p)}}{4}(\mp 2R_{ab}-S^G+2R^{(p)}\cos\alpha-2R^{(p)}\cos\theta^{(p)})$$
$$\left\{2\cos\gamma^{(p)}\left[r_2(-1+\omega_2)\cos\theta^{(p)}+R^{(p)}\omega_2\sin(\alpha-\theta^{(p)})\right]\right.$$
$$\left.+\sin\theta^{(p)}\left[\mp 2R_{ab}\omega_2\pm 2r_2\phi_2+(\pm 2R_{ab}+S^G)\omega_2\cos\gamma^{(p)}\right]\right\}=0. \qquad (3.23)$$

According to the gear theory, the gear mathematical model can be obtained by representing the locus equation of the rack cutter on the coordinate system of the generated gear

33

and the meshing equation. The locus equation of the rack cutter represented in the gear coordinate system $S_1(X_1, Y_1, Z_1)$ can be attained by applying the following homogeneous coordinate transformation from the coordinate system $S_c^{(g)}(X_c^{(g)}, Y_c^{(g)}, Z_c^{(g)})$ to $S_1(X_1, Y_1, Z_1)$ is:

$$\mathbf{R}_1 = \mathbf{M}_{1c} \mathbf{R}_c^{(g)}, \tag{3.24}$$

and the homogeneous coordinate transformation matrix:

$$\mathbf{M}_{1c} = \begin{bmatrix} \cos\phi_1 & -\sin\phi_1 & 0 & r_1(\cos\phi_1 + \phi_1\sin\phi_1) \\ \sin\phi_1 & \cos\phi_1 & 0 & r_1(\sin\phi_1 - \phi_1\cos\phi_1) \\ 0 & 0 & 1 & 0 \\ 0 & 0 & 0 & 1 \end{bmatrix}. \tag{3.25}$$

Using the equations Eqs.(3.18), (3.24) and (3.25), the locus of the rack cutter represented in the gear coordinate system $S_1(X_1, Y_1, Z_1)$ can be obtained as:

$$\mathbf{R}_1 = \mathbf{M}_{1c} \mathbf{R}_c^{(g)} = \begin{bmatrix} \cos\phi_1 & -\sin\phi_1 & 0 & r_1(\cos\phi_1 + \phi_1\sin\phi_1) \\ \sin\phi_1 & \cos\phi_1 & 0 & r_1(\sin\phi_1 - \phi_1\cos\phi_1) \\ 0 & 0 & 1 & 0 \\ 0 & 0 & 0 & 1 \end{bmatrix} \begin{bmatrix} x_c^{(g)} \\ y_c^{(g)} \\ z_c^{(g)} \\ 1 \end{bmatrix},$$

thus

$$\mathbf{R}_1 = \begin{bmatrix} x_1 \\ y_1 \\ z_1 \\ 1 \end{bmatrix} = \begin{bmatrix} F_2\cos\phi_1 + \left[\left(-F_3 + F_1\cos\gamma^{(g)}\right)\sin\phi_1\right] \\ \left(F_3 - F_1\cos\gamma^{(g)}\right)\cos\phi_1 + F_2\sin\phi_1 \\ F_1\sin\gamma^{(g)} \\ 1 \end{bmatrix}, \tag{3.26}$$

where

$$F_1 = \left[\pm \frac{S^G}{2} \pm R^{(g)} \left(\cos \theta^{(g)} - \cos \alpha \right) + R_{ab} \right],$$

$$F_2 = \left(r_1 - R^{(g)} \sin \alpha + R^{(g)} \sin \theta^{(g)} \right),$$

and $F_3 = \left(R_{ab} - r_1 \phi_1 \right)$.

The mathematical model of the gear with curvilinear-teeth generated by a disk-type circular-arc rack cutter can be attained by solving the locus equation Eq.(3.26) with the meshing equation Eq.(3.22).

Similarly, the locus of the rack cutter surface Σ_p represented in the pinion coordinate system $S_2 \left(X_2, Y_2, Z_2 \right)$ can be obtained as follows:

$$\mathbf{R}_2 = \mathbf{M}_{2c} \mathbf{R}_c^{(p)} = \begin{bmatrix} G_2 \cos \phi_2 + \left[\left(G_3 - G_1 \cos \gamma^{(p)} \right) \sin \phi_2 \right] \\ \left(G_3 - G_1 \cos \gamma^{(p)} \right) \cos \phi_2 - G_2 \sin \phi_2 \\ G_1 \sin \gamma^{(p)} \\ 1 \end{bmatrix}, \tag{3.27}$$

where

$$G_1 = \left[\pm \frac{S^G}{2} \pm R^{(p)} \left(\cos \theta^{(p)} - \cos \alpha \right) + R_{ab} \right],$$

$$G_2 = \left(-r_2 - R^{(p)} \sin \alpha + R^{(p)} \sin \theta^{(p)} \right),$$

$$G_3 = \left(R_{ab} - r_2 \phi_2 \right).$$

and the homogeneous coordinate transformation matrix is:

$$\mathbf{M}_{2c} = \begin{bmatrix} \cos \phi_2 & \sin \phi_2 & 0 & -r_2 \left(\cos \phi_2 + \phi_2 \sin \phi_2 \right) \\ -\sin \phi_2 & \cos \phi_2 & 0 & r_2 \left(\sin \phi_2 - \phi_2 \cos \phi_2 \right) \\ 0 & 0 & 1 & 0 \\ 0 & 0 & 0 & 1 \end{bmatrix}. \tag{3.28}$$

The mathematical model of the gear with curvilinear-teeth generated by a disk-type circular-arc cutter can be attained by solving the locus equation Eq.(3.27) with the equation of meshing Eq.(3.23).

3.2.3 Computer Graphs

The equations of the circular-arc gear and pinion with curvilinear-teeth generated by a disk-type circular-arc cutter are expressed in Eqs.(3.26) and (3.27) with meshing equations Eqs.(3.22) and (3.23), respectively. Table 3-1 lists the major design parameters of a circular-arc gear pair with curvilinear-teeth generated by disk-type circular-arc cutters. Base on the developed gear mathematical models, three-dimensional tooth profiles of the gear and pinion are plotted by commercial software CATIA$^{®}$ as displayed in Fig. 3-12 and Fig. 3-13, respectively.

Table 3-1 Some major design parameters for the gear set

Design parameters	Pinion	Gear
Number of Teeth ($T^{(i)}$)	18	36
Normal Module (M)	3mm/tooth	
Normal Pressure Angle (α)	20$^{°}$	
Radius of the Disk-Type Cutter (R_{ab}) (Fig. 3-7)	30mm	
Radius of Rack Cutter Normal Section ($R^{(i)}$) (Fig. 3-6 & Fig. 3-8)	40mm	40mm
Face Width (W) (Fig. 3-7)	30mm	

In addition, Fig. 3-14 illustrates the tooth surface deviation of various radii of the circular-arc rack cutters. Fig. 3-14(a) depicts the tooth surface deviation of the normal profile at the middle section of the tooth flank ($Z = 0$ mm) with different radii of convex rack cutter Σ_p, and Fig. 3-14(b) depicts the tooth surfaces of concave rack cutter Σ_g.

3.3 Remarks

The normal section of the rack cutter is designed as a circular-arc for the generation of circular-arc gears with curvilinear-teeth gear. A new topology for tooth surfaces has been achieved by applying the imaginary circular-arc rack cutter with a curvilinear-trace generation mechanism. The mathematical model of the circular-arc gear with curvilinear-teeth generated by a disk-type circular-arc cutter has been derived based on the theory of gearing. Furthermore, a computer program applicable to the generation of the tooth profile has been developed on the basis of the derived equations. Further characteristics of the circular-arc curvilinear-tooth gear, such as TCA and contact patterns, can also be performed with the aid of the developed mathematical models.

Based on the study of this chapter, the following geometric characteristics of the circular-arc curvilinear-tooth gear can be drawn:

1. The involute gear is a special case of the circular-arc gear when the radius of the rack cutter profile $R^{(g)}$ tends to infinity.

2. The spur gear and helical gear is a special case of the curvilinear-tooth gear when the radius of the disk-type rack cutter (i.e. the R_{ab} in Fig. 3-1 and Fig. 3-7) tends to infinity, the curvilinear-tooth gear becomes a spur gear.
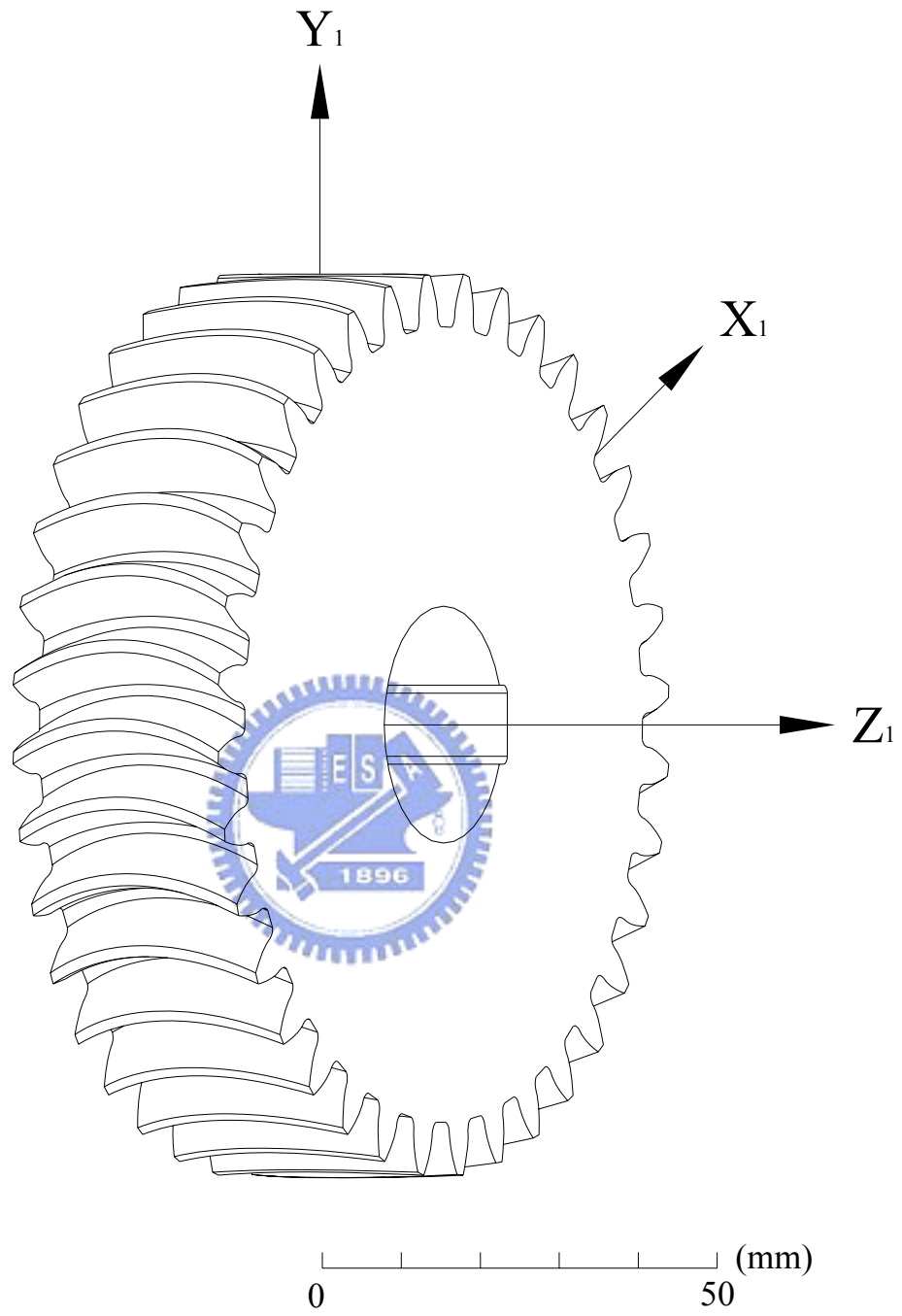
Fig. 3-12 Computer graph of the circular-arc gear with curvilinear-teeth
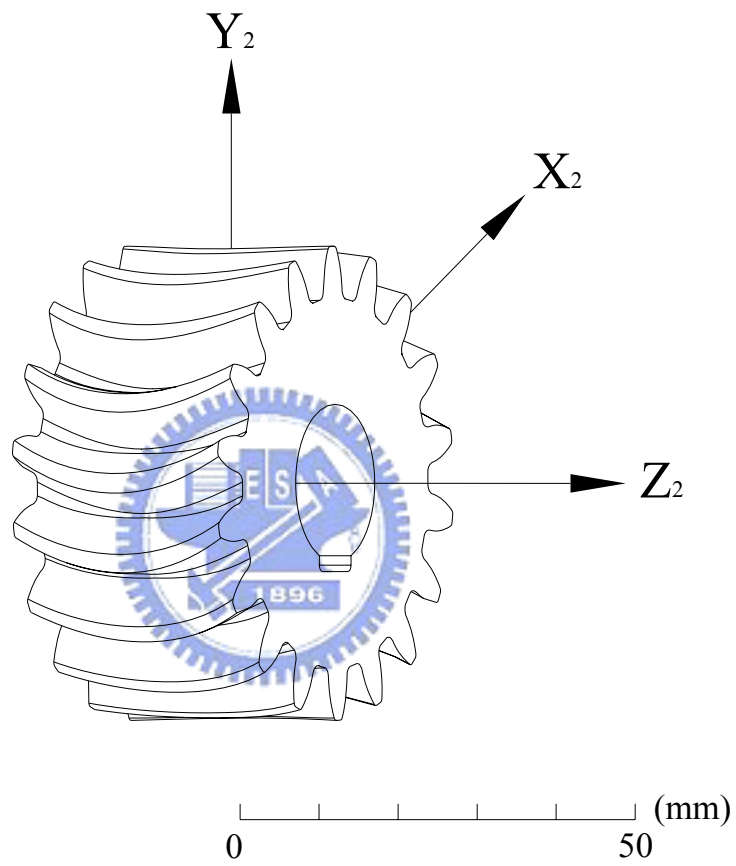
Fig. 3-13 Computer graph of the circular-arc pinion with curvilinear-teeth
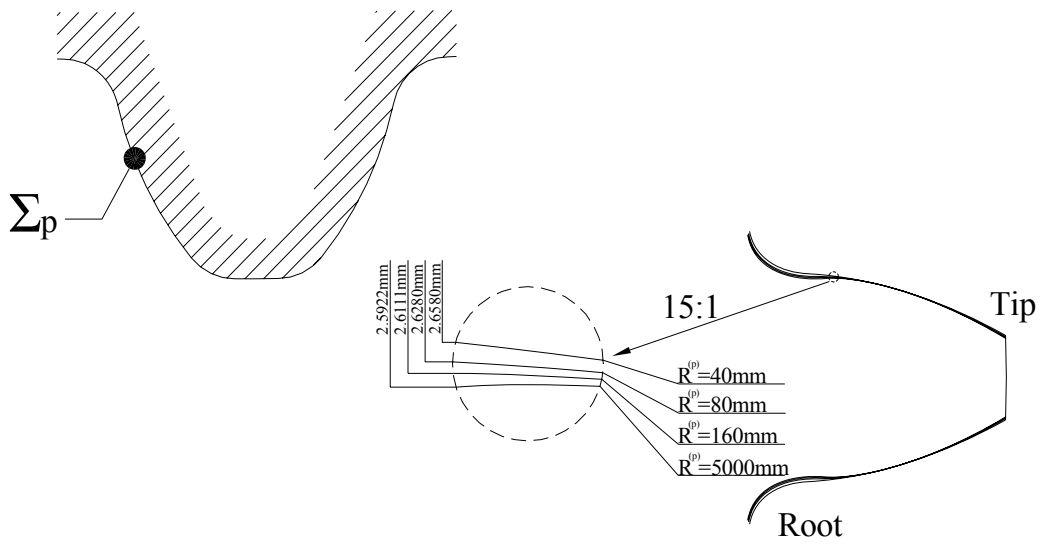
(a) Rack cutter Σ_p for gear generation
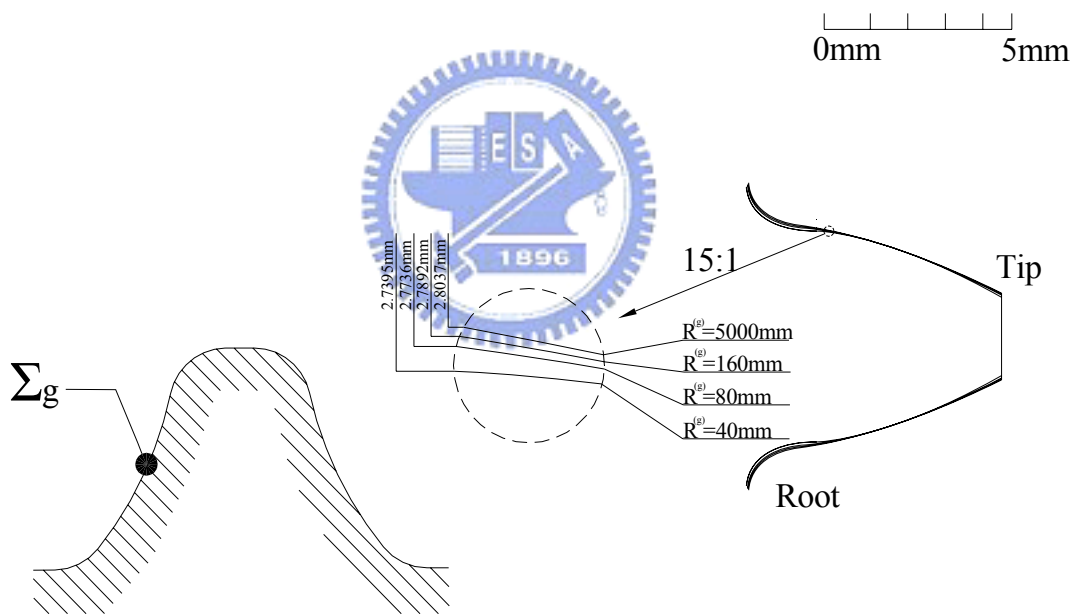
(b) Rack cutter Σ_g for gear generation

Fig. 3-14 Tooth surface profiles with different radii of circular-arc rack cutters

3. The curvilinear-tooth gear has no axial thrust force during operation similar to the herringbone gear because of its symmetrical geometric characteristic.

4. The transverse gear chordal thickness measured at the middle section is larger than those of other sections as shown in Fig. 3-15.
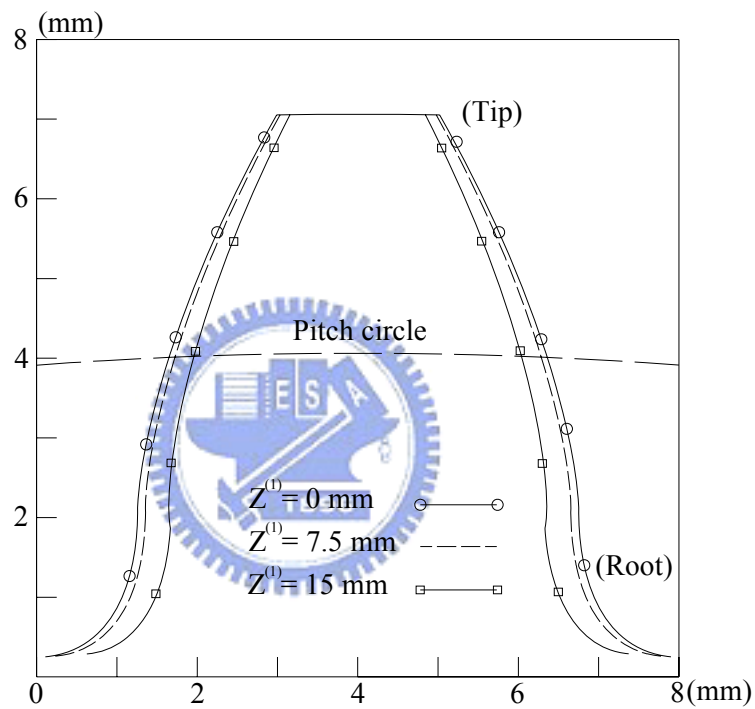
Fig. 3-15 Normal profiles at different cross sections of the gear

CHAPTER 4

Tooth Undercutting Analysis

4.1 Introduction

Tooth undercutting is an important issue for gear manufacture and design. When tooth undercutting occurs, the gear thickness near the tooth fillet will be decreased. The load capacity and the length action line are consequently reduced. Undercutting also induced noise and vibration. Besides, the contact ratio also decreases with undercutting.

Actually, tooth undercutting is the singular points appeared on the tooth surface. Thus, the problem of tooth non-undercutting is the existence of singular points on the generated gear tooth surface. However, gear with a bit of tooth undercutting sometimes can be a benefit for solving the gear interference problem and storing of lubricating oil.

In this chapter, the tooth undercutting conditions among the cutting parameters and gear design parameters on the generated tooth profiles are investigated based on the theory of gearing proposed by Litvin [10][20].

4.2 Conditions of Tooth Undercutting

The concept for checking the undercutting of a gear tooth surface is to check the appearance of singular points on the generated gear tooth surfaces. Singularities of the generated surface Σ_1 occurs when the relative velocity of the contact point over the generated surface equals to zero. The gear surface of the circular-arc curvilinear-tooth gear is generated by the imaginary rack cutter Σ_g. The position vectors of Σ_1 and Σ_g at the instantaneous contact points should equal to each other if they are expressed in the same

coordinate system in the process of generation. Therefore, if the rack cutter surface Σ_g and

the generated gear surface Σ_1 are expressed in the fixing coordinate system $S_f(X_f, Y_f, Z_f)$

shown in Fig. 3-9, the relationship will be found:

$$\mathbf{R}_f^{(g)} = \mathbf{R}_f^{(1)}. \tag{4.1}$$

By differentiating Eq.(4.1) with respect to time, it results in:

$$\mathbf{V}_{tr}^{(g)} + \mathbf{V}_r^{(g)} = \mathbf{V}_{tr}^{(1)} + \mathbf{V}_r^{(1)}. \tag{4.2}$$

After transposition, the $\mathbf{V}_r^{(1)}$ can be expressed as:

$$\mathbf{V}_r^{(1)} = \mathbf{V}_{tr}^{(g)} + \mathbf{V}_r^{(g)} - \mathbf{V}_{tr}^{(1)} = \mathbf{V}_r^{(g)} + \mathbf{V}_{tr}^{(g1)}, \tag{4.3}$$

where $\mathbf{V}_{tr}^{(g)}$ and $\mathbf{V}_{tr}^{(1)}$ are the transfer velocities move of the cutter and blank at the contact

point, respectively, and $\mathbf{V}_r^{(g)}$ and $\mathbf{V}_r^{(1)}$ represent the relative velocity of the cutter surface

and tooth surface at the contact point, respectively.

A singular point is occurred when the derivatives of $\mathbf{V}_r^{(1)}$ becomes to zero. Therefore,

the necessary conditions of tooth undercutting which allows the determination of the limit on

the rack cutter surface Σ_g can be expressed by:

$$\mathbf{V}_r^{(g)} + \mathbf{V}_{tr}^{(g1)} = 0, \tag{4.4}$$

and the differential meshing equation:

$$\frac{d}{dt} f\left(\gamma^{(g)}, \theta^{(g)}, \phi_1\right) = 0. \tag{4.5}$$

Tooth undercutting curve can be found by solving Eqs.(4.4) and (4.5). This undercutting curve is expressed on the rack cutter surface. To avoid tooth undercutting of the generated gear tooth surfaces, the generating rack cutter surface must be limited with the constraints.
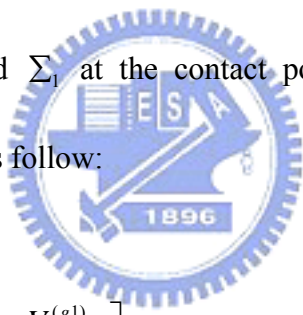
Now, Eqs.(4.4) and (4.5) yield that:

$$\frac{\partial \mathbf{R}_c^{(g)}}{\partial \theta^{(g)}} \frac{d\theta^{(g)}}{dt} + \frac{\partial \mathbf{R}_c^{(g)}}{\partial \gamma^{(g)}} \frac{d\gamma^{(g)}}{dt} = -\mathbf{V}_c^{F1}, \tag{4.6}$$

$$\frac{\partial f}{\partial \theta^{(g)}} \frac{d\theta^{(g)}}{dt} + \frac{\partial f}{\partial \gamma^{(g)}} \frac{d\gamma^{(g)}}{dt} = -\frac{\partial f}{\partial \phi_1} \frac{d\phi_1}{dt}. \tag{4.7}$$

In Eqs.(4.6) and (4.7), $\mathbf{R}_c^{(g)}$ represents the equation of rack cutter surface Σ_g expressed in coordinate system $S_c^{(g)}\left(X_c^{(g)}, Y_c^{(g)}, Z_c^{(g)}\right)$, and $\mathbf{V}_c^{F1}$ means the relative velocity between two surfaces Σ_g and Σ_1 at the contact point. Eqs.(4.6) and (4.7) can be also expressed by the matrix form as follow:
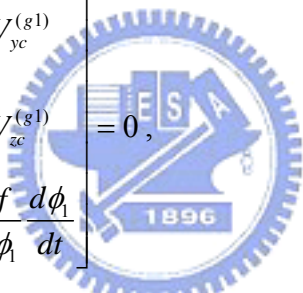
$$\begin{bmatrix} \dfrac{\partial x_c^{(g)}}{\partial \theta^{(g)}} & \dfrac{\partial x_c^{(g)}}{\partial \gamma^{(g)}} \\[2mm] \dfrac{\partial y_c^{(g)}}{\partial \theta^{(g)}} & \dfrac{\partial y_c^{(g)}}{\partial \gamma^{(g)}} \\[2mm] \dfrac{\partial z_c^{(g)}}{\partial \theta^{(g)}} & \dfrac{\partial z_c^{(g)}}{\partial \gamma^{(g)}} \\[2mm] \dfrac{\partial f}{\partial \theta^{(g)}} & \dfrac{\partial f}{\partial \gamma^{(g)}} \end{bmatrix} \begin{bmatrix} \dfrac{d\theta^{(g)}}{dt} \\[2mm] \dfrac{d\gamma^{(g)}}{dt} \end{bmatrix} = \begin{bmatrix} -V_{xc}^{(g1)} \\[2mm] -V_{yc}^{(g1)} \\[2mm] -V_{zc}^{(g1)} \\[2mm] -\dfrac{\partial f}{\partial \phi_1}\dfrac{d\phi_1}{dt} \end{bmatrix}. \tag{4.8}$$

Based on the theory of Linear Algebra, the sufficient conditions for Eq.(4.8) existing, the only solution is the rank of the augmented matrix of Eq.(4.8) is two. It means the following four equations must be conformed in the meantime:

$$\Delta_1 = \begin{vmatrix} \dfrac{\partial x_c^{(g)}}{\partial \theta^{(g)}} & \dfrac{\partial x_c^{(g)}}{\partial \gamma^{(g)}} & -V_{xc}^{(g1)} \\[3mm] \dfrac{\partial y_c^{(g)}}{\partial \theta^{(g)}} & \dfrac{\partial y_c^{(g)}}{\partial \gamma^{(g)}} & -V_{yc}^{(g1)} \\[3mm] f_{\theta^{(g)}} & f_{\gamma^{(g)}} & -\dfrac{\partial f}{\partial \phi_1}\dfrac{d\phi_1}{dt} \end{vmatrix} = 0 \,, \tag{4.9}$$

$$\Delta_2 = \begin{vmatrix} \dfrac{\partial x_c^{(g)}}{\partial \theta^{(g)}} & \dfrac{\partial x_c^{(g)}}{\partial \gamma^{(g)}} & -V_{xc}^{(g1)} \\[3mm] \dfrac{\partial z_c^{(g)}}{\partial \theta^{(g)}} & \dfrac{\partial z_c^{(g)}}{\partial \gamma^{(g)}} & -V_{zc}^{(g1)} \\[3mm] f_{\theta^{(g)}} & f_{\gamma^{(g)}} & -\dfrac{\partial f}{\partial \phi_1}\dfrac{d\phi_1}{dt} \end{vmatrix} = 0 \,, \tag{4.10}$$

$$\Delta_3 = \begin{vmatrix} \dfrac{\partial y_c^{(g)}}{\partial \theta^{(g)}} & \dfrac{\partial y_c^{(g)}}{\partial \gamma^{(g)}} & -V_{yc}^{(g1)} \\[3mm] \dfrac{\partial z_c^{(g)}}{\partial \theta^{(g)}} & \dfrac{\partial z_c^{(g)}}{\partial \gamma^{(g)}} & -V_{zc}^{(g1)} \\[3mm] f_{\theta^{(g)}} & f_{\gamma^{(g)}} & -\dfrac{\partial f}{\partial \phi_1}\dfrac{d\phi_1}{dt} \end{vmatrix} = 0 \,, \tag{4.11}$$

$$\Delta_4 = \begin{vmatrix} \dfrac{\partial x_c^{(g)}}{\partial \theta^{(g)}} & \dfrac{\partial x_c^{(g)}}{\partial \gamma^{(g)}} & -V_{xc}^{(g1)} \\[3mm] \dfrac{\partial y_c^{(g)}}{\partial \theta^{(g)}} & \dfrac{\partial y_c^{(g)}}{\partial \gamma^{(g)}} & -V_{yc}^{(g1)} \\[3mm] \dfrac{\partial z_c^{(g)}}{\partial \theta^{(g)}} & \dfrac{\partial z_c^{(g)}}{\partial \gamma^{(g)}} & -V_{zc}^{(g1)} \end{vmatrix} = 0 \,. \tag{4.12}$$

Eq.(4.12) is the meshing equation of gear C exactly. Eq.(4.9) to (4.12) are the conditions of tooth undercutting, and they can also be expressed as:

$$F\left(\theta^{(g)}, \gamma^{(g)}, \phi_1\right) = \Delta_1^2 + \Delta_2^2 + \Delta_3^2 = 0 \,, \tag{4.13}$$

and $f\left(\gamma^{(g)}, \theta^{(g)}, \phi_1\right) = 0$. \hfill (4.14)

With a similar process, tooth undercutting conditions of the circular-arc curvilinear-tooth pinion can be obtained as follows:

$$F\left(\theta^{(p)}, \gamma^{(p)}, \phi_2\right) = \Delta_1^2 + \Delta_2^2 + \Delta_3^2 = 0, \tag{4.15}$$

$$f\left(\gamma^{(p)}, \theta^{(p)}, \phi_2\right) = 0, \tag{4.16}$$

$$\text{and } \Delta_1 = \begin{vmatrix} \dfrac{\partial x_c^{(p)}}{\partial \theta^{(p)}} & \dfrac{\partial x_c^{(p)}}{\partial \gamma^{(p)}} & -V_{xc}^{(p2)} \\[3mm] \dfrac{\partial y_c^{(p)}}{\partial \theta^{(p)}} & \dfrac{\partial y_c^{(p)}}{\partial \gamma^{(p)}} & -V_{yc}^{(p2)} \\[3mm] f_{\theta^{(p)}} & f_{\gamma^{(p)}} & -\dfrac{\partial f}{\partial \phi_2}\dfrac{d\phi_2}{dt} \end{vmatrix} = 0, \tag{4.17}$$

$$\Delta_2 = \begin{vmatrix} \dfrac{\partial x_c^{(p)}}{\partial \theta^{(p)}} & \dfrac{\partial x_c^{(p)}}{\partial \gamma^{(p)}} & -V_{xc}^{(p2)} \\[3mm] \dfrac{\partial z_c^{(p)}}{\partial \theta^{(p)}} & \dfrac{\partial z_c^{(p)}}{\partial \gamma^{(p)}} & -V_{zc}^{(p2)} \\[3mm] f_{\theta^{(p)}} & f_{\gamma^{(p)}} & -\dfrac{\partial f}{\partial \phi_2}\dfrac{d\phi_2}{dt} \end{vmatrix} = 0, \tag{4.18}$$

$$\Delta_3 = \begin{vmatrix} \dfrac{\partial y_c^{(p)}}{\partial \theta^{(p)}} & \dfrac{\partial y_c^{(p)}}{\partial \gamma^{(p)}} & -V_{yc}^{(p2)} \\[3mm] \dfrac{\partial z_c^{(p)}}{\partial \theta^{(p)}} & \dfrac{\partial z_c^{(p)}}{\partial \gamma^{(p)}} & -V_{zc}^{(p2)} \\[3mm] f_{\theta^{(p)}} & f_{\gamma^{(p)}} & -\dfrac{\partial f}{\partial \phi_2}\dfrac{d\phi_2}{dt} \end{vmatrix} = 0, \tag{4.19}$$

$$\Delta_4 = \begin{vmatrix} \dfrac{\partial x_c^{(p)}}{\partial \theta^{(p)}} & \dfrac{\partial x_c^{(p)}}{\partial \gamma^{(p)}} & -V_{xc}^{(p2)} \\[3mm] \dfrac{\partial y_c^{(p)}}{\partial \theta^{(p)}} & \dfrac{\partial y_c^{(p)}}{\partial \gamma^{(p)}} & -V_{yc}^{(p2)} \\[3mm] \dfrac{\partial z_c^{(p)}}{\partial \theta^{(p)}} & \dfrac{\partial z_c^{(p)}}{\partial \gamma^{(p)}} & -V_{zc}^{(p2)} \end{vmatrix} = 0. \tag{4.20}$$

Tooth undercutting means the singular points locates in the range of $\theta^{(g)}_{min}$ to $\theta^{(g)}_{max}$, where $\theta^{(g)}_{min}$ and $\theta^{(g)}_{max}$ are relative to the design parameters of tools A, B and they are defined in Fig. 3-6. However, the range of parameter $\theta^{(g)}$ is not identical with every case. It depends on the radius $R^{(g)}$ of the circular-arc curve of the rack cutter. For example, if $R^{(g)} = 30\,\text{mm}$, then $\theta^{(g)}$ varies from $14.01°$ to $26.23°$, but if $R^{(g)} = 200\,\text{mm}$, $\theta^{(g)}$ varies from $20.92°$ to $21.22°$. Thus, a new parameter $l^{(g)}_c$ is defined as: $l^{(g)}_c = \dfrac{x_r(\theta^{(g)}_{uc}) - x_r(\theta^{(g)}_{min})}{\cos \alpha}$ and $\theta^{(g)}_{uc}$ is the angle of $\theta^{(g)}$ illustrated in Fig. 4-1. The $\theta^{(g)}_{uc}$ indicates the position where singular point is appeared. The working range of the rack cutter is $0 \le l^{(g)}_c \le \dfrac{A+B}{\cos \alpha}$, parameter $l^{(g)}_c = 0.0\,\text{mm}$ means the starting point of the generating line. If the singular point occurs in the working range of the rack cutter, it indicates that the gear tooth is undercut. Similarly, parameter $l^{(p)}_c$ can be defined by the same process.

Fig. 4-1 Schema of normal cross section of the circular-arc rack cutter Σ_g

4.3 Numerical Examples for Tooth Undercutting of Circular-Arc Curvilinear-Tooth Gears

Some examples are given to find the relationships between the design parameters of the gears and the conditions of undercutting.

Example 4-1

A numerical example here is given to find a set of singular points on the tooth surface of circular-arc curvilinear-tooth gear. The main design parameter is given as listed in Table 4-1.

Based on the undercutting conditions discussed in last section 4.2, the singular points of the gear can be obtained and shown in Table 4-2. Positions of undercutting points are illustrated in Table 4-2. Symbol $l_{cL}^{(g)}$ represents the parameter of the surface coordinate of the convex tooth surface, while $l_{cR}^{(g)}$ means the surface coordinate of the concave tooth surface. It is found that the distributions of undercutting points are symmetrical with the surface $Z_1 = 0$ mm because of its symmetrical shape, and the undercutting is most easily occurred on cross section $Z_1 = 0$ mm. The locations of the singular points on these two surfaces are not the same since the two surfaces are different. The undercutting is first occurred on the middle region of the tooth flank. Table 4-2 indicates that the convex tooth (right side tooth surface) surfaces are easier to undercut. However, the locations of singular points of these two surfaces are almost the same near the middle section of the tooth flank. The undercutting line of the gear is also shown in Fig. 4-2.

Table 4-1 Some major design parameters of the generated gear

Design Parameters	Gear
Number of Teeth ($T^{(i)}$)	36
Normal Module(M)	3mm/tooth
Normal Pressure Angle (α)	20°
Radius of the Disk-Type Cutter R_{ab} (Fig. 3-7)	30mm
Radius of Rack Cutter Normal Section ($R^{(i)}$) (Fig. 3-6)	50mm
Face Width (W) (Fig. 3-7)	30mm
Tool Settings of Rack Cutter (Fig. 3-6)	$A = 1.25M, \quad B = 1.25M$

Table 4-2 Location of singular points on tooth surface Σ_1

Cross section (Z_1) mm	$l_{cL}^{(g)}$ mm	$l_{cR}^{(g)}$
-15.0	-0.209	-0.001
-12.0	0.067	0.184
-9.0	0.254	0.314
-6.0	0.375	0.400
-3.0	0.444	0.450
0.0	0.466	0.466
3.0	0.444	0.263
6.0	0.375	0.226
9.0	0.254	0.162
12.0	0.067	0.067
15.0	-0.209	-0.066
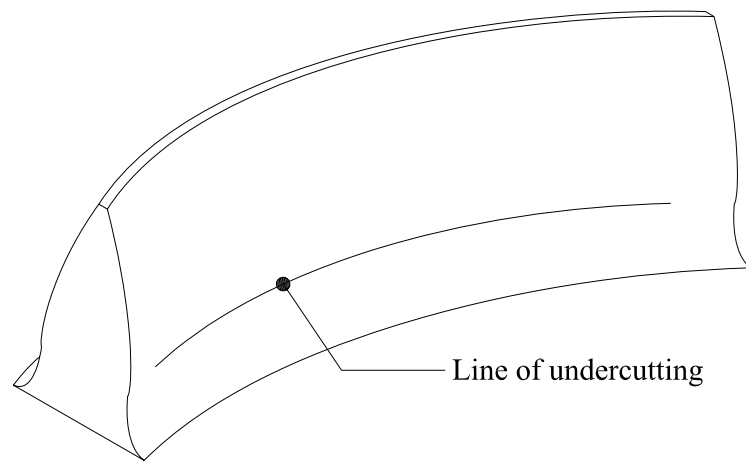
Fig. 4-2 Position of the undercutting line

Example 4-2

In this example, the study focuses on the undercutting with design parameters of pressure angle α and the radius R_{ab} of the disk-type cutter.
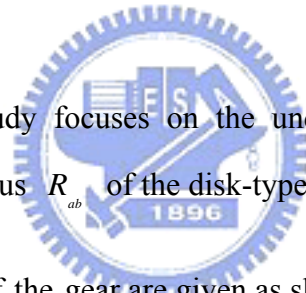
The design parameters of the gear are given as shown in Table 4-3 and the undercutting points are shown in Fig. 4-3. The undercutting condition is simply cared about the $l_{cR}^{(g)}$ since the convex tooth surfaces are easier to undercut. With the increase of the pressure angle value, tooth undercutting is avoided efficiently. However, the tooth undercutting is first occurs on the middle region of the tooth flank no matter what the value of pressure angle is. Fig. 4-4 shows the location of singular points on different tooth cross sections of the convex tooth surface when the curvilinear-tooth gear is generated by radii $R_{ab} = 20$mm, 30mm, 40mm and 5000mm, respectively. When $R_{ab} = 20$mm, the tooth undercutting appears at cross section $|Z_1| \leq 10.04$ mm.

Table 4-3 Some major design parameters of gear

Design Parameters	Gear
Number of Teeth ($T^{(i)}$)	36
Normal Module (M)	3mm/tooth
Radius of Rack Cutter Normal Section ($R^{(i)}$) (Fig. 3-6)	50mm
Face Width (W) (Fig. 3-7)	30mm
Tool Settings of Rack Cutter (Fig. 3-6)	$A = 1.25M,\ \ B = 1.25M$
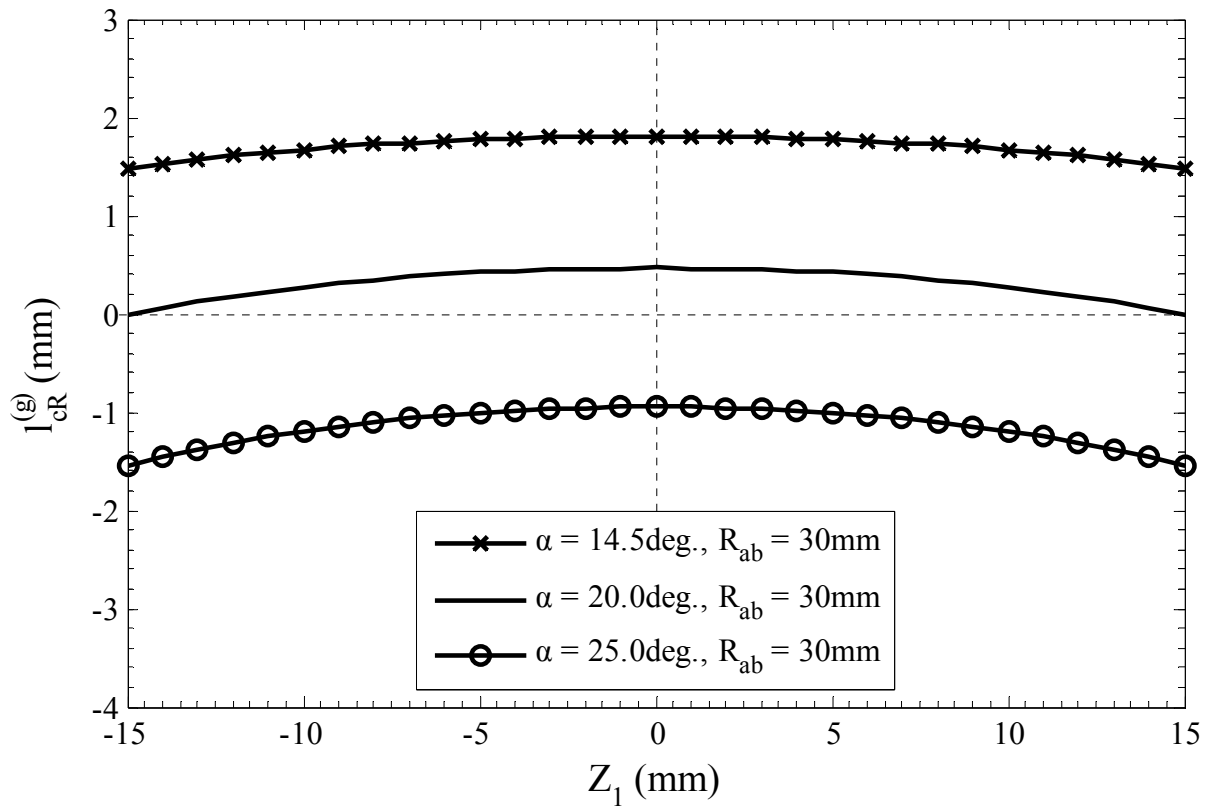
Fig. 4-3 Locations of undercutting points with different α

Fig. 4-4 Locations of undercutting points with different R_{ab}
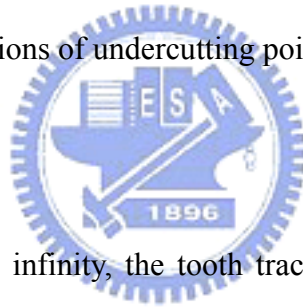
When R_{ab} approaches to infinity, the tooth trace of the gear becomes a straight line. Therefore, locations of the undercutting point on every cross section tend to the same as R_{ab} approaches to infinity. The phenomenon verifies the mathematical model by setting $R_{ab} = 5000\text{mm}$.

Example 4-3

The undercutting condition is also related to the teeth number of the gear. The design parameters are listed in Table 4-4 with different number of teeth Fig. 4-5 shows the locations of tooth undercutting points. It is found that gears with fewer teeth are easier to undercut.

Table 4-4 Some major design parameters of the gear with different number of teeth

| Design Parameters	Gear C
Normal Module (M)	3mm/tooth
Normal Pressure Angle (α)	$20°$
Radius of the Disk-Type Cutter (R_{ab}) (Fig. 3-7)	30mm
Radius of Rack Cutter Normal Section ($R^{(i)}$) (Fig. 3-6)	40mm
Face Width (W) (Fig. 3-7)	30mm
Tool Settings of Rack Cutter (Fig. 3-6)	$A = 1M, \quad B = 1M$
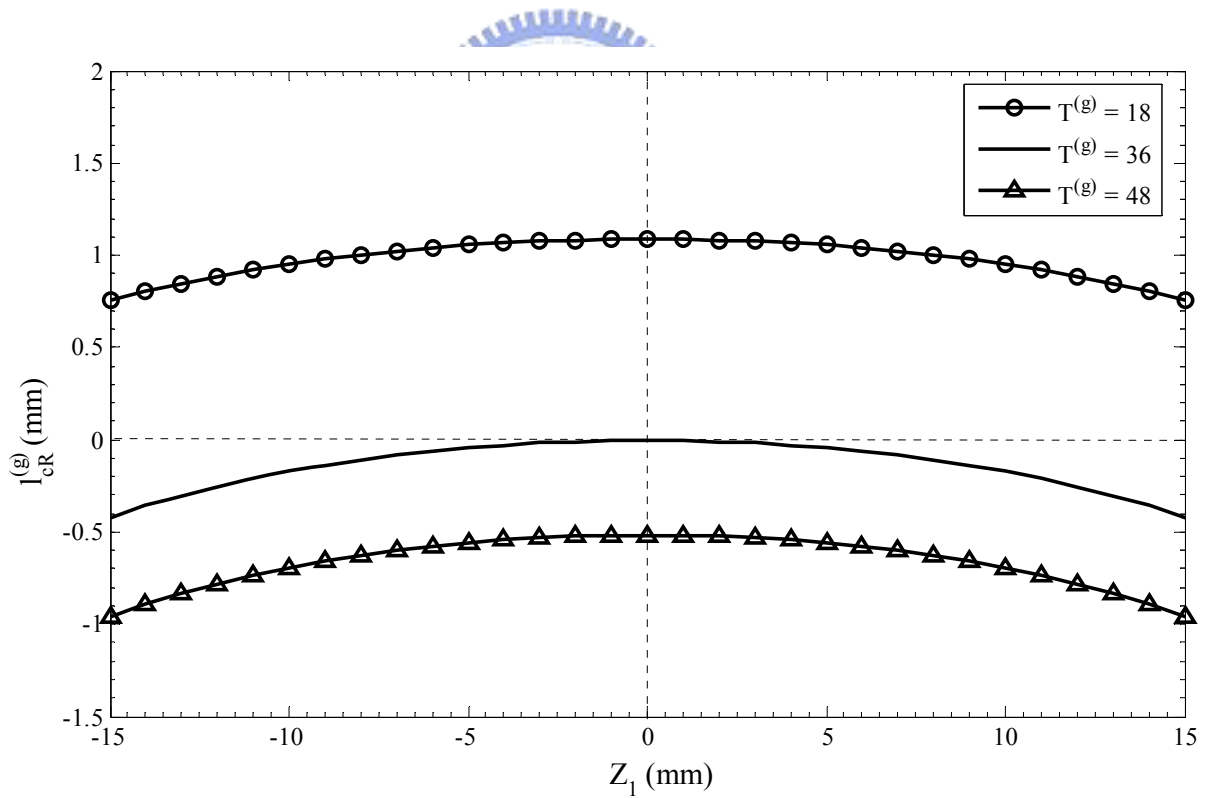
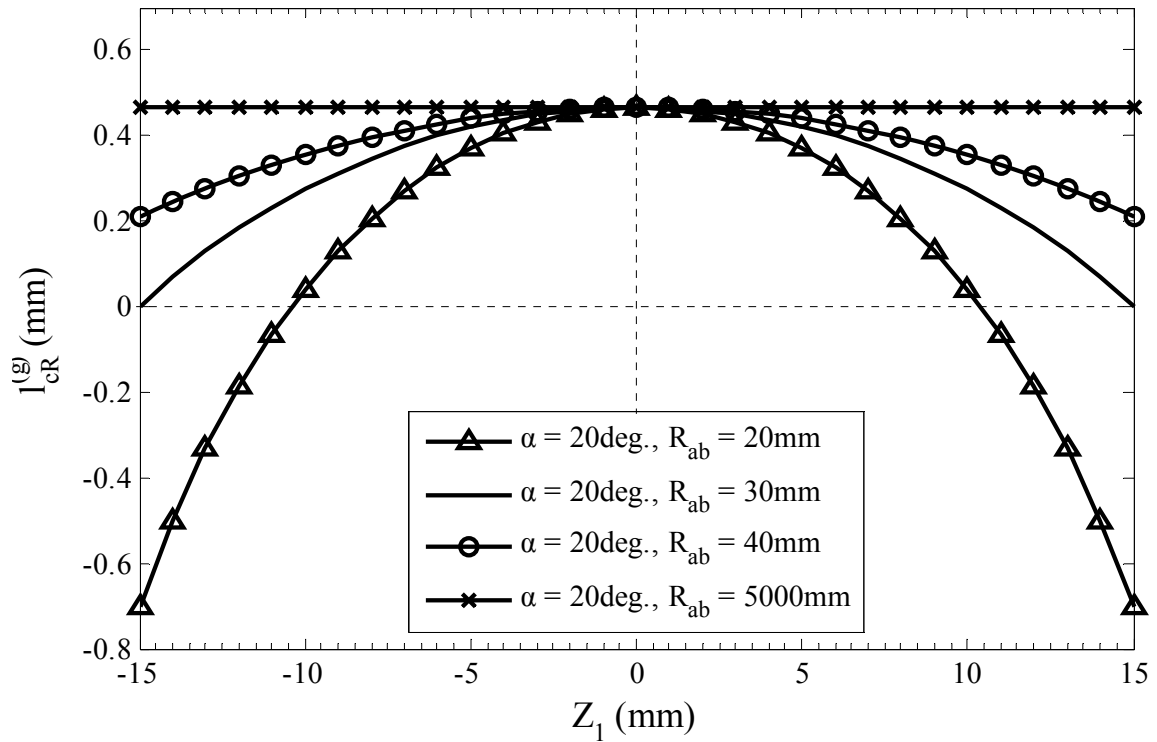Fig. 4-5 Locations of undercutting points with different number of teeth

Recall that the profile of cutters Σ_g and Σ_p are different, as shown in Fig. 2-6. Pressure angle of the circular-arc profile cutter is varying from the gear tip to gear root as shown in Fig. 4-6, where α_{ptip} is defined as the instance pressure angle on the tip of Σ_p and α_{gtip} indicates the instance pressure angle on the tip of Σ_g. Example 4-1 showed that the undercutting first appears on the gear root which is generated by the tip of the cutter. Example 4-2 proved that undercutting is avoided efficiently with the increase of the pressure angle value. As shown in Fig. 4-6, α_{ptip} is greater than α_{gtip} and pressure angle α due to the circular-arc profile cutters. Therefore, cutter Σ_g is easier to undercut.
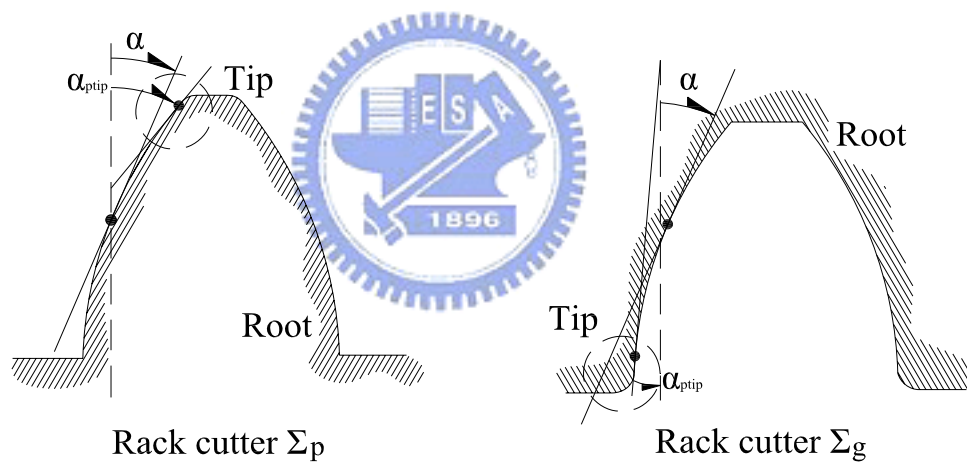
Fig. 4-6 Pressure angles of rack cutters Σ_g and Σ_p

Gears with fewer teeth are easier to undercut. Consequently, the minimum teeth number can be found to prevent tooth undercutting. Tooth undercutting is first occurs on the middle region of the tooth flank. Thus, if tooth undercutting is not occurred on the middle section ($Z_1 = 0\,\text{mm}$) of the curvilinear gear, then there is no singular point on the tooth surface

anymore. The minimum teeth number of circular-arc curvilinear tooth gear can be obtained by following the flowchart shown in Fig. 4-7.

Fig. 4-8 shows the minimum number of gear teeth to avoid tooth undercutting. It denotes a smaller pressure angle value and a smaller radius value of the circular-arc profile of the rack cutter, a higher number of teeth are acceptable for non-undercutting.

Example 4-4

Tooth undercutting decreases the strength of the gear root seriously. The circular-arc curvilinear-tooth gear is easy to occur tooth undercutting on the middle cross section when the circular-arc profile cutter has a smaller radius or a smaller pressure angle. Besides, cutter-shifting is a method to prevent tooth undercutting.

As shown in Fig. 4-9, the basic line of the rack cutter (axis $Y_c^{(g)}$) is tangent to the pitch circle of the gear blank at point I. Shifted cutting means to remove a distance of xM from the rotated center of the gear blank, where x means the shifting coefficient, and M is the normal module of the gear. Gears generated by the cutter with shifting can reduce the tooth undercutting efficiently. Axis $Y_c^{(g)}$ and $Y_a^{(g)}$ overlap when cutting the standard circular-arc curvilinear-tooth gear. The equations of the cutter surface and tooth surface can be obtained by the same process in section 3.2 only with consideration of the shifting coefficient xM.

The sufficient conditions of the singular point appears on the tooth surface Σ_1 are shown in Eqs.(4.13) and (4.14). With the consideration of the shifting coefficient x, there are four unknowns in the Eqs.(4.13) and (4.14): x, $\theta^{(g)}$, $\gamma^{(g)}$ and ϕ_1, and there are only two equations. Obviously, in order to solve these non-linear equations, two unknowns must be set
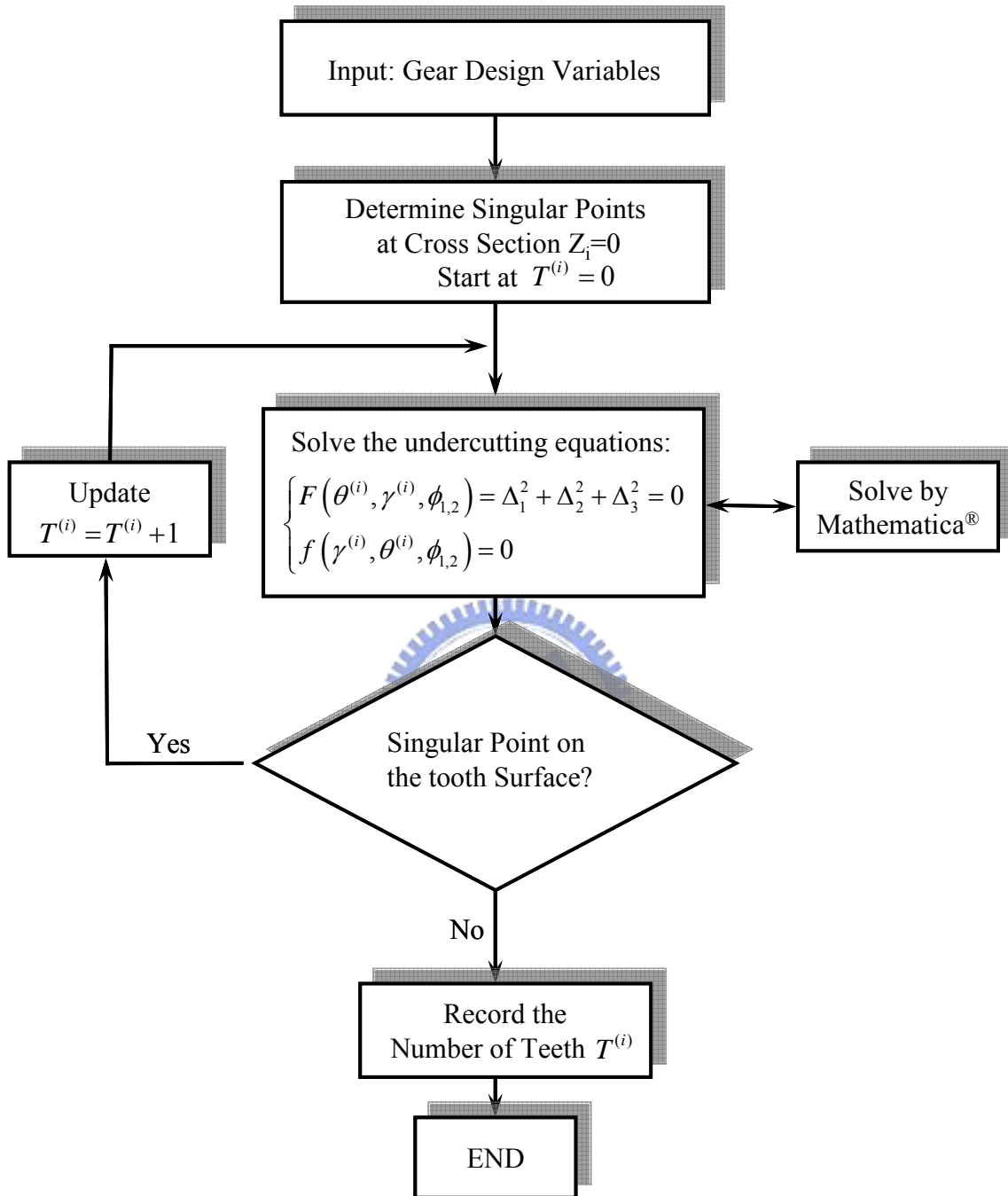
Fig. 4-7 Flowchart for determination of the minimum teeth number
without tooth undercutting
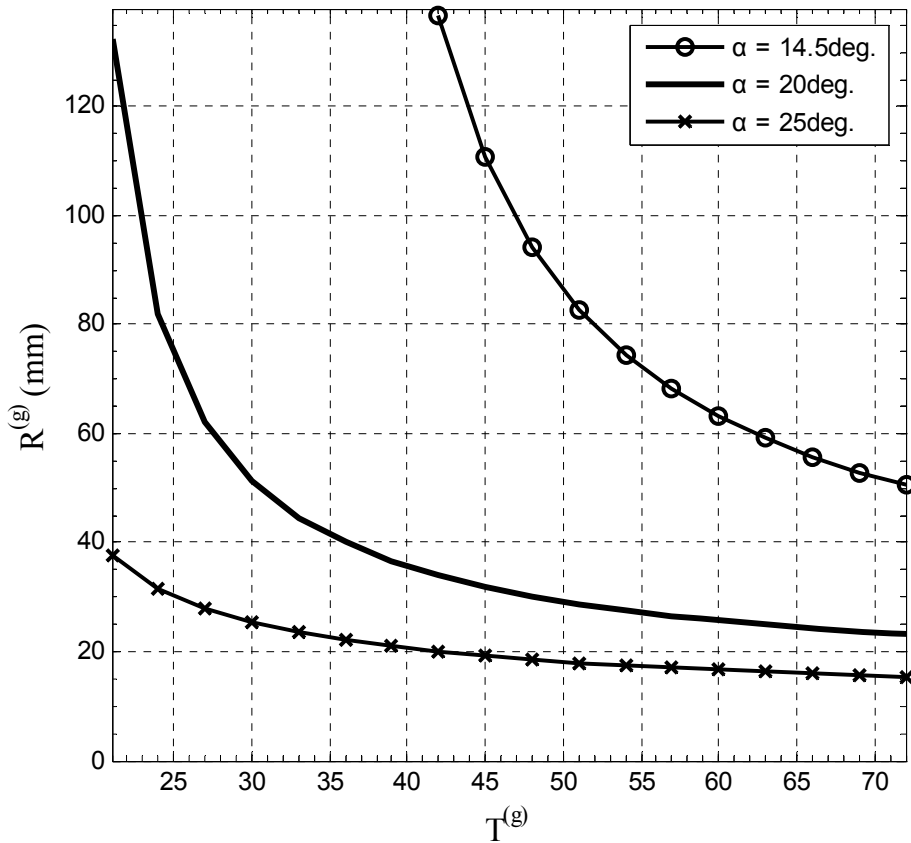
Fig. 4-8 The minimum teeth number for non-undercutting

as given values. Based on the analysis results in previous section, the tooth undercutting is first occurs on the middle cross section of $Z_1 = 0$ mm. It means if the tooth undercutting can be avoided for the middle section, then there is no singular point on the tooth surface anymore.

Based on the tooth undercutting analysis model with the shifting coefficient, the tooth undercutting conditions can be obtained by the following flowchart as shown in Fig. 4-10. Fig. 4-11 shows the minimum shifting coefficient x versus number of gear teeth to avoid undercutting under different radii and pressure angles of the circular-arc profile rack cutter. A higher shifting coefficient can be used to prevent the undercutting with a smaller value of $R^{(g)}$ and α. The proper shifting coefficient can be easily chosen by using Fig. 4-11.
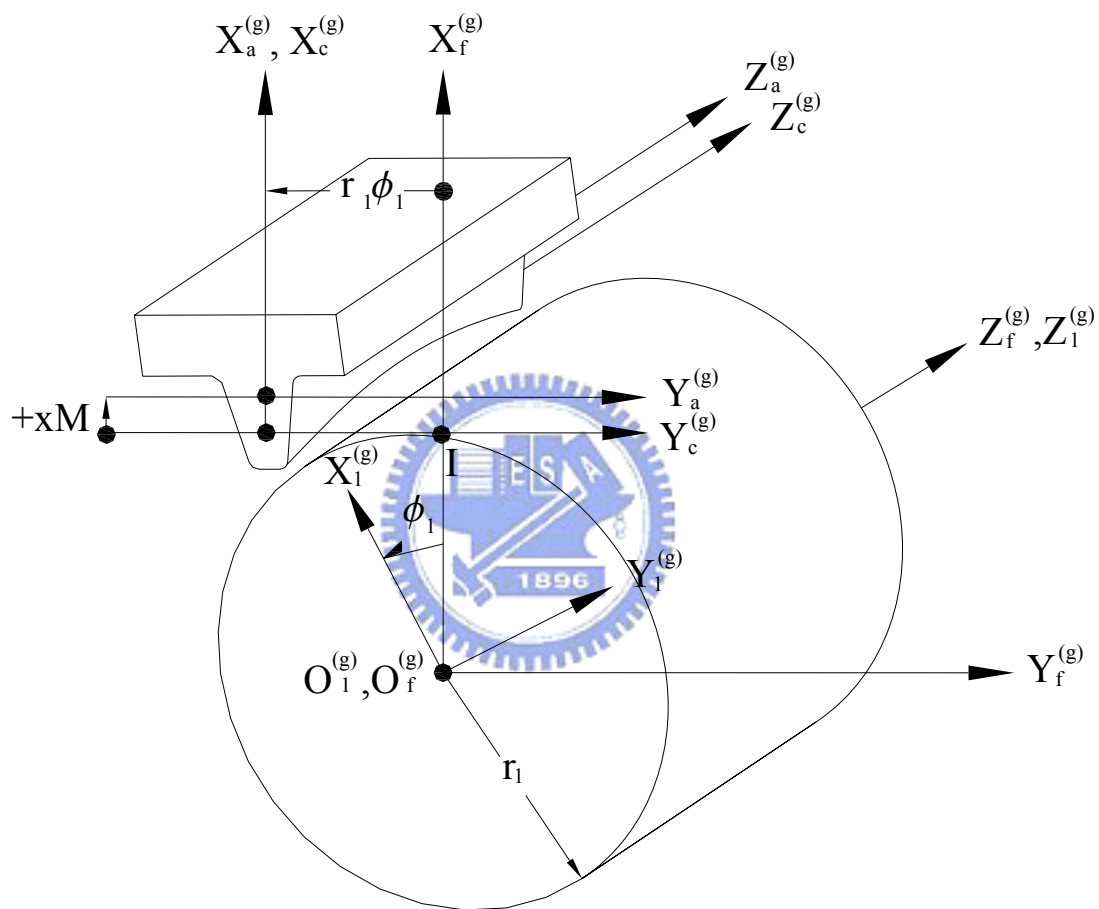
Fig. 4-9 The schematic of shifted cutting

Input: Gear Design Variables

Determine Singular Points
at Cross Section Z_i=0mm
Start at Shifting Coefficient $x = 0$

Update
$x = x + dx$

Solve the undercutting equations:

$$\begin{cases} F\left(\theta^{(i)}, \gamma^{(i)}, \phi_{1,2}\right) = \Delta_1^2 + \Delta_2^2 + \Delta_3^2 = 0 \\ f\left(\gamma^{(i)}, \theta^{(i)}, \phi_{1,2}\right) = 0 \end{cases}$$

Solve by
Mathematica®

Singular Point on
the tooth Surface?

Yes

No

Record the x

END
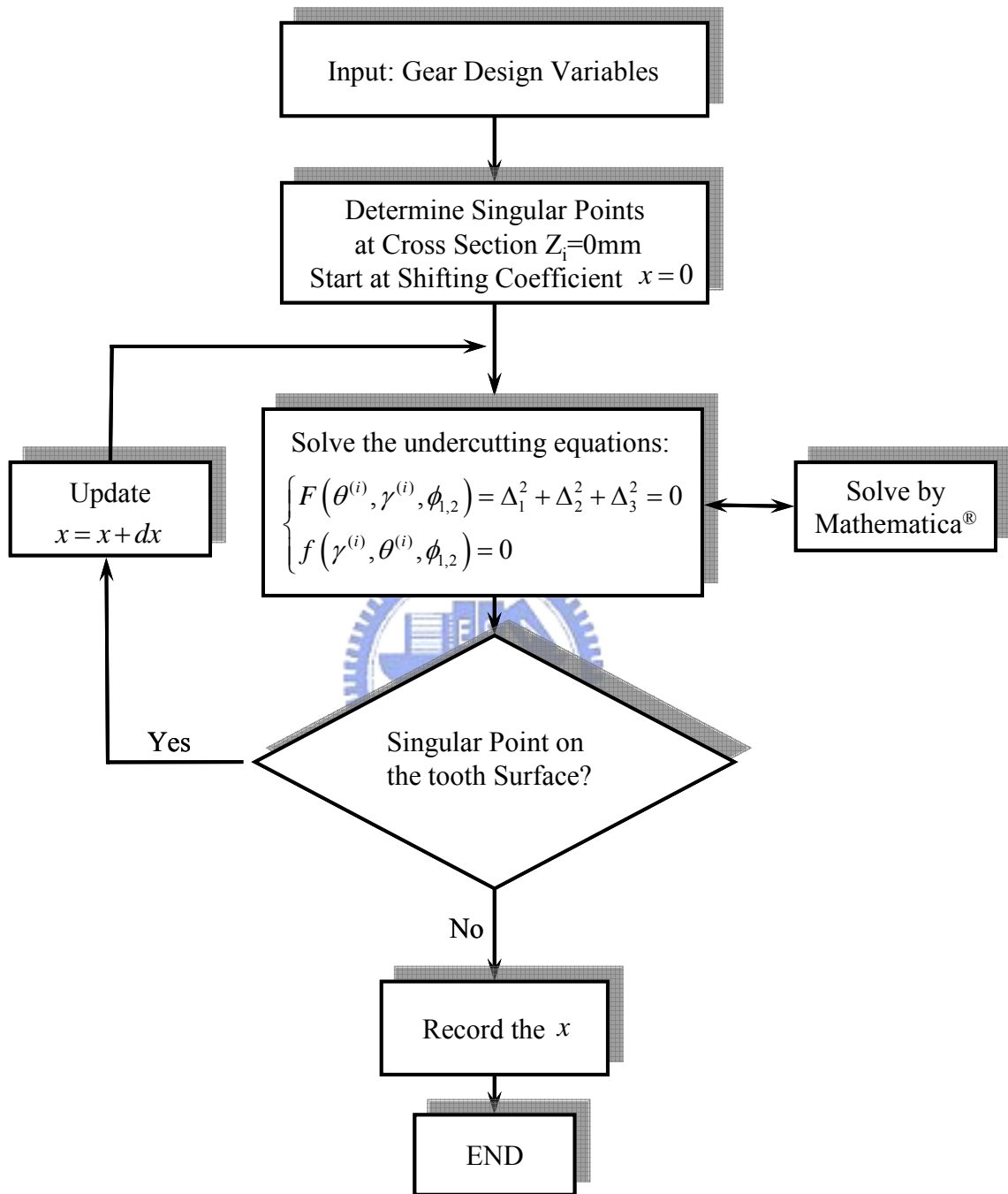
Fig. 4-10 Flowchart for determination of the shifting coefficient x
without tooth undercutting

59
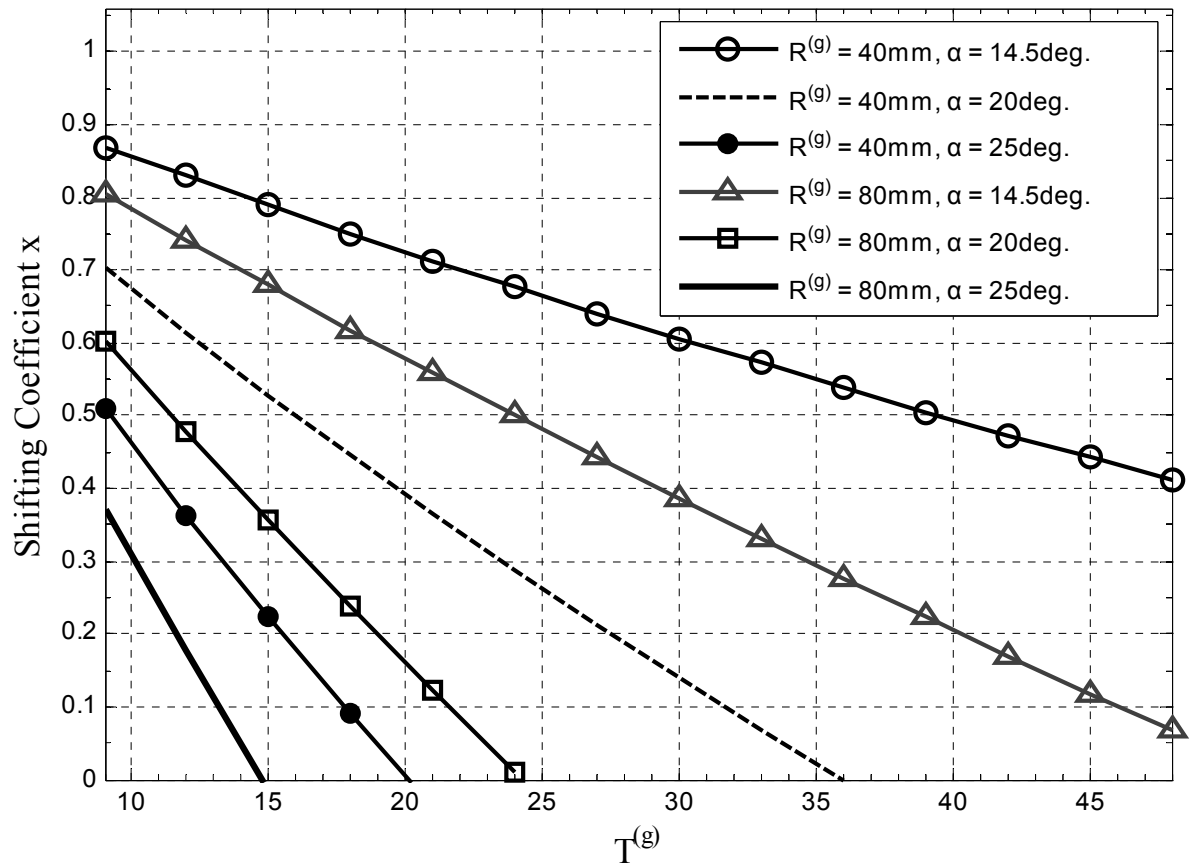
Fig. 4-11 The minimum shifting coefficient x versus number of gear teeth
to avoid undercutting

4.4 Remarks

The conditions of tooth undercutting for the circular-arc curvilinear-tooth gear are investigated utilizing the undercutting conditions and the mathematical model. A computer program applicable to check the tooth undercutting has been developed based on the derived mathematical model and tooth undercutting analysis. The undercutting characteristics of the gears generated by the rack cutter Σ_g and Σ_p are quite different. Tooth undercutting can be predicted by applying the developed undercutting computer program. Designers and manufactures can choose the proper design parameters from the developed equations and figures when manufacturing the circular-arc curvilinear-tooth gear.

CHAPTER 5

Tooth Contact Analysis

5.1 Introduction

The kinematical errors (KE) of a gear set, is defined as the difference between the actual and the ideal rotation angle of the output shaft with reference to the input shaft. In the past, there were mainly two important factors in determining the performance of gear units: load capacity and fatigue life. In recent years, however, the noise radiations of running gears become important. Designers now must design gears with significantly consideration the significance of this extra factor. There are several factors may cause the noise of a gearbox, such as the misalignment of assembly; the precision of the profile, the roughness of the tooth surface and so on. All of these factors may cause the KE of the gear. Therefore, it can be said that the KE is the main reason to cause the noise of the gear.

Computerize simulation of meshing and bearing contact is a significant achievement that could substantially improve the technology and quality of gears. The mathematical model of the circular-arc curvilinear-tooth gear has been presented in CHAPTER 3. The contact and meshing analyses can be attained by applying the developed mathematical and the tooth contact analysis (TCA) program. The TCA investigates the meshing characteristics of gear drives based on the knowledge of gear geometry. When performing TCA, the following assumptions have been made:

1. Only rigid body motion is considered, i.e., no elastic deformation is considered;

2. The effect of temperature, friction, and dynamic loading are neglected;

3. Thermal expansion and inertial force due to gear rotation are also ignored.

The KE can be predicted by the TCA, the contact ratio of the gear pair can also be obtained by the results of TCA. The contact ratio is an important design index for gear tooth bending, load sharing and contact stress. Namely, increasing the contact ratio can develop the loading capacity of the gear set.

In this chapter, the mathematical model of the circular-arc curvilinear-tooth gear will be first transformed to a fixed coordinate system. The different conditions for the gear set will be considered. The KE will also be studied and illustrated by numerical examples and computer graphs.

5.2 Analysis on Kinematical Errors.

The gear is generated by an imaginary rack cutter that has a circular-arc normal section and moves along a curved-template guide during the gear manufacturing process. Owing to the gear tooth surface of the gear set is in point contact rather than in line contact, it can be presumed that the contact point will fall on the middle region of the gear tooth surface.

The mathematical model and the unit normal vectors of the circular-arc curvilinear-tooth gear should be expressed in the same coordinate system for the tooth contact analysis. As shown in Fig. 5-1, coordinate systems $S_1(X_1,Y_1,Z_1)$ and $S_2(X_2,Y_2,Z_2)$ is attached to the gear and pinion separately, in which Z_1 and Z_2 stands for the rotation-axis of the gear and pinion. ϕ_1' and ϕ_2' represent the actual rotation-angle of the gear and pinion under assembly errors, respectively. Coordinate system $S_f(X_f,Y_f,Z_f)$ is the fixed coordinate system, and coordinate systems $S_v(X_v,Y_v,Z_v)$ and $S_h(X_h,Y_h,Z_h)$ are setup for simulation with the horizontal misaligned angle $\Delta\gamma_h$ and vertical misaligned angle $\Delta\gamma_v$, as shown in Fig. 5-1. C is the ideal center distance of the gear pair, and ΔC is the center distance error.

In CHAPTER 3, the mathematical models and the unit normal vectors of the gear and pinion, expressed in Eqs.(3.11), (3.12), (3.22), (3.23), (3.26) and (3.27), are represented in their corresponding coordinate systems $S_1(X_1,Y_1,Z_1)$ and $S_2(X_2,Y_2,Z_2)$, respectively. The position vector and unit normal vector can be transformed from coordinate systems $S_1(X_1,Y_1,Z_1)$ to the fixed coordinate system $S_f(X_f,Y_f,Z_f)$ by applying homogeneous coordinate transformation matrix equations:

$$\mathbf{R}_f^{(1)} = \mathbf{M}_{fh}\mathbf{M}_{hv}\mathbf{M}_{v1}\mathbf{R}_1, \tag{5.1}$$

and

$$\mathbf{n}_f^{(1)} = \mathbf{L}_{fh}\mathbf{L}_{hv}\mathbf{L}_{v1}\mathbf{n}_1, \tag{5.2}$$
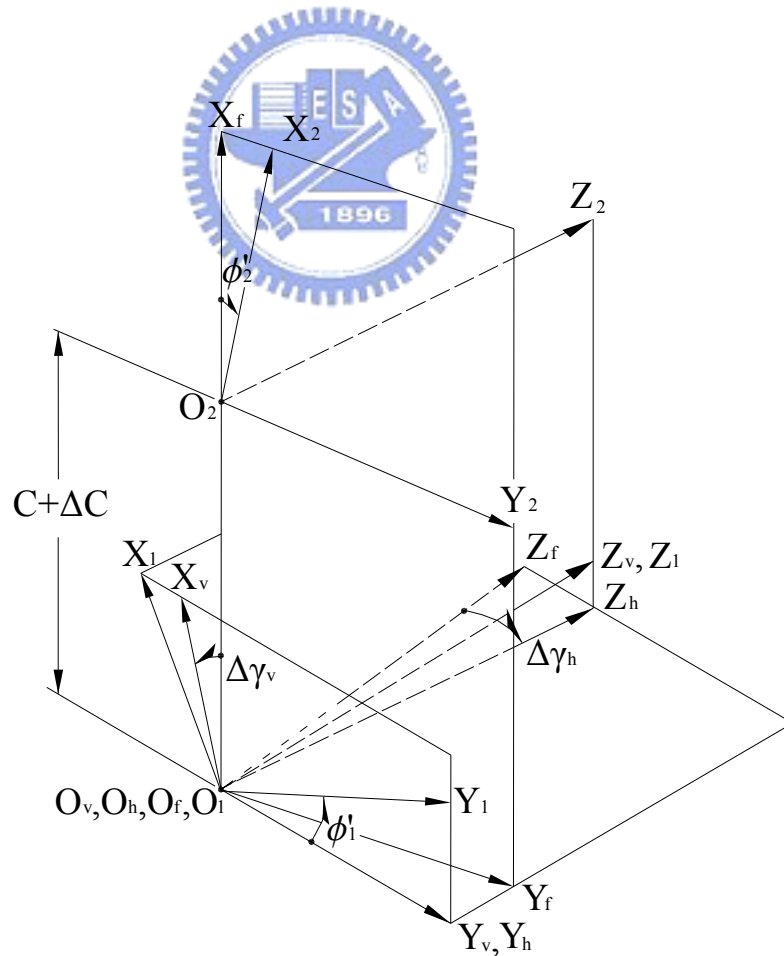

Fig. 5-1 Coordinate systems for simulation of a gear pair meshed with assembly errors

where

$$\mathbf{M}_{fh} = \begin{bmatrix} 1 & 0 & 0 & 0 \\ 0 & \cos\Delta\gamma_h & \sin\Delta\gamma_h & 0 \\ 0 & -\sin\Delta\gamma_h & \cos\Delta\gamma_h & 0 \\ 0 & 0 & 0 & 1 \end{bmatrix}, \tag{5.3}$$

$$\mathbf{M}_{hv} = \begin{bmatrix} \cos\Delta\gamma_v & 0 & \sin\Delta\gamma_v & 0 \\ 0 & 1 & 0 & 0 \\ -\sin\Delta\gamma_v & 0 & \cos\Delta\gamma_h & 0 \\ 0 & 0 & 0 & 1 \end{bmatrix}, \tag{5.4}$$

$$\mathbf{M}_{v1} = \begin{bmatrix} \cos\phi_1' & \sin\phi_1' & 0 & 0 \\ -\sin\phi_1' & \cos\phi_1' & 0 & 0 \\ 0 & 0 & 1 & 0 \\ 0 & 0 & 0 & 1 \end{bmatrix}, \tag{5.5}$$

$$\mathbf{L}_{fh} = \begin{bmatrix} 1 & 0 & 0 \\ 0 & \cos\Delta\gamma_h & \sin\Delta\gamma_h \\ 0 & -\sin\Delta\gamma_h & \cos\Delta\gamma_h \end{bmatrix}, \tag{5.6}$$

$$\mathbf{L}_{hv} = \begin{bmatrix} \cos\Delta\gamma_v & 0 & \sin\Delta\gamma_v \\ 0 & 1 & 0 \\ -\sin\Delta\gamma_v & 0 & \cos\Delta\gamma_v \end{bmatrix}, \tag{5.7}$$

$$\mathbf{L}_{v1} = \begin{bmatrix} \cos\phi_1' & \sin\phi_1' & 0 \\ -\sin\phi_1' & \cos\phi_1' & 0 \\ 0 & 0 & 1 \end{bmatrix} \tag{5.8}$$

Therefore, the position vector and the unit normal vector of the circular-arc curvilinear-tooth gear surface can be expressed in coordinate system $S_f(X_f, Y_f, Z_f)$ as follows:

$$\mathbf{R}_f^{(1)} = \begin{bmatrix} x_f^{(1)} \\ y_f^{(1)} \\ z_f^{(1)} \end{bmatrix} \tag{5.9}$$

64

$$= \begin{bmatrix} (x_1 \cos \phi_1' + y_1 \sin \phi_1') \cos \Delta \gamma_v + z_1 \sin \Delta \gamma_v \\ (-x_1 \sin \phi_1' + y_1 \cos \phi_1') \cos \Delta \gamma_h + [-(x_1 \cos \phi_1' + y_1 \sin \phi_1') \sin \Delta \gamma_v + z_1 \cos \Delta \gamma_v] \sin \Delta \gamma_h \\ -(-x_1 \sin \phi_1' + y_1 \cos \phi_1') \sin \Delta \gamma_h + [-(x_1 \cos \phi_1' + y_1 \sin \phi_1') \sin \Delta \gamma_v + z_1 \cos \Delta \gamma_v] \cos \Delta \gamma_h \end{bmatrix},$$

and

$$\mathbf{n}_f^{(1)} = \begin{bmatrix} n_{fx}^{(1)} \\ n_{fy}^{(1)} \\ n_{fz}^{(1)} \end{bmatrix} \tag{5.10}$$

$$= \begin{bmatrix} (n_{1x} \cos \phi_1' + n_{1y} \sin \phi_1') \cos \Delta \gamma_v + n_{1z} \sin \Delta \gamma_v \\ (-n_{1x} \sin \phi_1' + n_{1y} \cos \phi_1') \cos \Delta \gamma_h + [-(n_{1x} \cos \phi_1' + n_{1y} \sin \phi_1') \sin \Delta \gamma_v + n_{1z} \cos \Delta \gamma_v] \sin \Delta \gamma_h \\ -(-n_{1x} \sin \phi_1' + n_{1y} \cos \phi_1') \sin \Delta \gamma_h + [-(n_{1x} \cos \phi_1' + n_{1y} \sin \phi_1') \sin \Delta \gamma_v + n_{1z} \cos \Delta \gamma_v] \cos \Delta \gamma_h \end{bmatrix}.$$

Similarly, the position vector and the unit normal vector of the circular-arc curvilinear-tooth pinion surface, originally represented in coordinate system $S_2(X_2, Y_2, Z_2)$, can be transformed to the fixed coordinate system $S_f(X_f, Y_f, Z_f)$ by applying the following equations:

$$\mathbf{R}_f^{(2)} = \mathbf{M}_{f2} \mathbf{R}_2, \tag{5.11}$$

and

$$\mathbf{n}_f^{(2)} = \mathbf{L}_{f2} \mathbf{n}_2, \tag{5.12}$$

where

$$\mathbf{M}_{f2} = \begin{bmatrix} \cos \phi_2' & -\sin \phi_2' & 0 & C' \\ \sin \phi_2' & \cos \phi_2' & 0 & 0 \\ 0 & 0 & 1 & 0 \\ 0 & 0 & 0 & 1 \end{bmatrix}, \tag{5.13}$$

$$\mathbf{L}_{f2} = \begin{bmatrix} \cos\phi_2' & -\sin\phi_2' & 0 \\ \sin\phi_2' & \cos\phi_2' & 0 \\ 0 & 0 & 1 \end{bmatrix},$$ (5.14)

and $C' = C + \Delta C$. Based on Eq.(5.11) to (5.14), the position vector and the unit normal vector of the pinion can be represent in the coordinate system $S_f(X_f, Y_f, Z_f)$ as follows:

$$\mathbf{R}_f^{(2)} = \begin{bmatrix} x_2 \cos\phi_2' - y_2 \sin\phi_2' + C' \\ x_2 \sin\phi_2' + y_2 \cos\phi_2' \\ z_2 \end{bmatrix},$$ (5.15)

and,

$$\mathbf{n}_f^{(2)} = \begin{bmatrix} n_{2x} \cos\phi_2' - n_{2y} \sin\phi_2' \\ n_{2x} \sin\phi_2' + n_{2y} \cos\phi_2' \\ n_{2z} \end{bmatrix}.$$ (5.16)

When the gear pair is meshed with each other, as shown in Fig. 5-2, the mating surfaces Σ_1 and Σ_2 must satisfy the conditions of tooth continuous tangency at the instant contact point P. The conditions of tooth continuous tangency can be expressed by considering that the position vectors and unit vectors of the two mating surfaces coincide with each other at the common contact point at any instant. Thus:

$$\mathbf{R}_f^{(1)} = \mathbf{R}_f^{(2)},$$ (5.17)

and

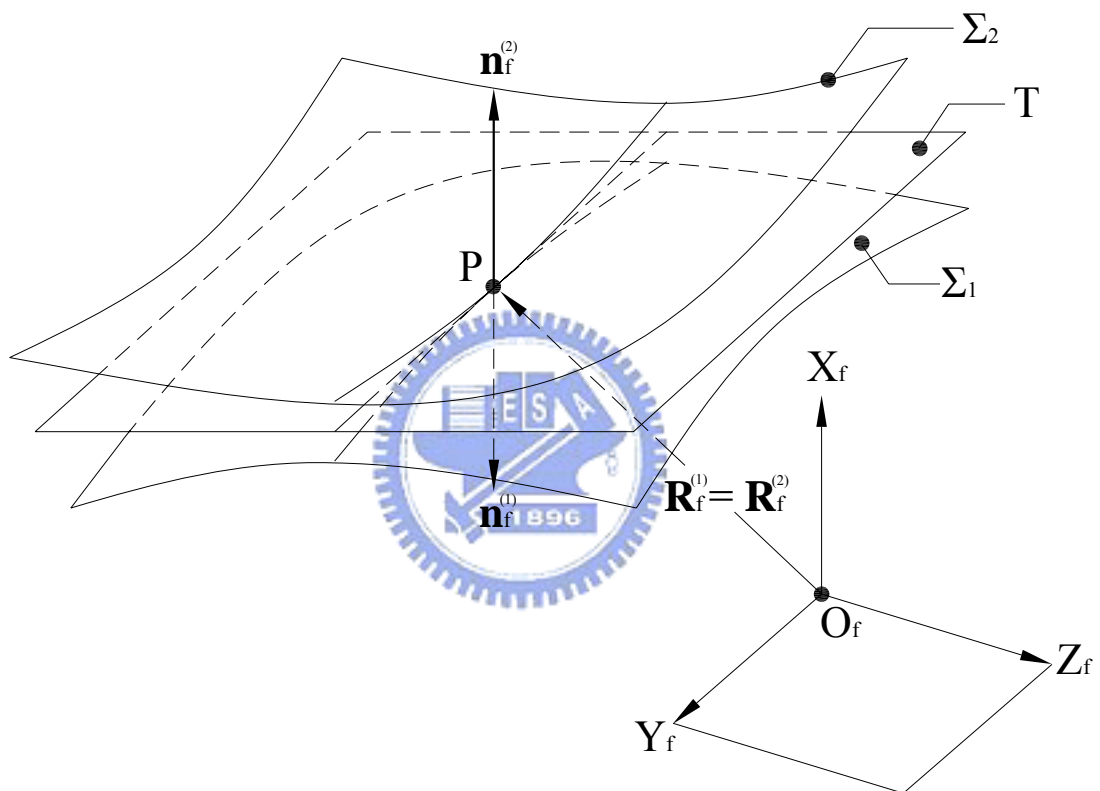$$\mathbf{n}_f^{(1)} \times \mathbf{n}_f^{(2)} = 0.$$ (5.18)

Fig. 5-2 Schematic of the relationship between two meshing gear tooth surfaces

Eq.(5.17) means the position vector of the contact point of the gear and pinion tooth surfaces are equal to each other, and Eq.(5.18) indicates their surface unit normal vectors are also collinear.

In a three-dimensional space, Eq.(5.17) contains three independent equations. However, Eq.(5.18) contains only two independent equations since $\left|\mathbf{n}_f^{(1)}\right| = \left|\mathbf{n}_f^{(2)}\right| = 1$. Recall that there are two independent meshing equations during the generation of the gear and pinion by rack cutter Σ_g and Σ_p. Generally, the rotation angle ϕ_1' is considered as an input variable in solving these non-linear equations. Hence, the output rotation angle ϕ_2' is a function of ϕ_1'. The relationship between ϕ_1' and is an inverse ratio to their number of teeth under the ideal meshing condition (i.e. $T^{(p)}\phi_2' = T^{(g)}\phi_1'$,). Nevertheless, manufacturing errors and assembly misalignments are inevitable in practical situations. Therefore, under a real meshing condition, the KE of the mating gear pair can be expressed as follow:

$$\Delta\phi_2'(\phi_1') = \phi_2'(\phi_1') - \phi_1'\frac{T^{(g)}}{T^{(p)}}, \tag{5.19}$$

where $T^{(g)}$ and $T^{(p)}$ indicates the number of teeth of the gear and pinion, and $\Delta\phi_2'(\phi_1')$ is the KE of the gear set induced by the assembly errors.

5.3 Contact Ratio

The contact ratio of a gear set is defined as the average number of teeth in contact during the gear meshing. A higher contact ratio of a gear set can increase its load capacity efficiently and decrease the impact force per tooth. Virtually, the increase of contact ratio can be achieved by the decrease of the pressure angle of the gear set. However, the bending and

compressive stresses will be increased with the decrease of the pressure angle since the tooth thickness of the gear fillet is reduced.

In general, a gear set with a minimum contact ratio of 1.4 is desirable, and it should never be less than 1.2 [21]. However, the contact ratio can be defined by the gear's rotation angle, measured from the starting point of contact to the end point of contact. Thus, the value of contact ratio can be obtained from the result of the teeth contact analysis and expressed by the following equation [10]:

$$m_c = T^{(g)}(\frac{\phi_{1E} - \phi_{1S}}{360°}) , \tag{5.20}$$

where $\phi_{1E} - \phi_{1S}$ denotes the rotation angle of the gear while one pair of teeth is in mesh within the range of tooth surface. The angle ϕ_{1E} and ϕ_{1S} can be determined based on the TCA simulation results. Table 5-1 illustrates the contact ratios versus different major design parameters. Contact ratio decreases with the decreasing of the radius of the cutter's circular-arc profiles and an acuter pressure angle. However, the contact ratio takes no effect with the variations of the radii R_{ab} of the disk-type tool.
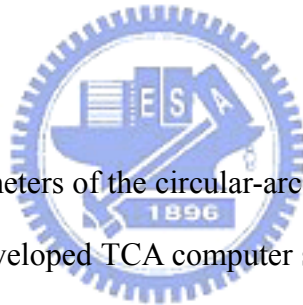
5.4 Numerical Examples for Kinematical Errors of Circular-Arc Curvilinear-Tooth Gears

Several examples are used to present the KE characteristics of the gear pair. Example 5-1 shows the positions of contact points on the gear pair with or without misalignments. Relationships between pressure angle and KE are also discussed in this example. Example 5-2 and Example 5-3 clarify the effects of the KE and the radii of the cutter's circular-arc profile. Example 5-4 explains the relations between KE and the radius of the disk-type cutter.

Table 5-1 Contact Ratios under different design parameters

Design parameters ($M = 3mm/tooth, A = 0.8M, B = 0.8M$, $T^{(g)} = 36$ teeth, $T^{(p)} = 18$ teeth)				Contact Ratio
R_{ab} (mm)	$R^{(g)}$ (mm)	$R^{(p)}$ (mm)	α (deg)	
30	80	80	14.5	undercutting
30	80	80	20	1.66
30	80	80	25	1.42
30	40	40	20	1.70
20	80	80	20	1.66

Example 5-1

Some major design parameters of the circular-arc curvilinear-tooth gear pair are given in Table 5-2. According to the developed TCA computer simulation program, Table 5-3 to Table 5-6 list the analysis detail results of bearing contacts and KE of the gear pair. The contact points under ideal and error assembly conditions are distributed over the middle region of the gear tooth surface, because of tooth surfaces of the gear set have crowning effect and are in point contact. It can be said that the gear edge contact is efficiently avoided. However, the circular-arc curvilinear-tooth gear set is sensitive to the center distance assembly error ΔC.

KE of the circular-arc curvilinear-tooth gear under different pressure angles with assembly errors are shown in Fig. 5-3, Fig. 5-4 and Fig. 5-5. The circular-arc curvilinear-tooth gear set possesses no KE under ideal assembly conditions, and the KE is insensitive to the axial assembly misalignments $\Delta\gamma_h$ and $\Delta\gamma_v$. When the gear pair has assembly errors with distance variation ΔC, where $\Delta C = 0.1\,mm$ is 0.12% of center distance variation, the contact

points are still located on the contact line of $\gamma^{(g)} = 0°$, and it takes an acute effect of the KE for the gear pair. However, center distance variation ΔC will not induce KE for involute gear pairs. KE under the axial misalignment $\Delta\gamma_h = 0.1°$ takes no effect with variations of the pressure angle. However, KE increases under assembly errors conditions $\Delta C = 0.1\,\text{mm}$ and $\Delta\gamma_v = 0.1°$ with a larger pressure angle value.

Table 5-2 Some major design parameters of the circular-arc curvilinear-tooth gear pair

Design parameters	Pinion	Gear
Number of Teeth ($T^{(i)}$)	18	36
Normal Module (M)	3mm/tooth	3mm/tooth
Normal Pressure Angle (α)	20°	
Radius of the Disk-Type Cutter (R_{ab}) (Fig. 3-7)	30mm	
Radius of Rack Cutter Normal Section ($R^{(i)}$) (Fig. 3-6 & Fig. 3-8)	80mm	80mm
Face Width (W) (Fig. 3-7)	30mm	

Table 5-3 Bearing contacts and kinematical errors
of the gear pair under ideal assembly condition

ϕ_1' (deg.)	ϕ_2' (deg.)	$\theta^{(g)}$ (deg.)	$\theta^{(p)}$ (deg.)	$\gamma^{(g)}$ (deg.)	$\gamma^{(p)}$ (deg.)	KE(arc-sec.)
-5.000	-10.000	19.438	19.438	0.000	0.000	0.00
-4.000	-8.000	19.659	19.659	0.000	0.000	0.00
-3.000	-6.000	19.885	19.885	0.000	0.000	0.00
-2.000	-4.000	20.116	20.116	0.000	0.000	0.00
-1.000	-2.000	20.352	20.352	0.000	0.000	0.00
0.000	0.000	20.594	20.594	0.000	0.000	0.00
1.000	2.000	20.841	20.841	0.000	0.000	0.00
2.000	4.000	21.093	21.093	0.000	0.000	0.00
3.000	6.000	21.352	21.352	0.000	0.000	0.00
4.000	8.000	21.617	21.617	0.000	0.000	0.00
5.000	10.000	21.888	21.888	0.000	0.000	0.00

Table 5-4 Bearing contacts and KE of the gear pair
under center distance assembly error $\Delta C = 0.1\,\mathrm{mm}$

ϕ_1' (deg.)	ϕ_2' (deg.)	$\theta^{(g)}$ (deg.)	$\theta^{(p)}$ (deg.)	$\gamma^{(g)}$ (deg.)	$\gamma^{(p)}$ (deg.)	KE(arc-sec.)
-5.000	-9.995	19.477	19.403	0.000	0.000	17.36
-4.000	-7.996	19.698	19.623	0.000	0.000	14.06
-3.000	-5.997	19.924	19.849	0.000	0.000	10.67
-2.000	-3.998	20.155	20.079	0.000	0.000	7.21
-1.000	-1.999	20.391	20.314	0.000	0.000	3.65
0.000	0.000	20.633	20.555	0.000	0.000	0.00
1.000	1.999	20.880	20.801	0.000	0.000	-3.74
2.000	3.998	21.133	21.053	0.000	0.000	-7.59
3.000	5.997	21.392	21.310	0.000	0.000	-11.54
4.000	7.996	21.657	21.574	0.000	0.000	-15.60
5.000	9.995	21.928	21.844	0.000	0.000	-19.77

Table 5-5 Bearing contacts and kinematical errors
of the gear pair under axial misalignments $\Delta\gamma_h = 0.1°$

ϕ_1'(deg.)	ϕ_2'(deg.)	$\theta^{(g)}$(deg.)	$\theta^{(p)}$(deg.)	$\gamma^{(g)}$(deg.)	$\gamma^{(p)}$(deg.)	KE(arc-sec.)
-5.000	-10.000	19.438	19.438	-0.787	-0.687	0.75
-4.000	-8.000	19.659	19.659	-0.767	-0.667	0.59
-3.000	-6.000	19.885	19.885	-0.747	-0.647	0.44
-2.000	-4.000	20.116	20.116	-0.727	-0.627	0.29
-1.000	-2.000	20.352	20.352	-0.707	-0.607	0.14
0.000	0.000	20.593	20.593	-0.687	-0.587	0.00
1.000	2.000	20.840	20.840	-0.667	-0.567	-0.14
2.000	4.000	21.093	21.093	-0.647	-0.547	-0.27
3.000	6.000	21.352	21.352	-0.627	-0.527	-0.40
4.000	8.000	21.616	21.616	-0.607	-0.507	-0.52
5.000	10.000	21.887	21.887	-0.587	-0.487	-0.64

Table 5-6 Bearing contacts and kinematical errors
of the gear pair under axial misalignments $\Delta\gamma_v = 0.1°$

ϕ_1'(deg.)	ϕ_2'(deg.)	$\theta^{(g)}$(deg.)	$\theta^{(p)}$(deg.)	$\gamma^{(g)}$(deg.)	$\gamma^{(p)}$(deg.)	KE(arc-sec.)
-5.000	-10.000	19.438	19.437	-0.868	-0.904	-0.20
-4.000	-8.000	19.659	19.658	-0.872	-0.908	-0.17
-3.000	-6.000	19.885	19.884	-0.876	-0.912	-0.13
-2.000	-4.000	20.116	20.115	-0.880	-0.916	-0.09
-1.000	-2.000	20.352	20.351	-0.884	-0.921	-0.04
0.000	0.000	20.593	20.593	-0.888	-0.925	0.00
1.000	2.000	20.840	20.840	-0.892	-0.930	0.04
2.000	4.000	21.093	21.092	-0.896	-0.935	0.09
3.000	6.000	21.351	21.351	-0.901	-0.940	0.14
4.000	8.000	21.616	21.616	-0.906	-0.945	0.19
5.000	10.000	21.887	21.887	-0.910	-0.950	0.24
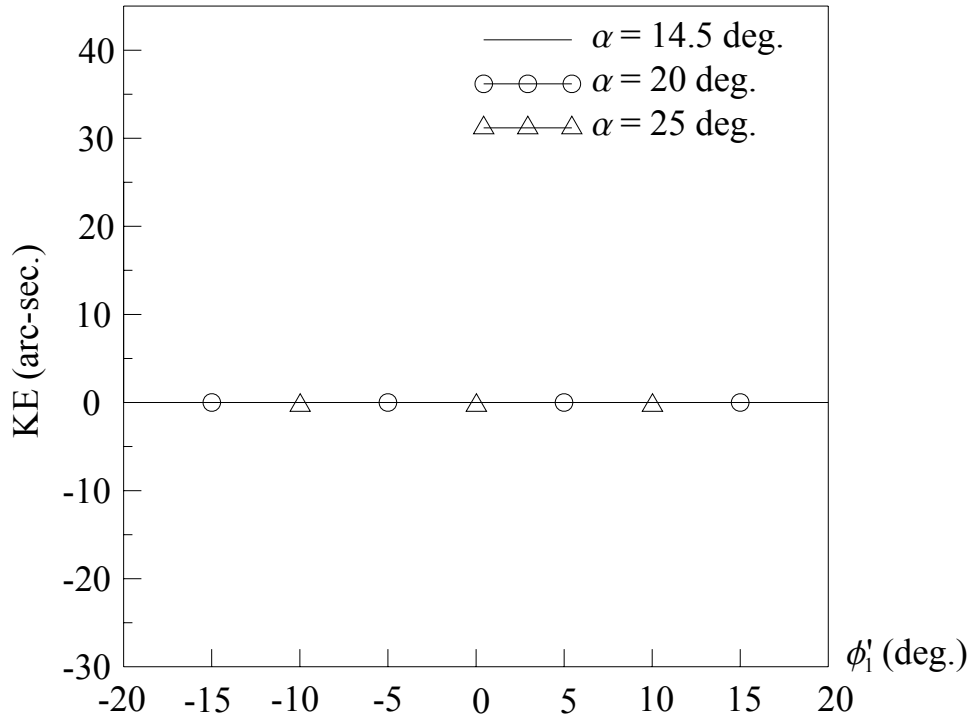
(a) Ideal Assembly Condition
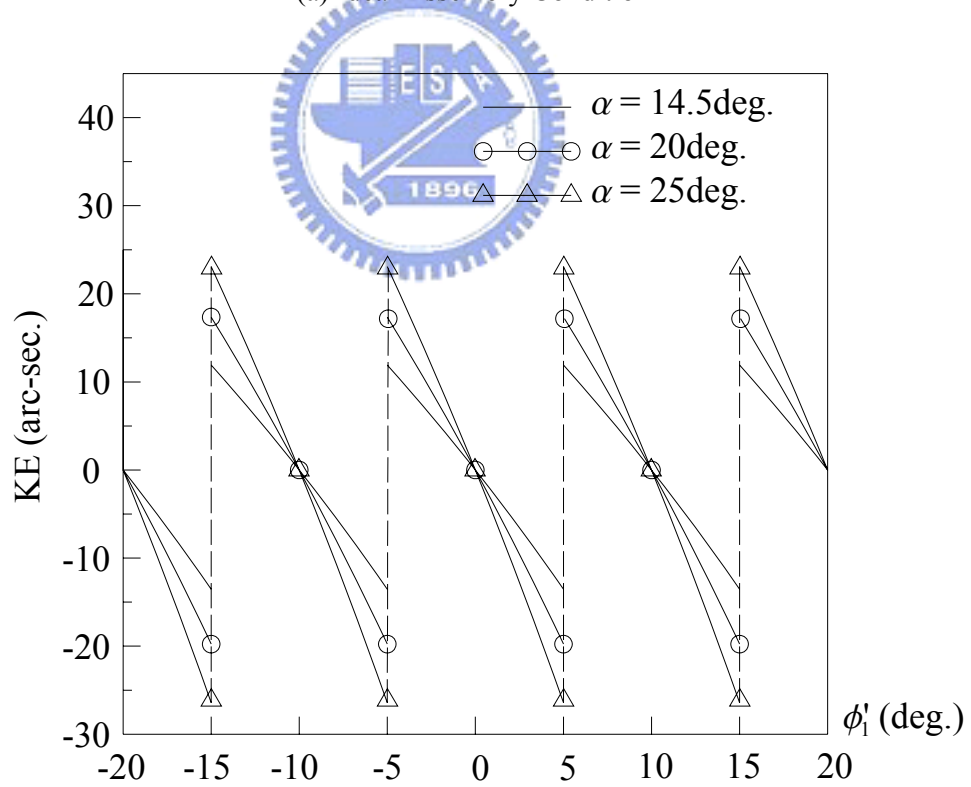
(b) $\Delta C = 0.1$mm

Fig. 5-3 Kinematical errors of the gear pair with different pressure angles under ideal assembly condition and assembly error $\Delta C = 0.1$mm
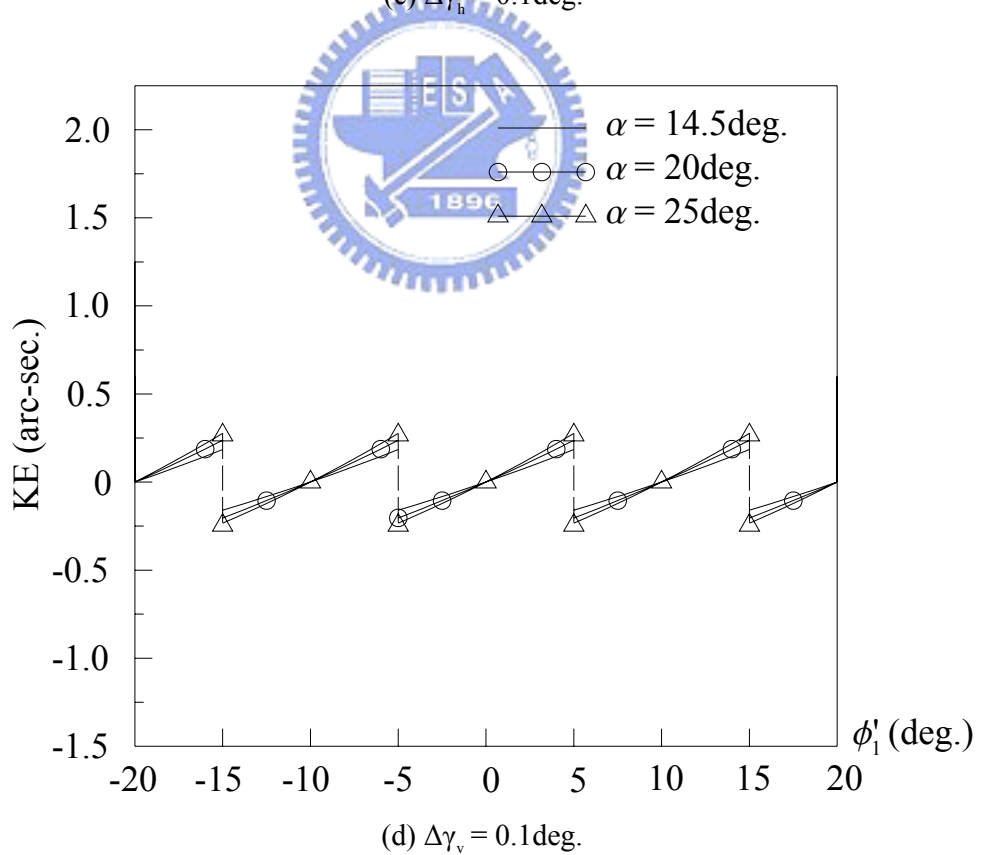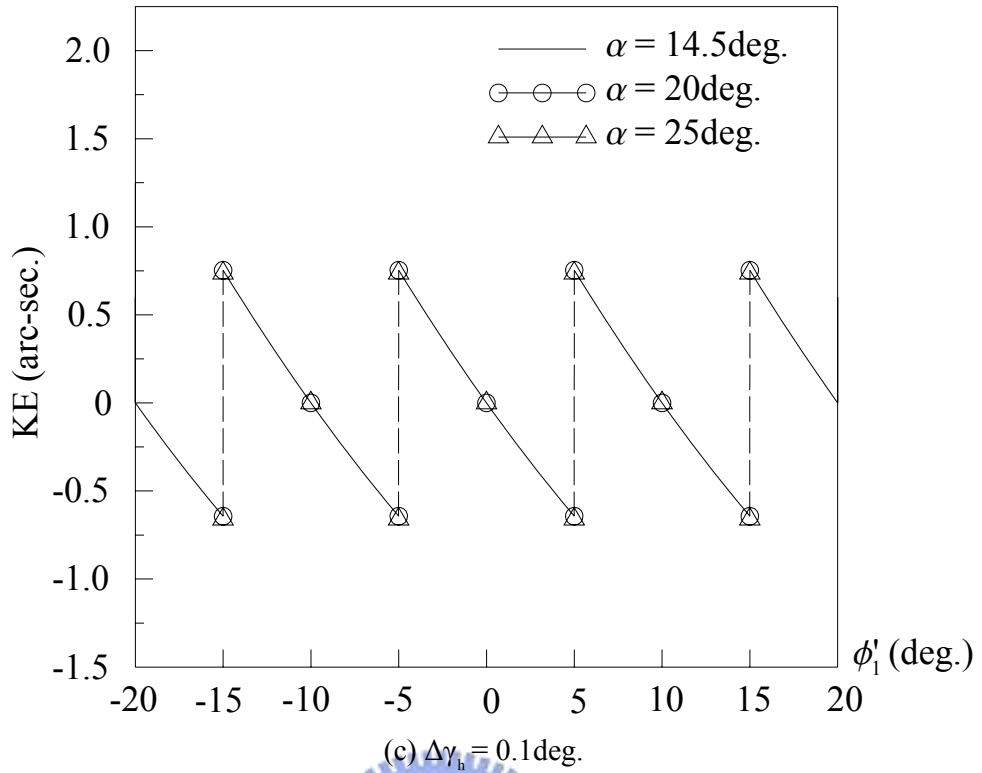
74

(c) $\Delta\gamma_h = 0.1\text{deg.}$

(d) $\Delta\gamma_v = 0.1\text{deg.}$

Fig. 5-4 Kinematical errors of the gear pair with different pressure angles under axial assembly misalignment $\Delta\gamma_h = 0.1°$ and $\Delta\gamma_v = 0.1°$
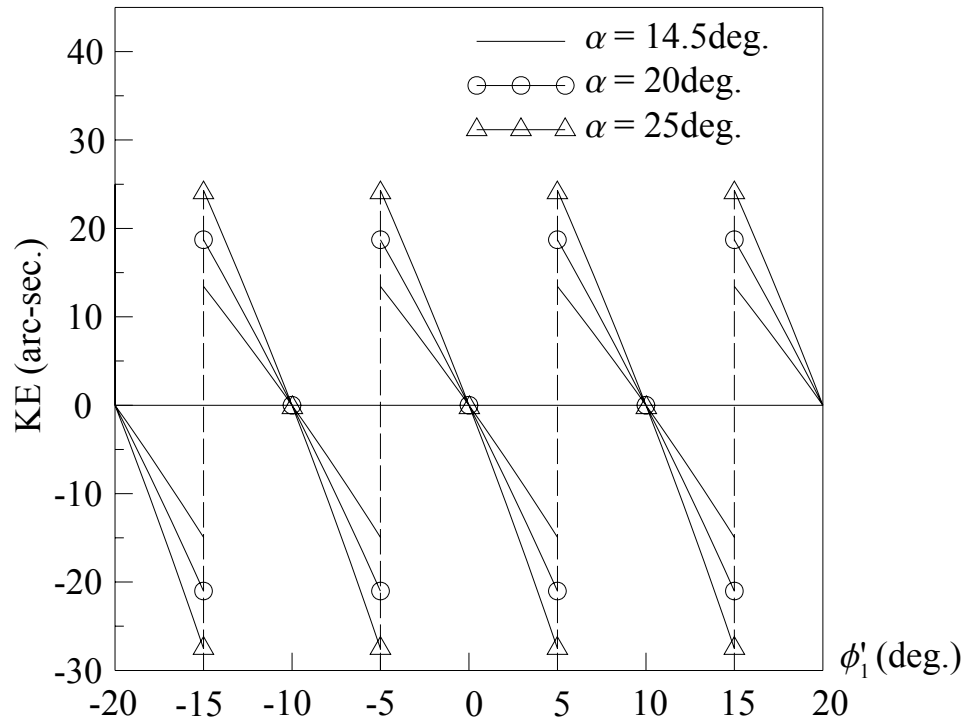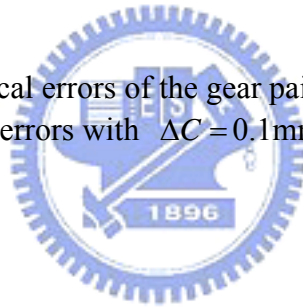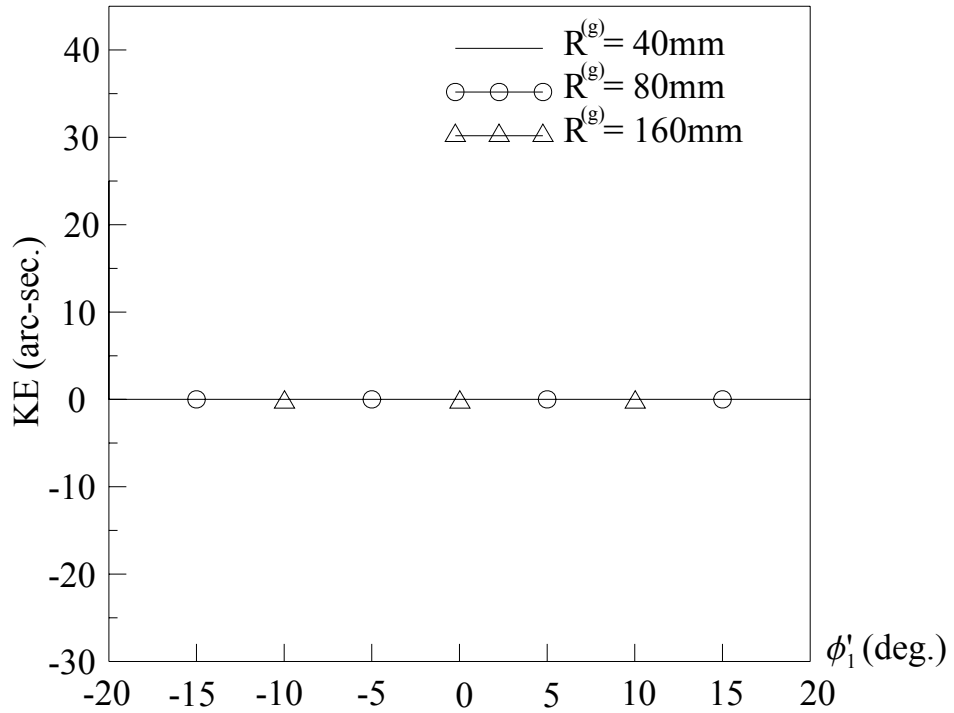
Fig. 5-5 Kinematical errors of the gear pair with different pressure angles under mixed assembly errors with $\Delta C = 0.1\text{mm}$, $\Delta\gamma_h = 0.1°$ and $\Delta\gamma_v = 0.1°$

Example 5-2

The relationships between KE and the radius $R^{(i)}$ of the circular-arc cutter profile are investigated in this example. The design parameters of the gear pair are the same as those listed in Table 5-2 with varying values of $R^{(i)}$. The example aims to investigate the gear pair meshing under different $R^{(i)}$, and it is defined that $R^{(g)} = R^{(p)}$ in this example.

The KE curves under different meshing conditions are shown in Fig. 5-6, Fig. 5-7 and Fig. 5-8. They illustrate that KE caused by $\Delta C = 0.1\text{mm}$ is decreased with the increase of $R^{(i)}$. Because gears with a involute profiles induce no KE with center distance assembly errors, it means $R^{(i)}$ approaches to infinity for the involute profiles. However, KE caused by

(a) Ideal Assembly Condition
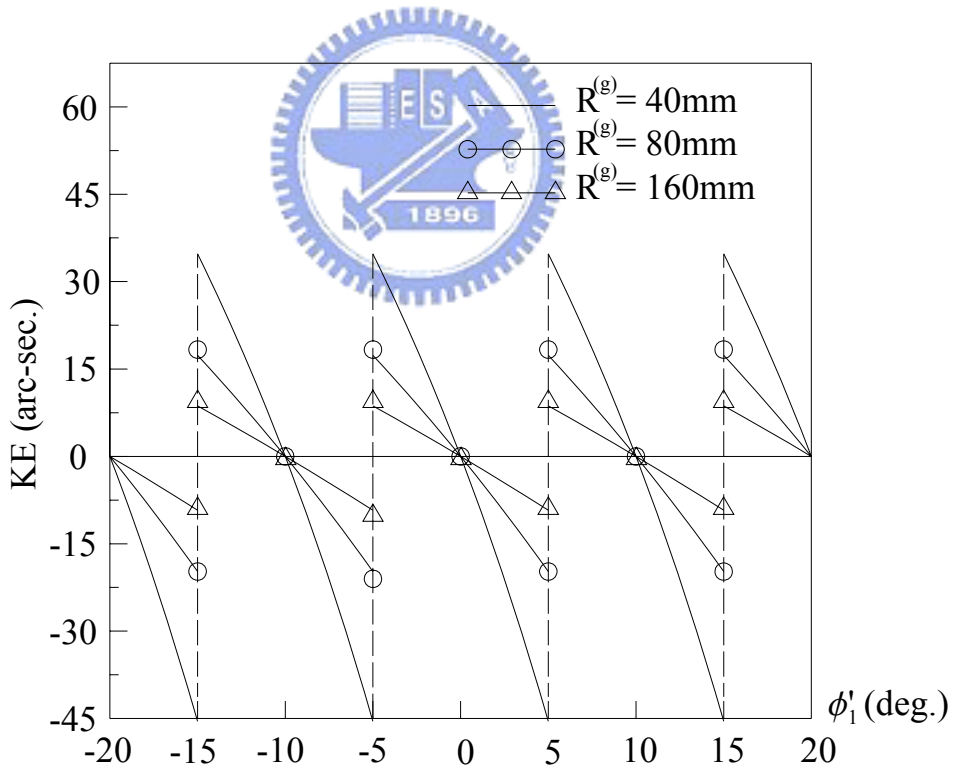
(b) $\Delta C = 0.1$mm

Fig. 5-6 Kinematical errors of the gear pair with different $R^{(i)}$ under ideal assembly condition and assembly error $\Delta C = 0.1$mm
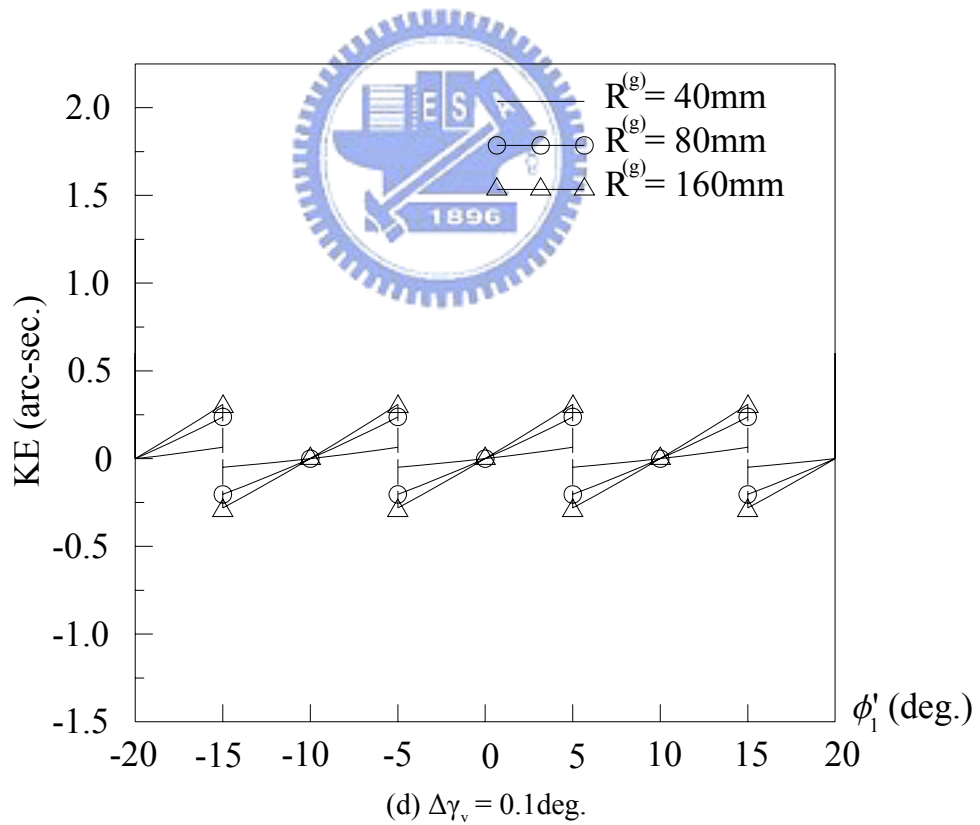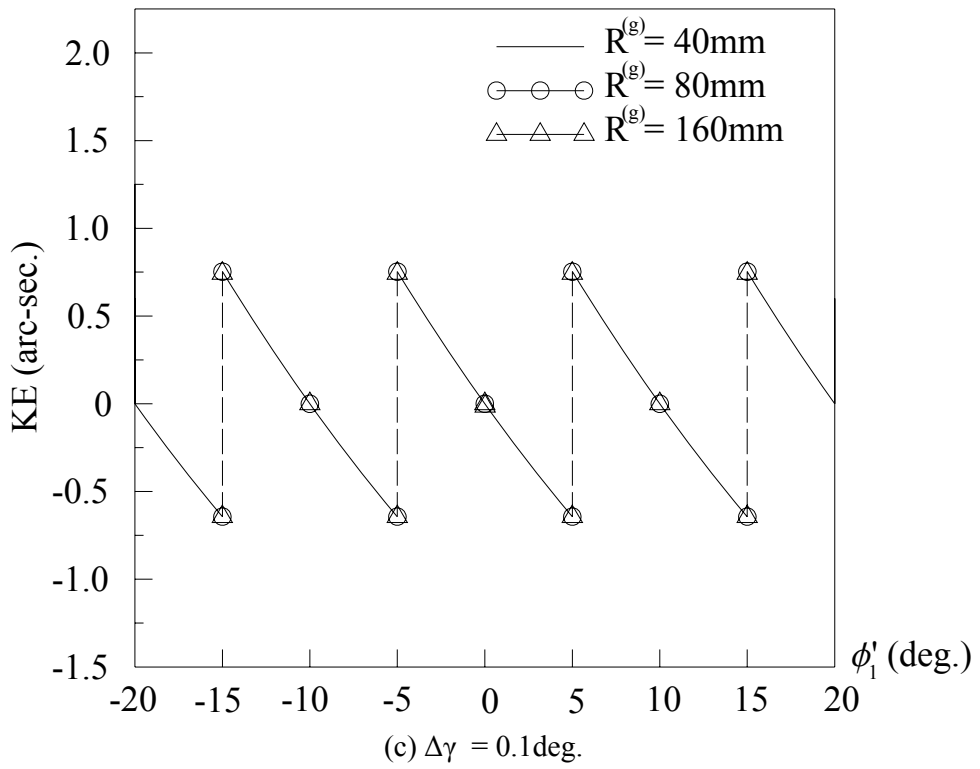
Fig. 5-7 Kinematical errors of the gear pair with different $R^{(i)}$
under axial assembly misalignment $\Delta\gamma_h = 0.1°$ and $\Delta\gamma_v = 0.1°$
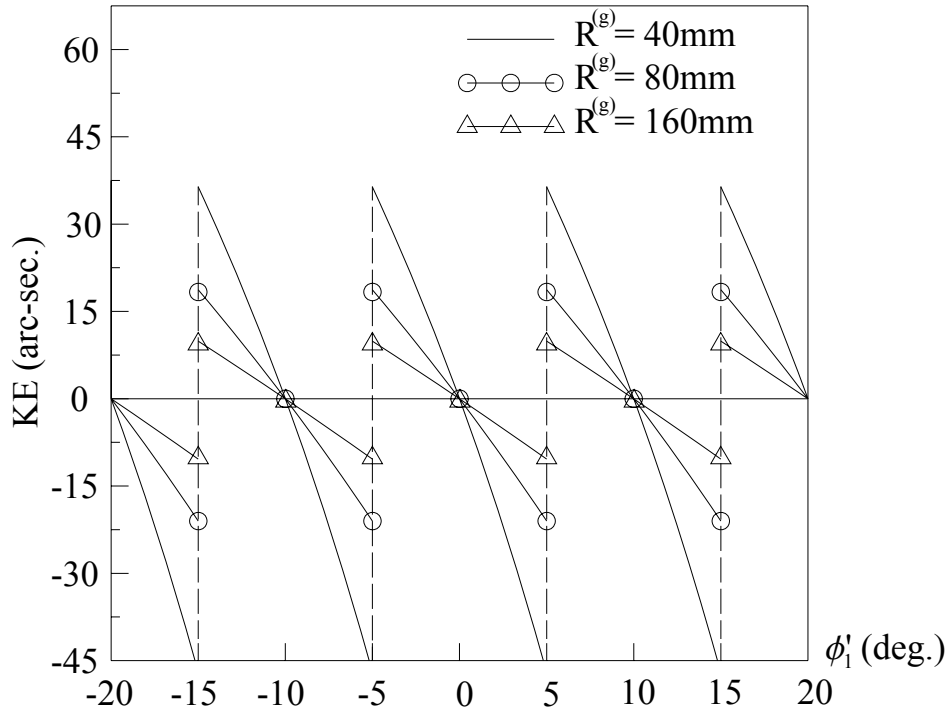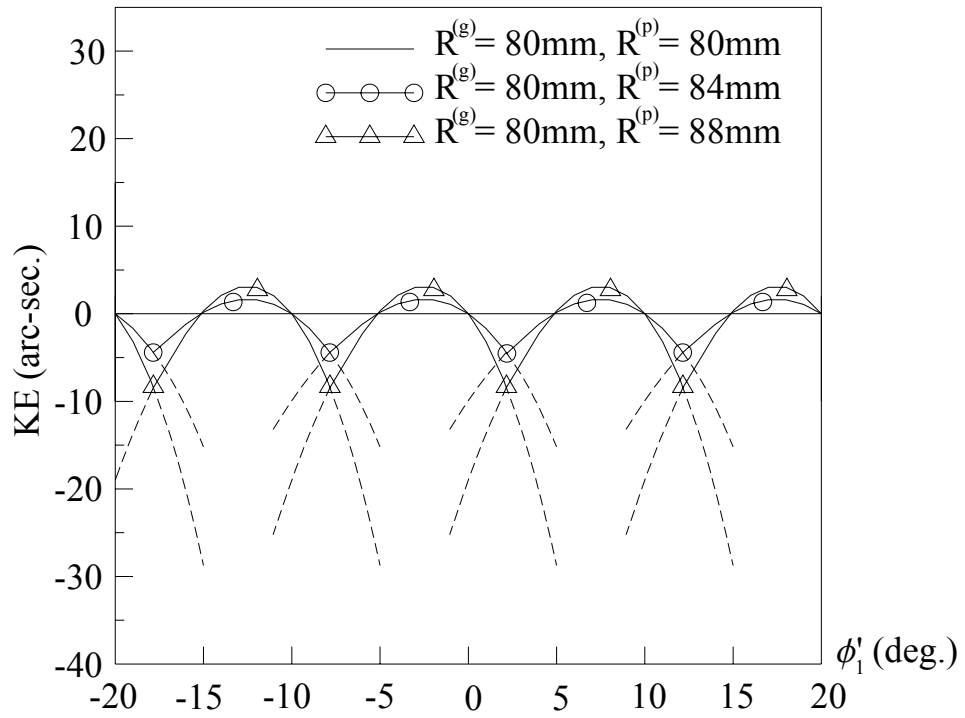
Fig. 5-8 Kinematical errors of the gear pair with different pressure angles
under mixed assembly errors with $\Delta C = 0.1\text{mm}$, $\Delta \gamma_h = 0.1°$ and $\Delta \gamma_v = 0.1°$

axial misalignment $\Delta \gamma_v = 0.1°$ increases with the increase of $R^{(i)}$. Fig. 5-8 shows the mixed

assembly misalignment conditions for the gear pair with a higher $R^{(i)}$, the results in a lower

level of KE is caused by the center distance $\Delta C = 0.1\text{mm}$ error.

Example 5-3

Example 5-1 and Example 5-2 are designed with the same radius ($R^{(g)} = R^{(p)}$) for the

rack cutter's circular-arc profile. A parameter ΔR is pre-designed in this example, and ΔR is

defined as $\Delta R = (R^{(p)} - R^{(g)})$. The major design parameters of the gear set are the same as

shown in Table 5-2. KE under different meshing conditions with ΔR as illustrated in Fig. 5-9

to Fig. 5-11, where ΔR is defined as 0mm, 4mm and 8mm. There is no KE under ideal

assembly conditions with $\Delta R = 0$ mm because the gear pair is generated by conjugate-shape

rack cutters [10][20].

(a) Ideal Assembly Condition
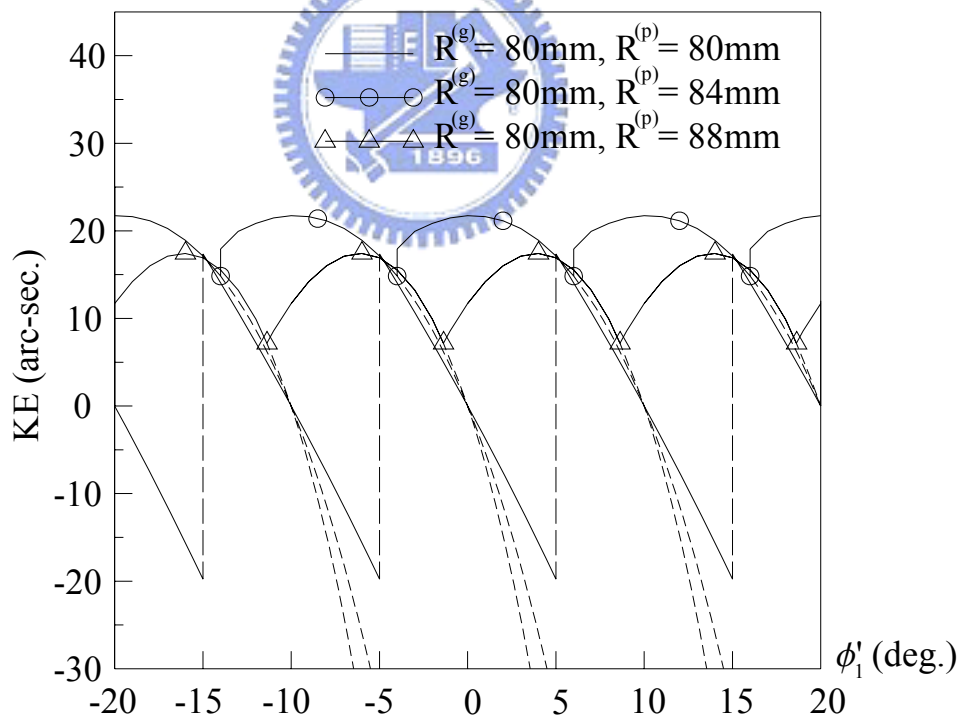
(b) $\Delta C = 0.1\text{mm}$

Fig. 5-9 Kinematical errors of the gear pair with different ΔR under ideal assembly condition and assembly error $\Delta C = 0.1\text{mm}$

(c) $\Delta\gamma_h = 0.1$deg.
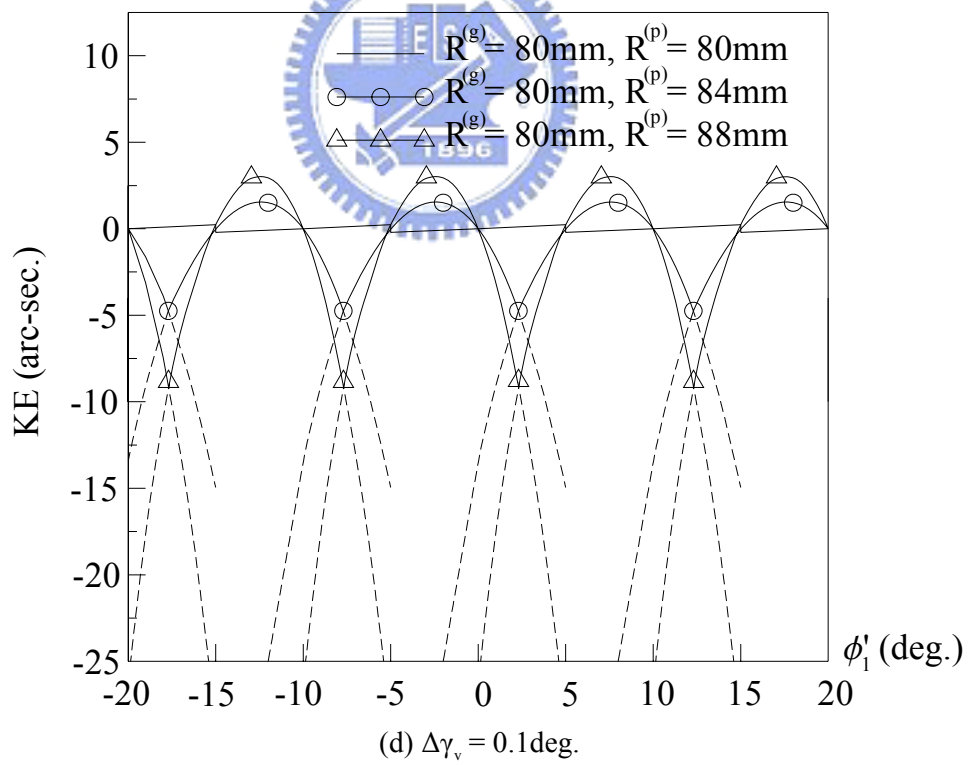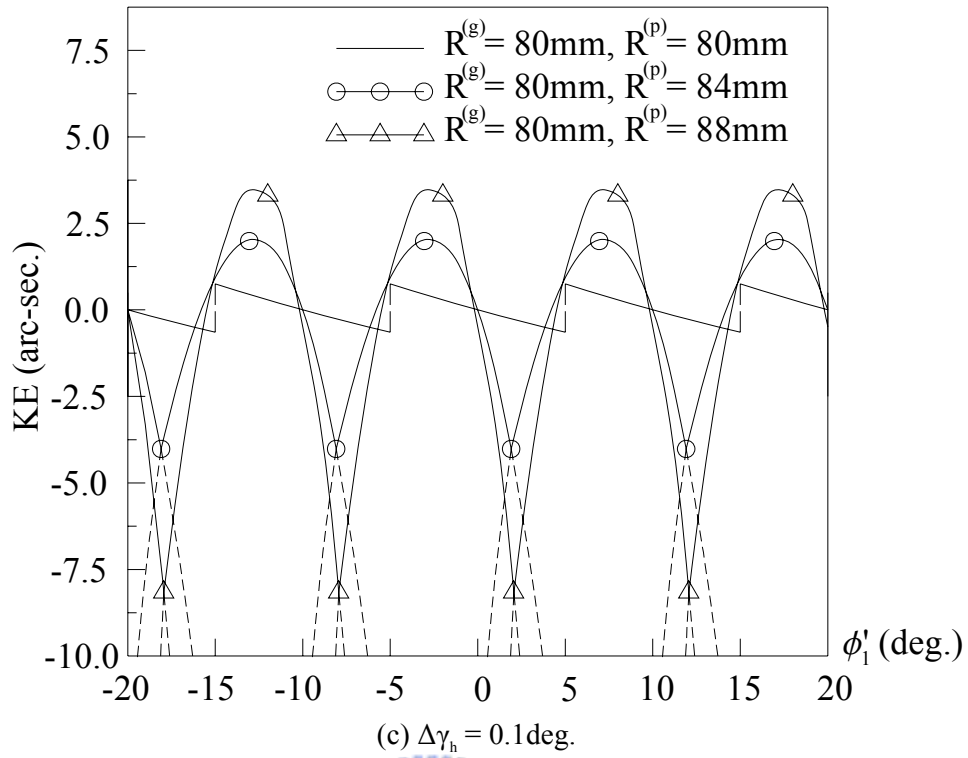

(d) $\Delta\gamma_v = 0.1$deg.

Fig. 5-10 Kinematical errors of the gear pair with different ΔR under axial assembly misalignment $\Delta\gamma_h = 0.1°$ and $\Delta\gamma_v = 0.1°$
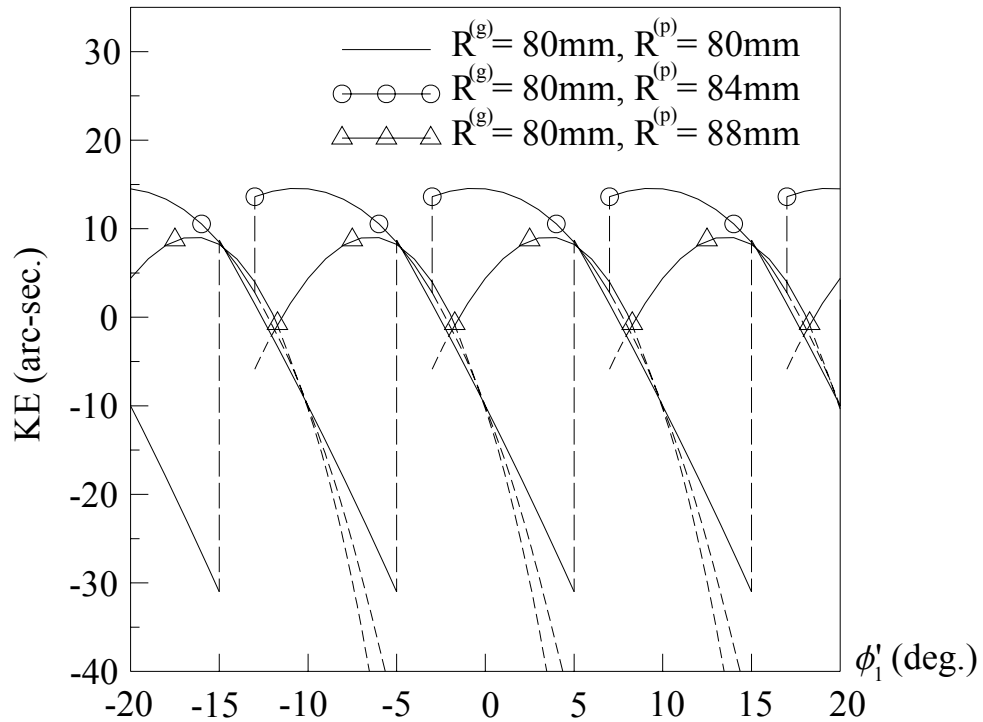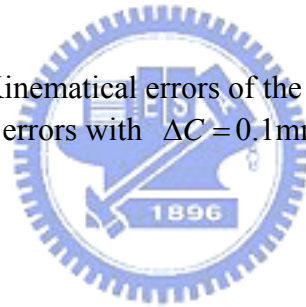
Fig. 5-11 Kinematical errors of the gear pair with ΔR
under mixed assembly errors with $\Delta C = 0.1\text{mm}$, $\Delta\gamma_h = 0.1°$ and $\Delta\gamma_v = 0.1°$

However, the gear pair with design parameter $\Delta R \neq 0$ possesses a parabolic type of KE under the ideal assembly condition. Relationships between KE and ΔR under different meshing conditions are shown in these figures. Center distance error ΔC has a great influence on the KE of the gear pair with its circular-arc profile. The KE caused by the center distance variation ΔC is decreased effectively with the parabolic type of KE by the pre-designing the design value ΔR.

Example 5-4

The relationships between KE and $R^{(i)}$ has been discussed before with considerations of different radii $R^{(g)}$, $R^{(p)}$ of the circular-arc rack cutters even a difference ΔR between them. In this example, the focus aims to investigate the KE of the gear pair with different radii

Fig. 5-12 Kinematical errors of the gear pair with different R_{ab} under ideal assembly condition and assembly error $\Delta C = 0.1$mm

(c) $\Delta\gamma_h = 0.1\text{deg.}$

(d) $\Delta\gamma_v = 0.1\text{deg.}$

Fig. 5-13 Kinematical errors of the gear pair with different R_{ab}
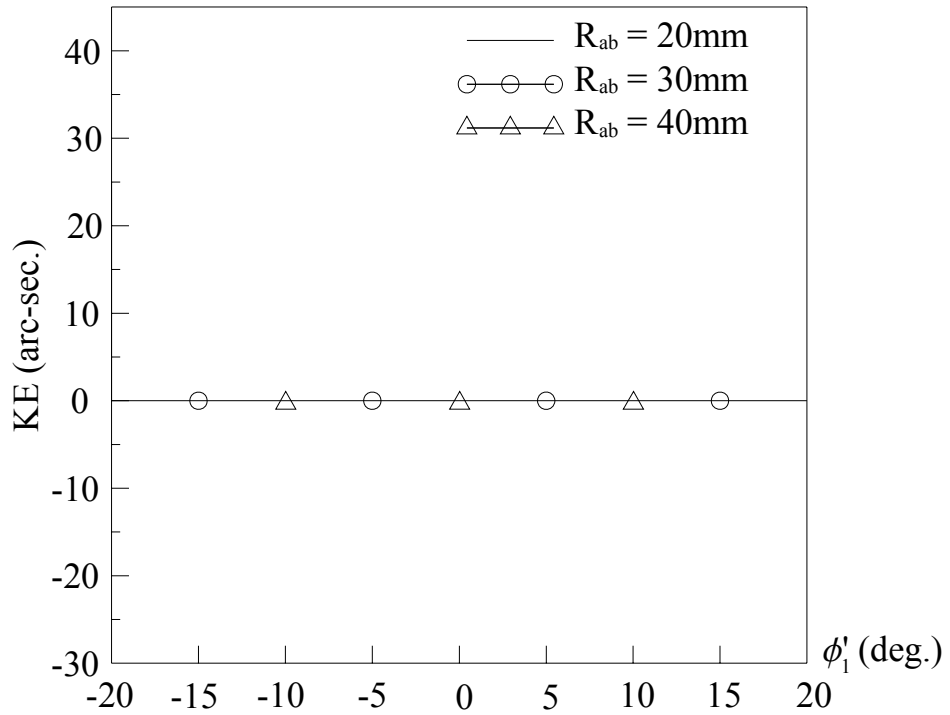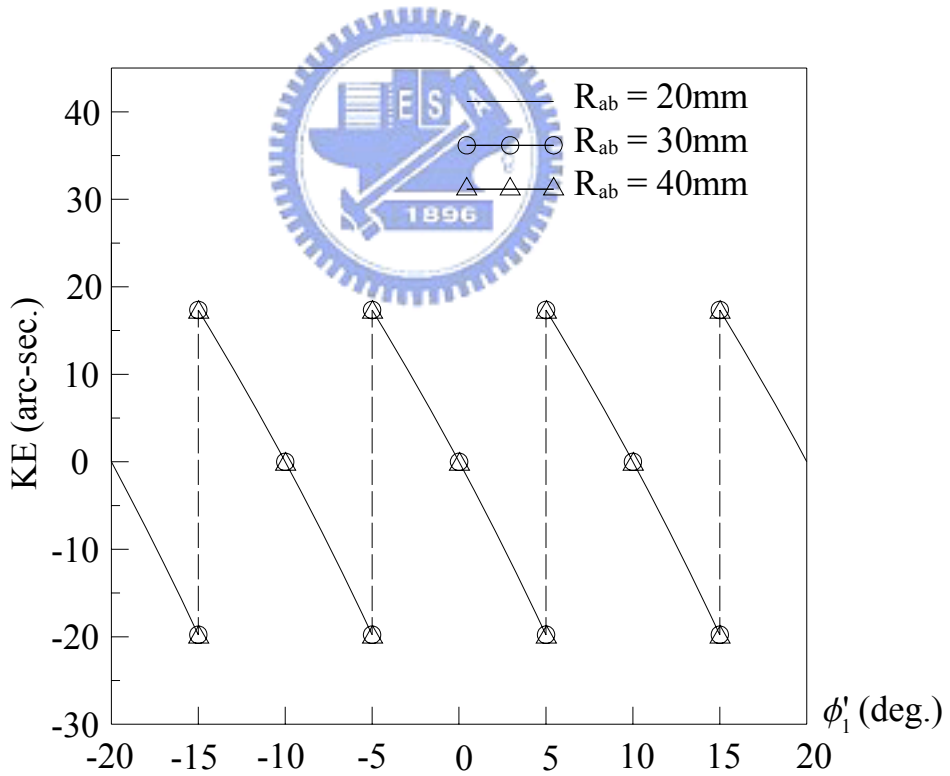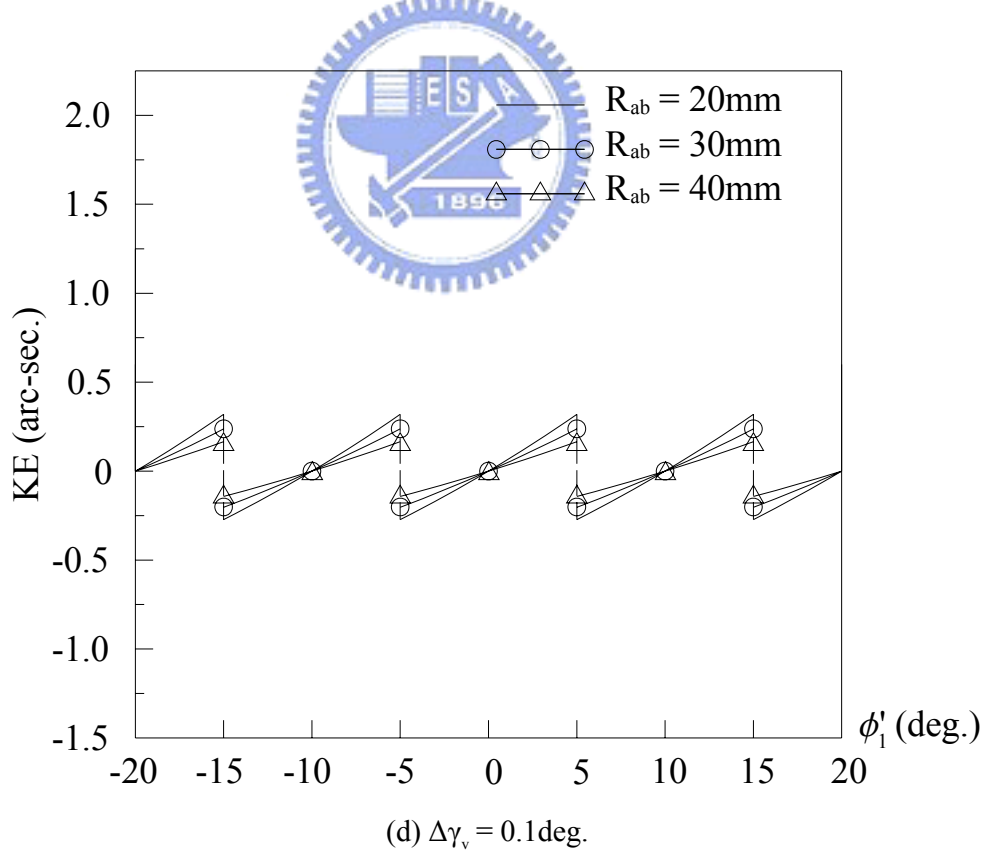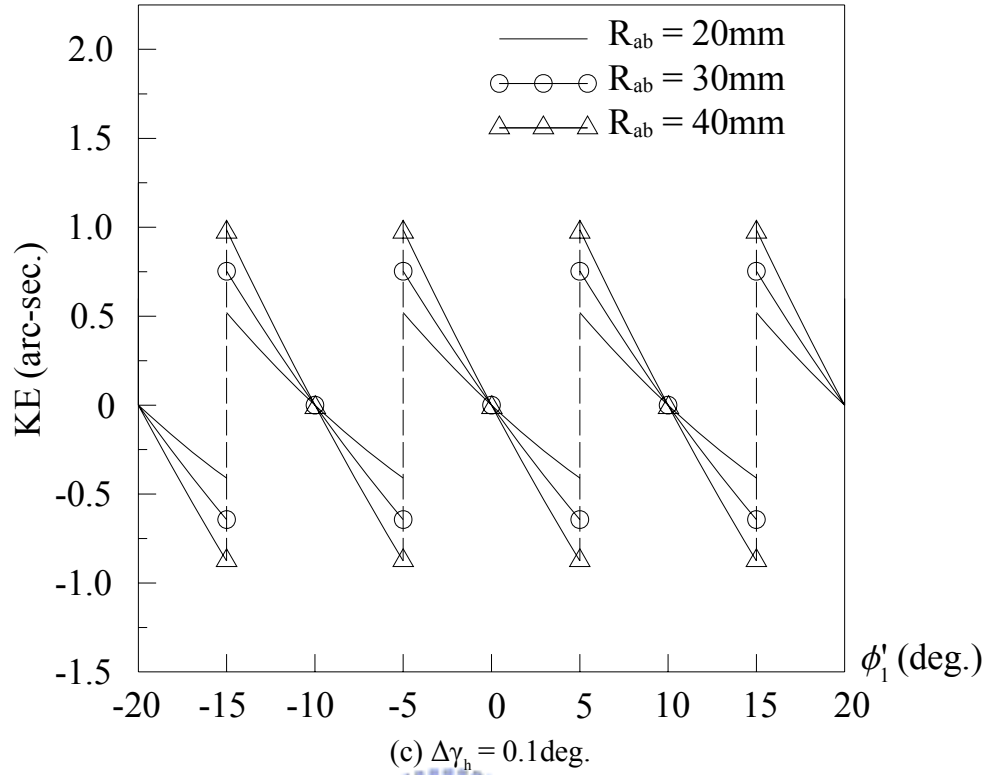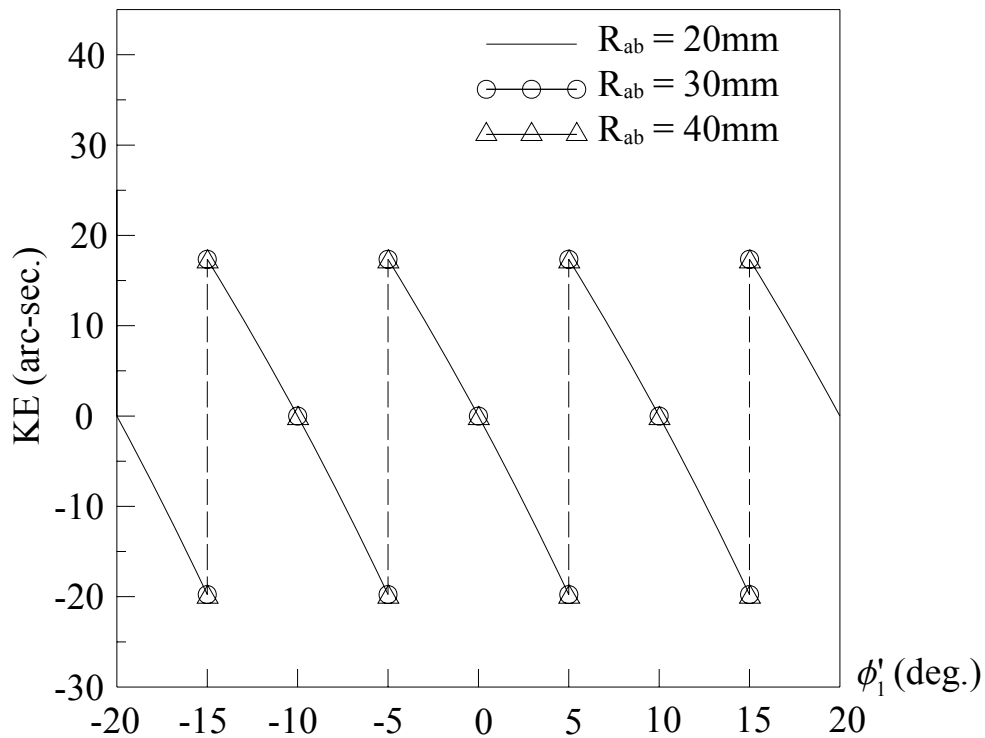under axial assembly misalignment $\Delta\gamma_h = 0.1°$ and $\Delta\gamma_v = 0.1°$

Fig. 5-14 Kinematical errors of the gear pair with ΔR
under mixed assembly errors with $\Delta C = 0.1\text{mm}$, $\Delta \gamma_h = 0.1°$ and $\Delta \gamma_v = 0.1°$
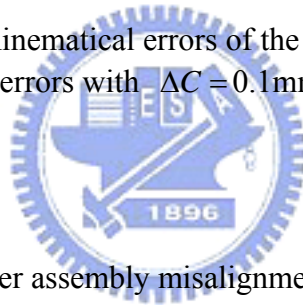
R_{ab} of the disk-type cutter under assembly misalignments.

The design parameters in this example are shown in Table 5-2 but the radius R_{ab} of the disk-type cutter is changed. The KE curves of the gear pair under different meshing conditions are shown in Fig. 5-12, Fig. 5-13 and Fig. 5-14.

The gear pair has no KE with conjugate-shape rack cutter under ideal assembly conditions, and the KE caused by the center distance error is the same as that of changing value R_{ab}. It can be considered that the contact point on the gear pair is on the cross section of $Z^{(i)} = 0\,\text{mm}$ (or $\gamma^{(i)} = 0°$) under the ideal assembly condition and with center distance error. Therefore, the KE is depend on the profile of the gear pair and has no relationship with the trace of the gear pair. KE is decreased with the decreasing of the R_{ab} under a horizontal

misaligned angle $\Delta\gamma_h$, it means the larger curvature (i.e. a smaller R_{ab}) of the tooth-trace enlarges the tolerance to the horizontal misaligned angle $\Delta\gamma_h$. However, KE is increased with the decreasing of the R_{ab} under an horizontal misaligned angle $\Delta\gamma_h$. The main portion of KE of the circular-arc curvilinear-tooth gear pair is caused by the center distance error. Consequently, the value of R_{ab} is not sensitive to the KE of the gear pair.

5.5 Remarks

In this chapter, computer simulation programs have been developed for the TCA of the proposed circular-arc curvilinear-tooth gear pair. Therefore, the effects of the gear design parameters and assembly errors on the KE of the mating gear pair can be predicted by the computer simulations. According to the numerical results, the following conclusions can be drawn:

1. The contact ratio of the gear pair is related to the radius of the generated rack cutter. A higher contact ratio of the gear pair can be obtained with a smaller radius of the cutter.

2. The bearing contact is localized near the middle region of the tooth flank by means of the curvilinear tooth trace. The gear pair is insensitive to axial misalignments because the contact type of the proposed gear pair is in point contact. Thus, edge contact can be efficiently avoided by the proposed gear pair.

3. The circular-arc curvilinear-tooth gear it is sensitive to the center distance assembly errors because of the profile of he mating gear pair is not in the involute type.

4. The resultant KE curve of the gear pair can be modified into a parabolic type by appropriately choosing the design parameter ΔR.

CHAPTER 6

Contact Pattern

6.1 Introduction

Owing to elasticity of tooth surfaces, the instantaneous contact of gear tooth surfaces at a point is spread over an elliptical area. The center of symmetry of the instantaneous contact ellipse coincides with the theoretical contact point. The bearing contact is formed as the set of contact ellipses. The goal for this chapter is to determine the orientation of the contact ellipse on the contact surface.

Spur gears, helical gears with parallel axes, and worm-gear drives are initially in line contact. However, the instantaneous line contact of gear tooth surfaces exists only theoretically for an ideal gear train without assembly and manufacturing errors. In practice, the line contact becomes point contact due to gear axial misalignments. Usually, the contact pattern can be measured by the gear pattern testing machine. The method is smeared with some coatings on the gear tooth surface, and the diameter of the coatings is 6.32 μm [10]. Then, the gear set is meshing and running for a period of time. The coatings on the deformed area will be scraped out, and the contact pattern is formed. It's said that the contact pattern is considered for the case when the gears are under a small load with a 6.32 μm elastic deformation. However, the contact pattern can be obtained by numerical simulation method. In this chapter, the contact patterns of this type of gear set will investigated by using the surface topology method [21]. Moreover, Litvin [10][20][23] proposed methodologies to directly evaluate the principal directions and curvatures of the generated surfaces in terms of design parameters of their corresponding generating tool surfaces.

6.2 Surface Topology Method

Fig. 6-1(a) displays the relationship among the tooth surfaces and common tangent plane, where point O_T means the instantaneous contact point of the two gear surfaces Σ_1 and Σ_2. Vector $\mathbf{n}$ is the common unit normal vector of these two tooth surfaces, and T indicates the common tangent plane to the mating tooth surfaces. A new coordinate system $S_T(X_T, Y_T, Z_T)$ is defined on the tangent plane by considering that the origin of coordinate system $S_T(X_T, Y_T, Z_T)$ is coincided with the instantaneous contact point O_T. Besides, axis Z_T of the coordinate system $S_T(X_T, Y_T, Z_T)$ coincides with the common unit normal vector $\mathbf{n}$ of two mating surfaces at their common tangent point O_T. Axes X_T and Y_T of the coordinate system $S_T(X_T, Y_T, Z_T)$ form the common tangent plane T to both mating tooth surfaces.
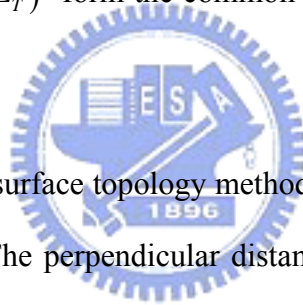
The main purpose of the surface topology method is to simulate the scraping of coatings near by to the contact point. The perpendicular distances measured from a point P on the tangent plane T to the mating tooth surfaces Σ_1 and Σ_2 are designated as d_1 and d_2, as illustrated in Fig. 6-1(b). Thus, the total distance of these two separated surfaces can be expressed as $d = d_1 + d_2$. The coatings proximity to the contact point will be scraped because of $d < 0.00632$ mm. The scraped region is formed the contact pattern.

When performing the surface topology method, the coordinate system $S_T(X_T, Y_T, Z_T)$ on the tangent plane is first established and the equations of the tooth surfaces are transformed to the coordinate system $S_T(X_T, Y_T, Z_T)$ by applying the homogeneous coordinate transformation method. Obviously, since axis Z_T coincides with the unit common normal vector $\mathbf{n}$ at the tangent point O_T, the absolute value of the coordinates $z_T^{(i)}(i=1,2)$
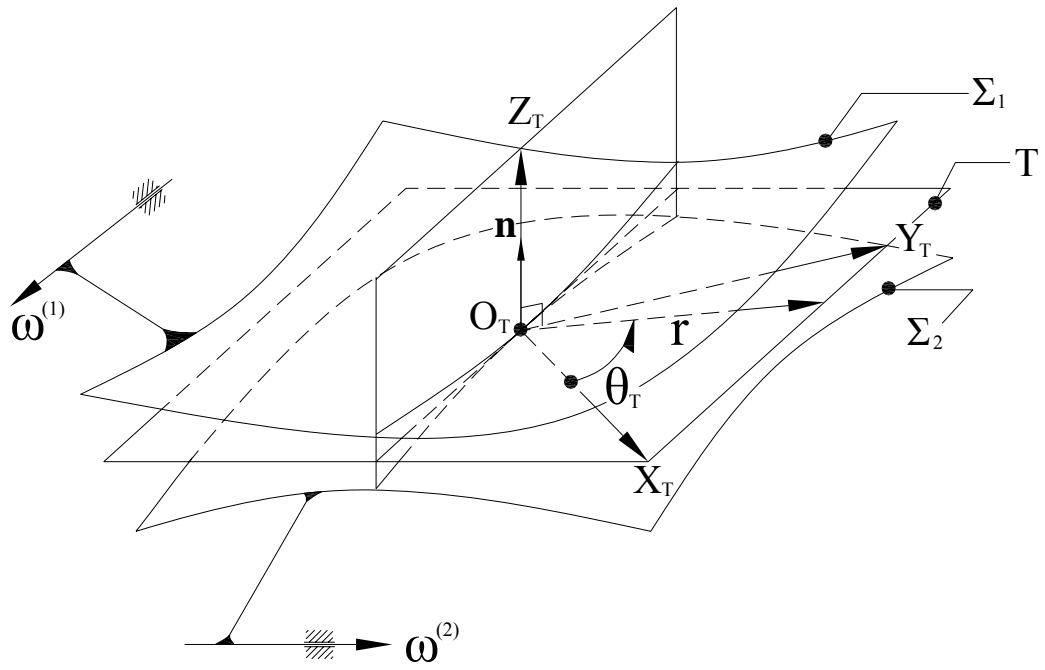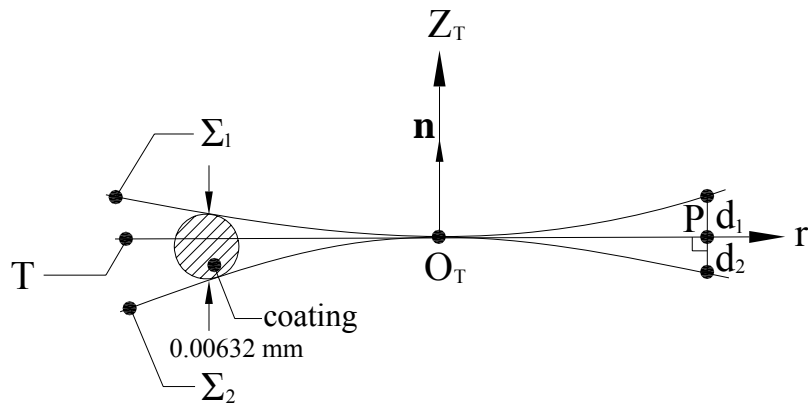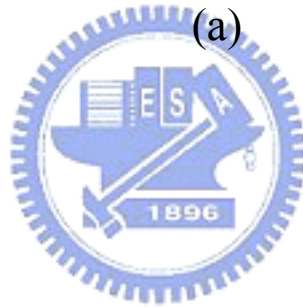
Fig. 6-1 Schematic relationship between the tooth surface and tangent plane

represents the distance measured from the common tangent plane T to both gear tooth surfaces, respectively.

In order to search the equal distance separation points of the mating surfaces around the neighborhood of the tangent point O_T, a polar coordinate system on the tangent plane T can be represented by two parameters θ_T and r, and the origin of polar coordinate system coincides with the contact point O_T. As shown in Fig. 6-1(b), r represents the distance measured outward from the contact point O_T to the searched separation point; θ_T is the angular position, and the range of θ_T is from 0 to 2π as searching the equal separation lines. Any point on the tangent plane can be represented by polar coordinates r and θ_T. The perpendicular distance measured from the tooth surface Σ_1 to the point (r,θ_T) on the common tangent plane T is the absolute value of $z_T^{(1)}$. Similarly, the perpendicular distance measured from the tooth surface Σ_2 to the point (r,θ_T) on the common tangent plane T is the absolute value of $z_T^{(2)}$. Hence, the distance between these two mating surfaces Σ_1 and Σ_2 can be determined by the absolute value of $z_T^{(1)}$ and $z_T^{(2)}$.

In practice, the equations of the mating tooth surfaces are transformed to the coordinate system $S_T\left(X_T,Y_T,Z_T\right)$ of the tangent plane. The geometrical relationships among coordinate systems $S_f\left(X_f,Y_f,Z_f\right)$, $S_m\left(X_m,Y_m,Z_m\right)$, $S_m\left(X_m,Y_m,Z_m\right)$ and $S_T\left(X_T,Y_T,Z_T\right)$ are shown in Fig. 6-2, where coordinate system $S_f\left(X_f,Y_f,Z_f\right)$ is the fixed coordinate system and $S_m\left(X_m,Y_m,Z_m\right)$ and $S_n\left(X_n,Y_n,Z_n\right)$ are the auxiliary coordinate systems. δ is the angle formed by axis Z_m and Z_n, and ε is the include angle of axis Z_n and Z_T. The position vector $\mathbf{R}_T^{(i)}$ of the gear tooth surface represented in coordinate system $S_T\left(X_T,Y_T,Z_T\right)$ can be obtained by applying the homogeneous coordinate transformation

matrix equation as follows:

$$\mathbf{R}_T^{(i)} = \mathbf{M}_{Tn}\mathbf{M}_{nm}\mathbf{M}_{mf}\mathbf{R}_f^{(i)} \tag{6.1}$$

$$= \mathbf{M}_{Tf}\mathbf{R}_f^{(i)}, \ (i=1,\ 2),$$

where

$$\mathbf{M}_{mf} = \begin{bmatrix} 1 & 0 & 0 & -p_x \\ 0 & 1 & 0 & -p_y \\ 0 & 0 & 1 & -p_z \\ 0 & 0 & 0 & 1 \end{bmatrix}, \tag{6.2}$$

$$\mathbf{M}_{nm} = \begin{bmatrix} 1 & 0 & 0 & 0 \\ 0 & \cos\delta & -\sin\delta & 0 \\ 0 & \sin\delta & \cos\delta & 0 \\ 0 & 0 & 0 & 1 \end{bmatrix}, \tag{6.3}$$

and

$$\mathbf{M}_{Tn} = \begin{bmatrix} \cos\varepsilon & 0 & -\sin\varepsilon & 0 \\ 0 & 1 & 0 & 0 \\ \sin\varepsilon & 0 & \cos\varepsilon & 0 \\ 0 & 0 & 0 & 1 \end{bmatrix}. \tag{6.4}$$

Therefore, the homogeneous coordinate transformation matrix for transforming from coordinate system $S_f\left(X_f, Y_f, Z_f\right)$ to coordinate system $S_T\left(X_T, Y_T, Z_T\right)$ becomes:

$$\mathbf{M}_{Tf} = \begin{bmatrix} \cos\varepsilon & -\sin\varepsilon\sin\delta & -\sin\varepsilon\cos\delta & -p_x\cos\varepsilon + \sin\varepsilon(p_y\sin\delta + p_z\cos\delta) \\ 0 & \cos\delta & -\sin\delta & -p_y\cos\delta + p_z\sin\delta \\ \sin\varepsilon & \cos\varepsilon\sin\delta & \cos\varepsilon\cos\delta & -p_x\sin\varepsilon - \cos\varepsilon(p_y\sin\delta + p_z\cos\delta) \\ 0 & 0 & 0 & 1 \end{bmatrix}.$$

$$\tag{6.5}$$

The equations for the gear and pinion can be expressed in the coordinate system

91

$S_T \left(X_T, Y_T, Z_T \right)$ as follows:

$$\mathbf{R}_T^{(1)} = \begin{bmatrix} x_T^{(1)} \\ y_T^{(1)} \\ z_T^{(1)} \end{bmatrix} \tag{6.6}$$

$$= \begin{bmatrix} X_f^{(1)} \cos\varepsilon - Y_f^{(1)} \sin\varepsilon \sin\delta - Z_f^{(1)} \sin\varepsilon \cos\delta - p_x \cos\varepsilon + \sin\varepsilon(p_y \sin\delta + p_z \cos\delta) \\ Y_f^{(1)} \cos\delta - Z_f^{(1)} \sin\delta - p_y \cos\delta + p_z \sin\delta \\ X_f^{(1)} \sin\varepsilon + Y_f^{(1)} \cos\varepsilon \sin\delta + Z_f^{(1)} \cos\varepsilon \cos\delta - p_x \sin\varepsilon - \cos\varepsilon(p_y \sin\delta + p_z \cos\delta) \end{bmatrix}$$

, and

$$\mathbf{R}_T^{(2)} = \begin{bmatrix} x_T^{(2)} \\ y_T^{(2)} \\ z_T^{(2)} \end{bmatrix} \tag{6.7}$$

$$= \begin{bmatrix} X_f^{(2)} \cos\varepsilon - Y_f^{(2)} \sin\varepsilon \sin\delta - Z_f^{(2)} \sin\varepsilon \cos\delta - p_x \cos\varepsilon + \sin\varepsilon(p_y \sin\delta + p_z \cos\delta) \\ Y_f^{(2)} \cos\delta - Z_f^{(2)} \sin\delta - p_y \cos\delta + p_z \sin\delta \\ X_f^{(2)} \sin\varepsilon + Y_f^{(2)} \cos\varepsilon \sin\delta + Z_f^{(2)} \cos\varepsilon \cos\delta - p_x \sin\varepsilon - \cos\varepsilon(p_y \sin\delta + p_z \cos\delta) \end{bmatrix},$$

where the p_x, p_y, and p_z designate the coordinates of the contact point of the two surfaces

represented in the fixed coordinate system $S_f \left(X_f, Y_f, Z_f \right)$. Position vectors $\mathbf{R}_f^{(1)}$ and $\mathbf{R}_f^{(2)}$

has already derived and expressed in Eqs.(6.9) and (6.15). Since the unit normal vector $\mathbf{n}$ at

the contact point is in the same direction with axis Z_T, the angle δ and ε can be obtained

by the geometrical relationship shown which can be expressed as follows in Fig. 6-2:

$$\delta = \tan^{-1}\left(\frac{n_y}{n_z} \right), \tag{6.8}$$

$$\varepsilon = \tan^{-1}\left(\frac{n_x}{\sqrt{n_y^2 + n_z^2}} \right), \tag{6.9}$$
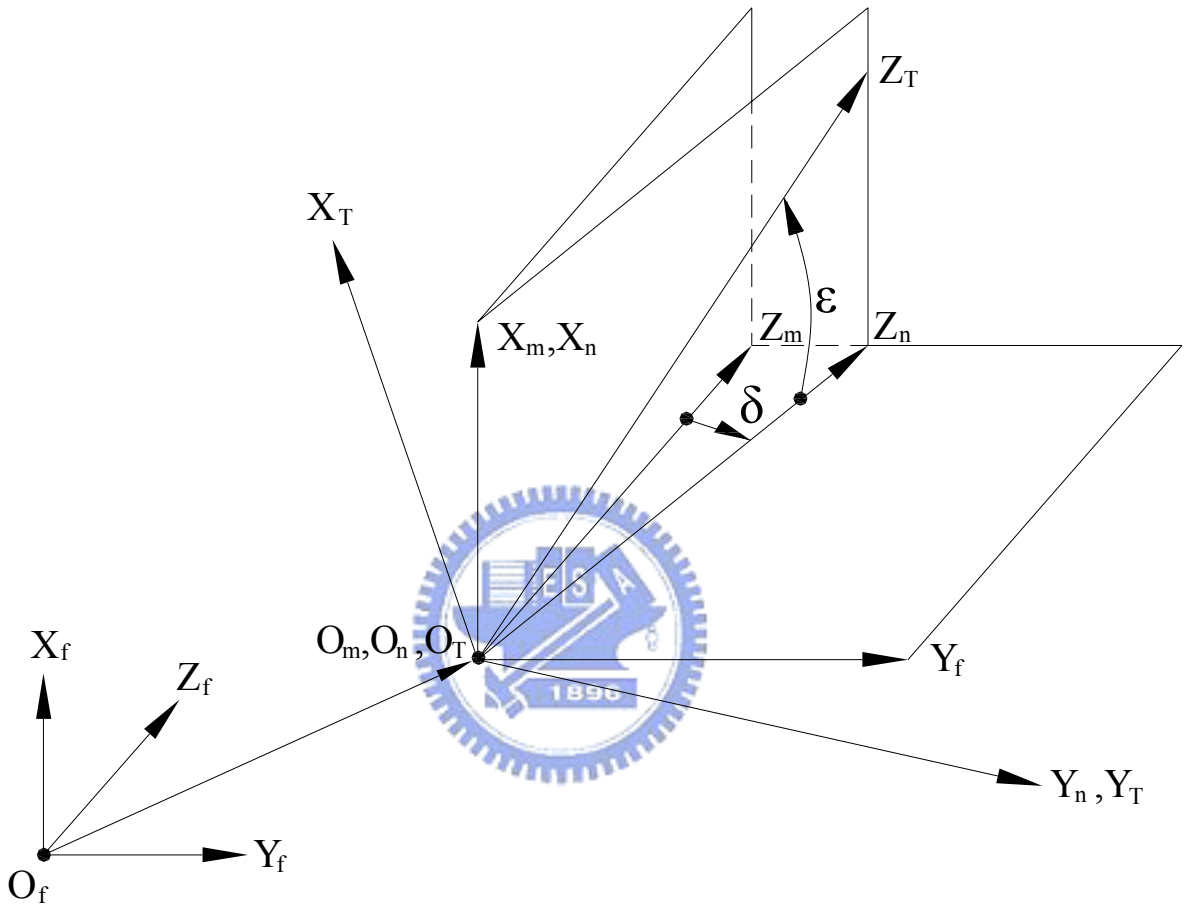
$$\overrightarrow{O_f O_T} = p_x \mathbf{i}_f + p_y \mathbf{j}_f + p_z \mathbf{k}_f$$

Fig. 6-2 Schematic relationship among the coordinate systems and tangent plane

where n_x, n_y and n_z is the three components of the unit normal vector on the contact point.

Based on the above-mentioned algorithm, a computer program is developed to determine the points when the amount of surface separation distance is chosen as the thickness of the coating for contact pattern tests.

## 6.3 Numerical Simulation of Contact Ellipses of Circular-Arc Curvilinear-Tooth Gears

Example 6-1

Table 6-1 Some major design parameters of the circular-arc curvilinear-tooth gear pair

Design parameters	Pinion	Gear
Number of Teeth ($T^{(i)}$)	18	36
Normal Module (M)	3mm/tooth	
Normal Pressure Angle (α)	20°	
Radius of the Disk-Type Cutter (R_{ab}) (Fig. 3-7)	30mm	
Radius of Rack Cutter Normal Section ($R^{(i)}$) (Fig. 3-6 & Fig. 3-8)	40mm	40mm
Face Width (W) (Fig. 3-7)	30mm	

The major design parameters of the proposed gear set are listed in Table 6-1. The contact patterns under different assembly conditions are acquired by the computer programs based on TCA. Fig. 6-3 depicts the contact path and the contact ellipses on the gear tooth surfaces under ideal and error assembly conditions. The contact ellipses are plotted when the gear rotates every 1° from -5° to 5°. It is found that the bearing contact points of the gear set are localized in the middle region of the tooth flank due to the curvilinear tooth trace. The contact ellipse moves upward with assembly error of $\Delta C = 0.1\,\text{mm}$. The contact ellipses under axial misalignments $\Delta\gamma_h$ and $\Delta\gamma_v$ are also shown in Fig. 6-4 and Fig. 6-5,

respectively. It is noted that the positions of the contact points of the gear set are located near the middle region of the tooth flank even under the axial misalignments.
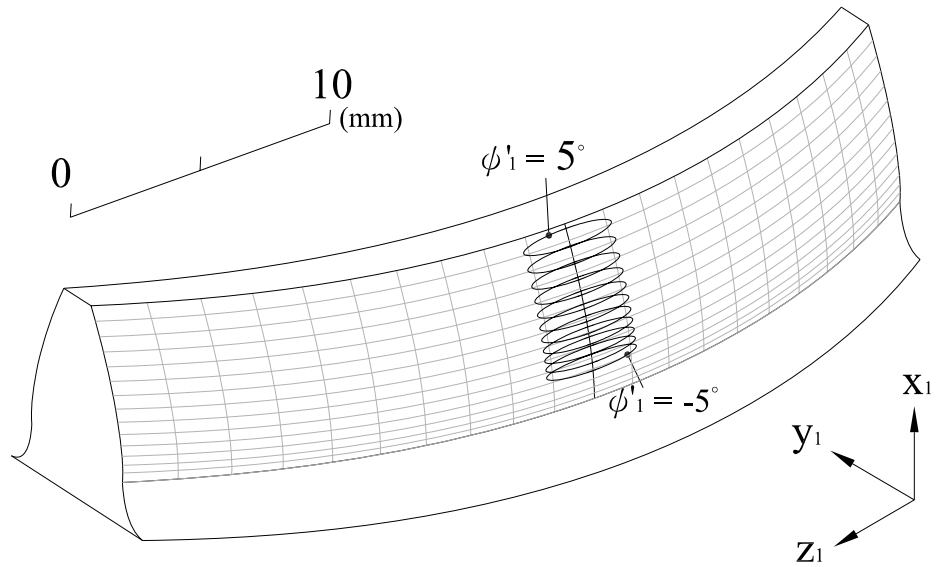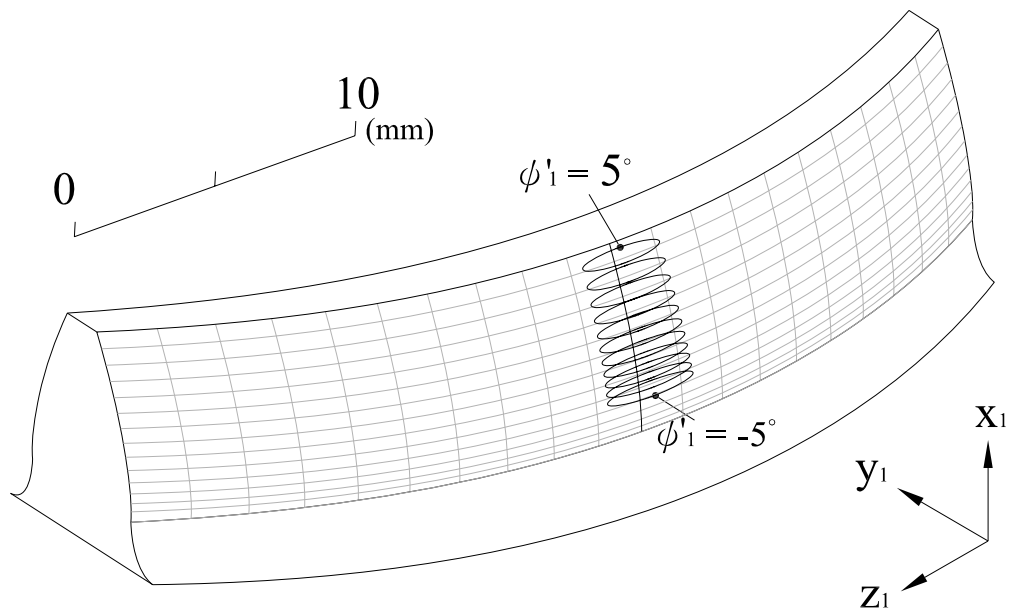

(a) Ideal assembly condition
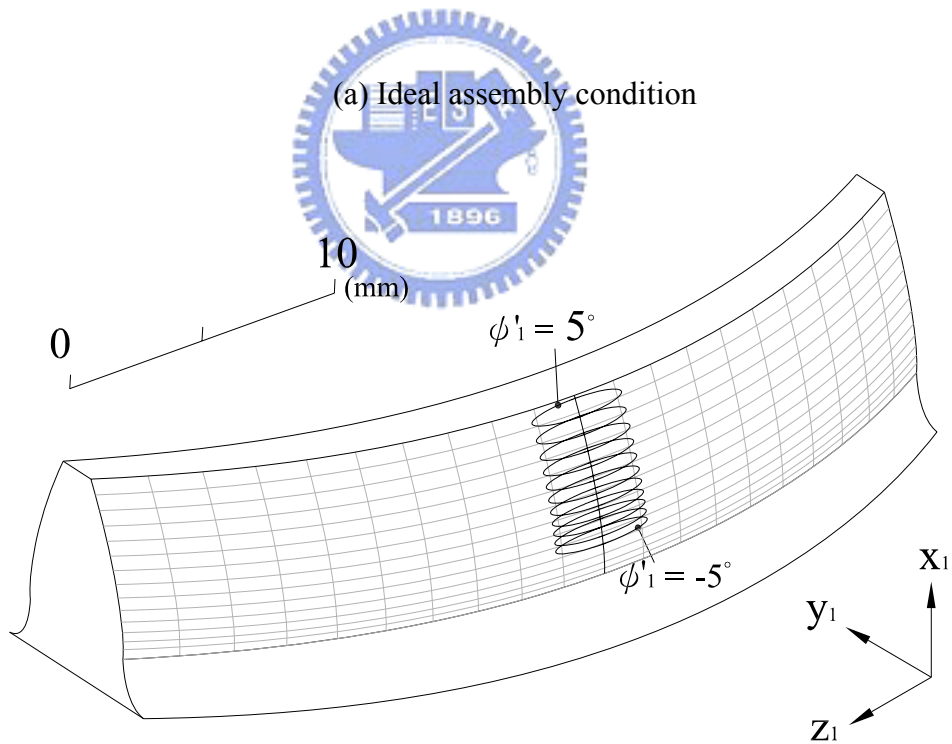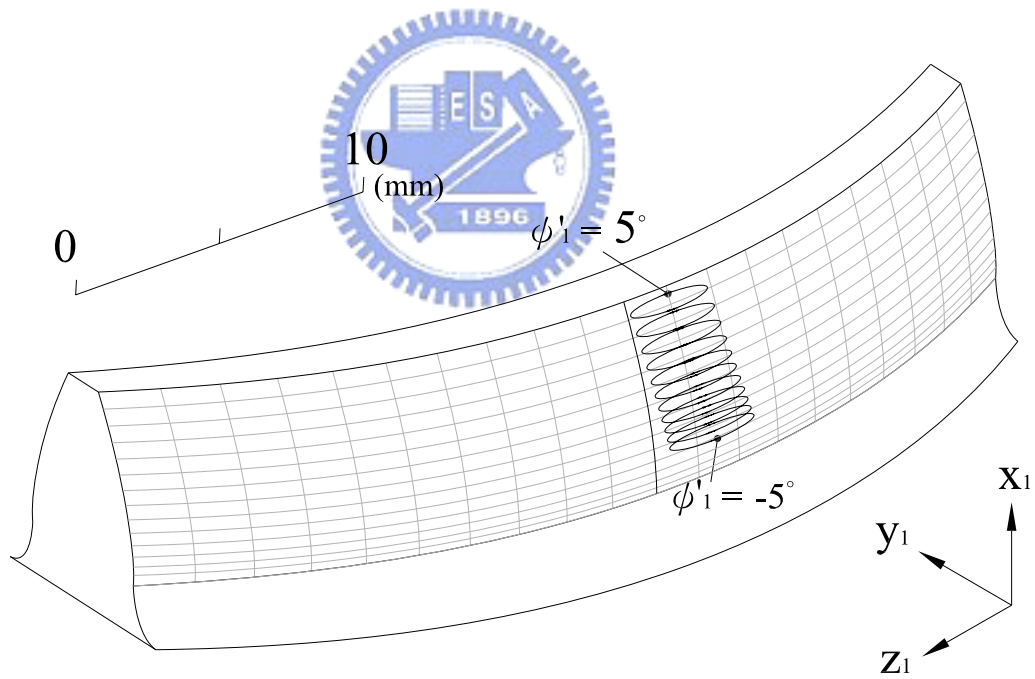
(b) With assembly error $\Delta C = 0.1\,\text{mm}$

Fig. 6-3 Contact patterns of the gear tooth surface under ideal and
error assembly conditions (Example 6-1)

(a) Horizontal axial misalignment $\Delta\gamma_h = 0.1°$

(b) Horizontal axial misalignment $\Delta\gamma_h = 0.5°$

Fig. 6-4 Contact patterns of the gear tooth surface under
horizontal axial misalignments (Example 6-1)
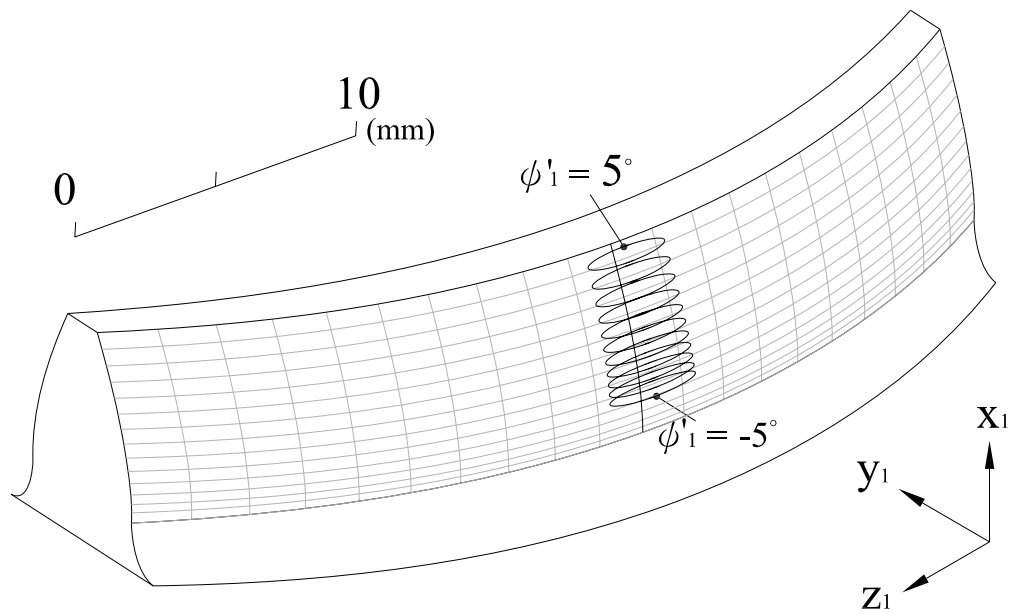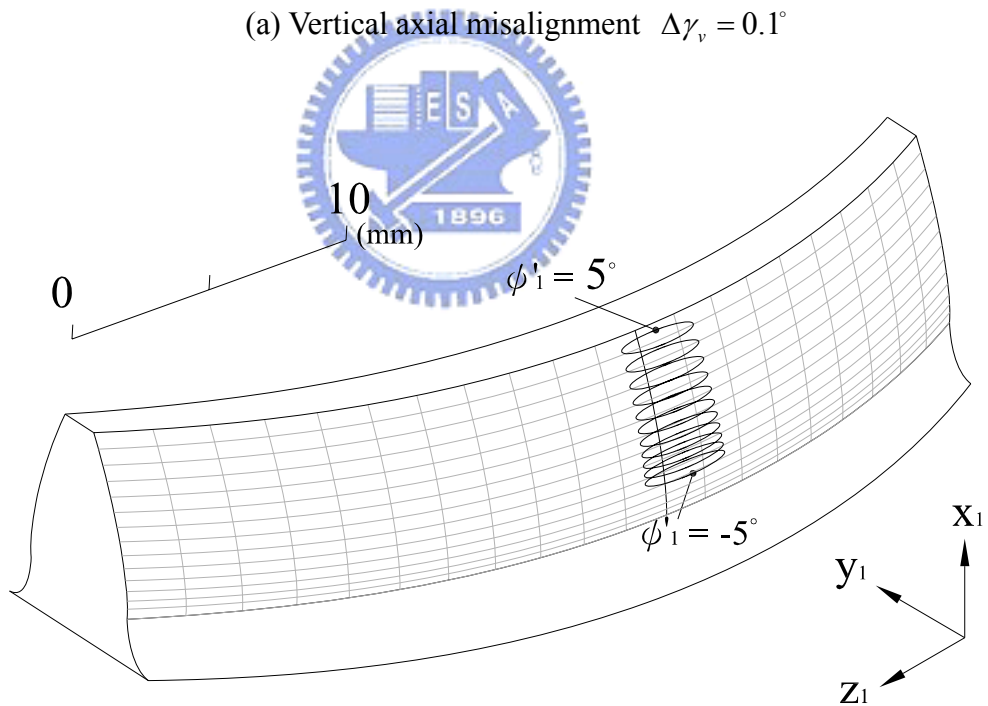
(a) Vertical axial misalignment $\Delta \gamma_v = 0.1°$

(b) Vertical axial misalignment $\Delta \gamma_v = 0.5°$

Fig. 6-5 Contact patterns of the gear tooth surface under
vertical axial misalignments (Example 6-1)

Example 6-2

The instantaneous contact of tooth surfaces at a point is spread over an elliptical area, as shown in Fig. 6-6. Symbol a and b represent the semi-major and semi-minor length of the ellipse. The relationship between the radii R_{ab} of the disk-type tool (Fig. 3-7) and semi-minor axis of the contact ellipse b will be discussed in this example.
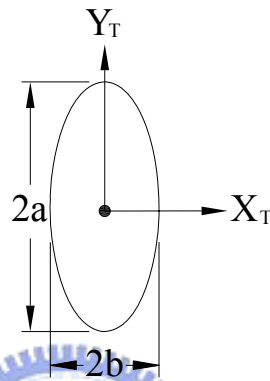

Fig. 6-6 Orientation and dimension of the contact ellipse

The major design parameters of the gear pair are the same as list in Table 6-1 except the value of R_{ab}. Fig. 6-7 shows the contact ellipses of the gear surface with $R_{ab} = 20\,\text{mm}$, $R_{ab} = 30\,\text{mm}$ and $R_{ab} = 40\,\text{mm}$ under ideal assembly condition. The contact points of the gear pair are all located on the middle region of the gear flank no matter $R_{ab} = 20\,\text{mm}$, $R_{ab} = 30\,\text{mm}$ or $R_{ab} = 40\,\text{mm}$, and the length of the major axis of contact ellipses increases evidently with the increase of the R_{ab}. This is due to the fact that a large radius R_{ab} induces a smaller crowning effect on the tooth flank. If the radius R_{ab} tends to infinity, the curvilinear-tooth gear becomes a spur gear, and the ellipse becomes a line contact. Fig. 6-8 shows the effects of design parameters R_{ab} and the semi-major axis length b of the contact ellipse. It is found that the semi-major axis length b is proportional to the R_{ab}. Gear designers can select the proper gear design parameters for their needs.
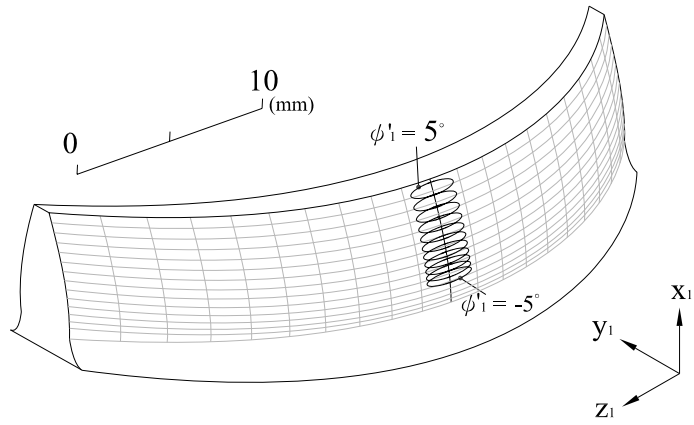
Gear with $R_{ab} = 20\,\text{mm}$ under ideal assembly condition
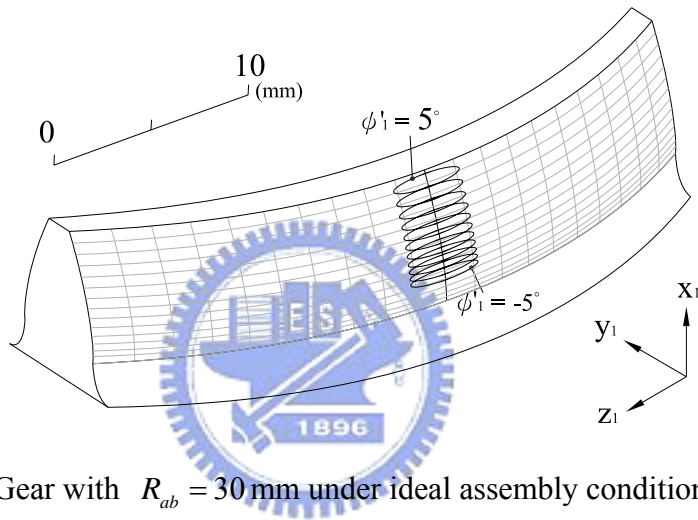
Gear with $R_{ab} = 30\,\text{mm}$ under ideal assembly condition
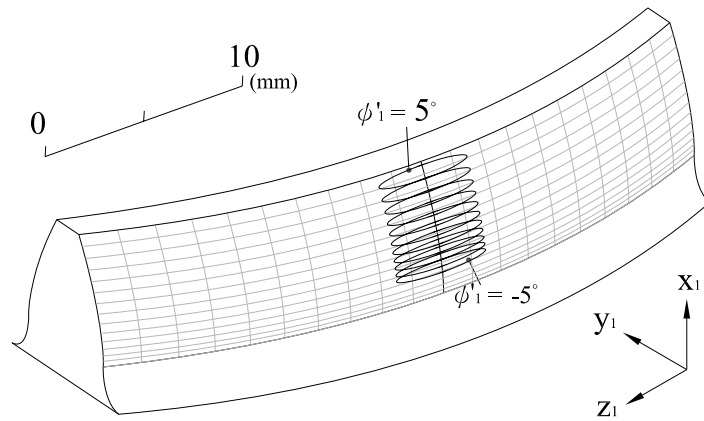
Gear with $R_{ab} = 40\,\text{mm}$ under ideal assembly condition

Fig. 6-7 Contact patterns of the gear tooth surfaces under ideal assembly condition with different value of R_{ab} (Example 6-2)
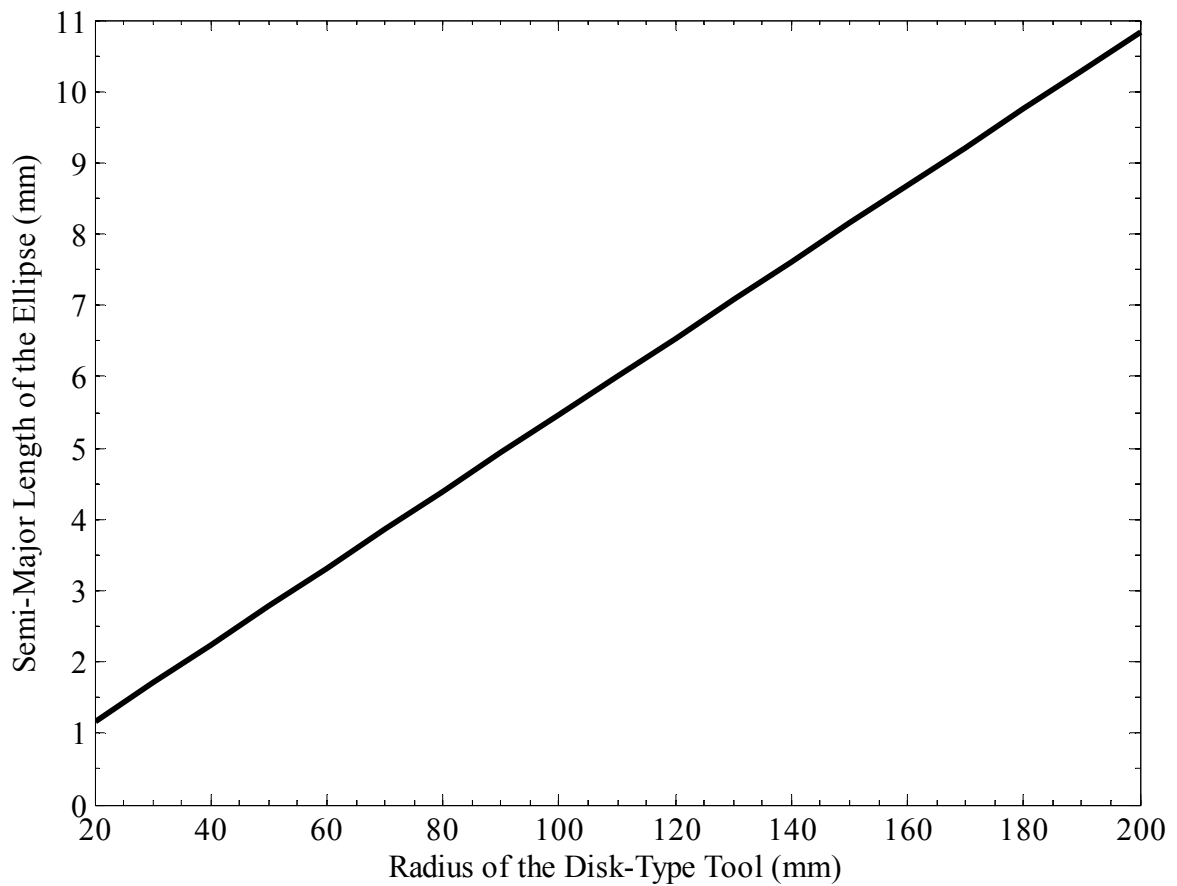
Fig. 6-8 Effects of design parameters R_{ab} versus
the semi-major axis length a of contact ellipse

Example 6-3

The main advantage of the circular-arc gear pair is efficiently to reduce the contact stress by a larger contact area on the contact tooth surfaces. However, contact ellipse is the key index to predict the contact situation. The area of the contact pattern depends on the lengths of major and minor axes. The gear parameters are chosen to investigate their effects on the corresponding contact patterns, while the radius of the disk-type cutter is fixed as $R_{ab} = 30\,\text{mm}$.

As the tooth undercutting condition of the gear generated by rack cutter Σ_g is severer than the pinion generated by rack cutter Σ_p discussed in CHAPTER 2, because the profiles of the circular-arc cutters Σ_g and Σ_p are different. According to the analysis results of Example 4-3, a larger number of teeth can effectual prevent the tooth undercutting. Therefore, the gear with a higher number of teeth is suggested and the gear pair should be generated by a concave rack cutter as shown in Fig. 3-6 to prevent tooth undercutting.

Major design parameters for this example are shown in Table 6-2. According to Fig. 6-9, the length of the minor-axis of contact ellipse is inverse proportional to the radius $R^{(g)}$. However, the dimension of the contact pattern is insensitive to the variation of $R^{(g)}$. Relationships between the design parameters $R^{(g)}$ to the length of semi-major axis and semi-minor axis under ideal assembly condition are shown in Fig. 6-10. Length of the semi-minor axis of contact ellipse increases significantly conspicuously with a smaller value of $R^{(g)}$, but the length of semi-major axis of contact ellipse nearly takes no effect with the variation of $R^{(g)}$. However, as stated in Example 6-2, the length of semi-major axis can be adjusted by the radii R_{ab} of the disk-type cutter.

Table 6-2 Some major design parameters of the circular-arc curvilinear-tooth gear pair

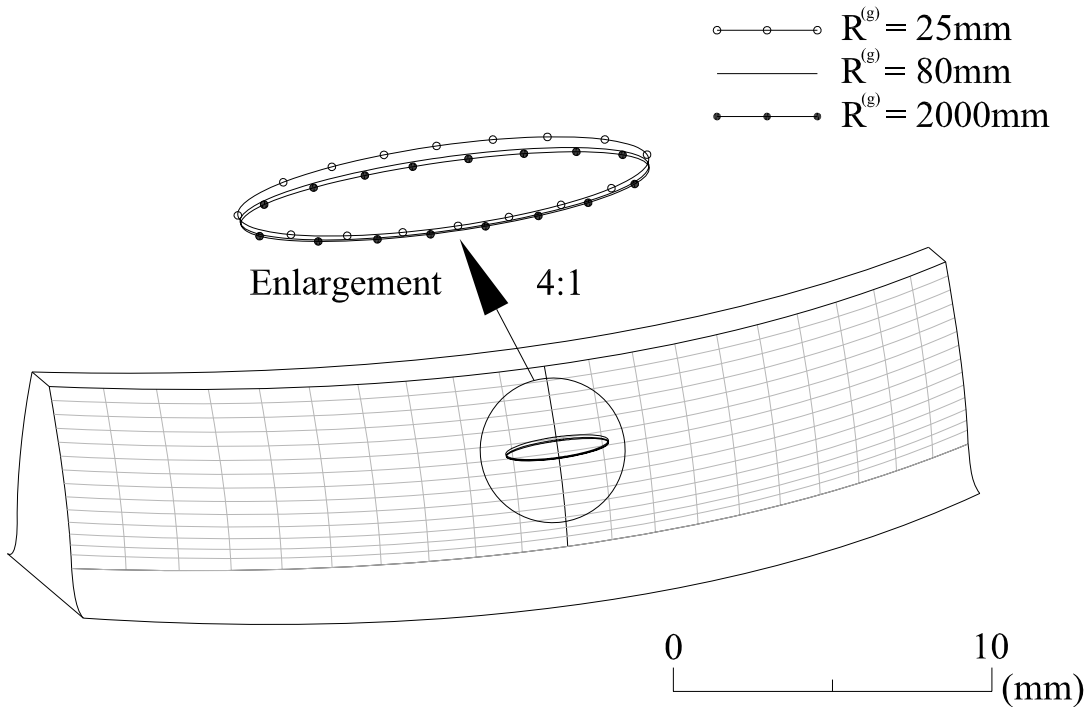| Design parameters	Pinion	Gear
Number of Teeth($T^{(i)}$)	18	72
Normal Module(M)	3mm	
Normal Pressure Angle(α)	20°	
Radius of the Disk-Type Cutter (R_{ab}) (Fig. 3-7)	30mm	
Face Width (W) (Fig. 3-7)	30mm	

Fig. 6-9 Contact ellipses on the gear tooth surface (Example 6-3)
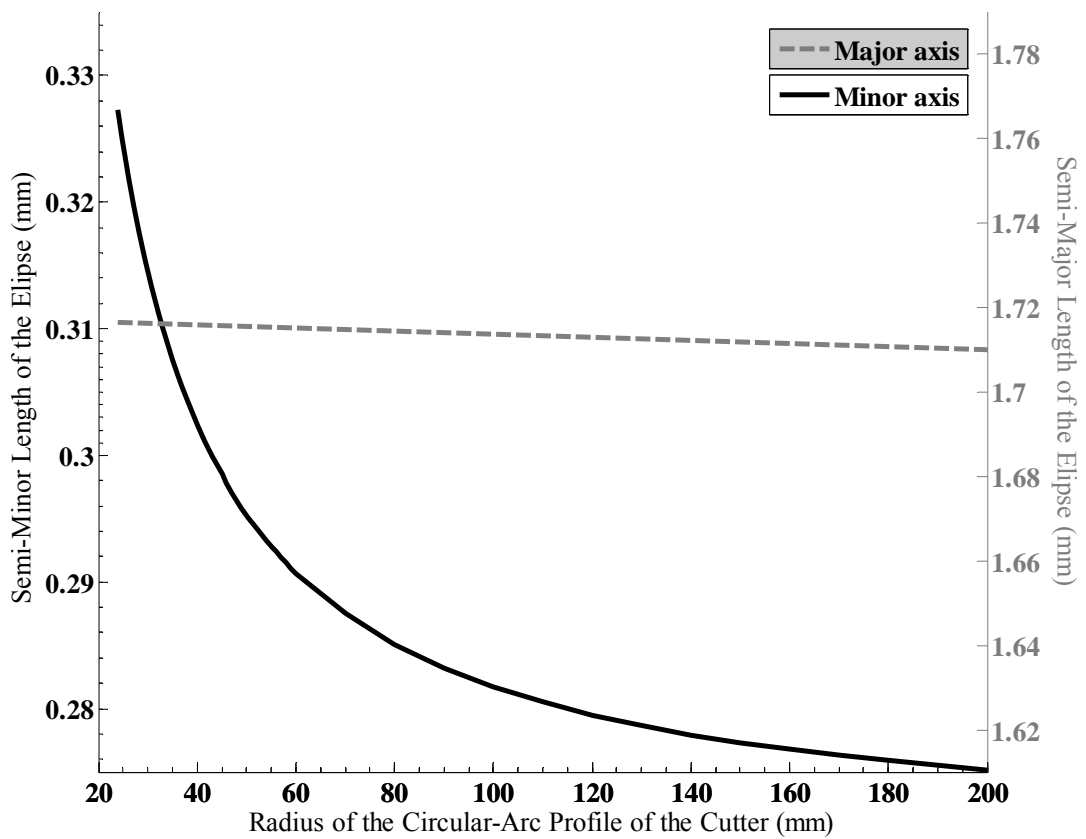
Fig. 6-10 Relationship of design parameter $R^{(g)}$ to the length of the contact ellipse

6.4 Remarks

In this chapter, the contact patterns are obtained by surface topology method. The instantaneous contact of tooth surface at a point is spread over an elliptical area. The effects of the assembly errors and major gear design parameters to the shape of contact ellipses are acquired by the developed computer simulation programs. According to the analysis results of numerical examples, some conclusions can be drawn as follows:

1. The contact patterns of the circular-arc curvilinear-tooth gear pair are localized near the middle region of the tooth flank due to the curvilinear tooth trace even the gear pair is meshing under axial misalignments.

2. Length of the major axis of the contact ellipse is highly related to the radius of the disk-type rack cutter.

3. Length of the minor-axis of the contact ellipse is related to the radii of the circular-arc profile of rack cutters.

CHAPTER 7

Conclusions and Future Works

Gears are widely used in industry for power transmissions. A new type of gear called circular-arc curvilinear-tooth gear, which is generated by a disk-type cutter with the normal cross section of circular-arc profiles, has been proposed in this thesis.

The mathematical model of the circular-arc curvilinear-tooth gear is developed in this study. Tooth undercutting is investigated based on the mathematical model of the gear. Besides, the contact characteristics of the gear pair such as KE and contact ellipses can also be investigated by computer simulation programs based on the developed mathematical model and the TCA.

7.1 Conclusions

Based on the analysis results obtained in the previous chapters, some conclusions can be made as follows:

1. The circular-arc curvilinear-tooth gear is generated by a disk-type cutter with the normal cross section of the circular-arc profiles. However it can be considered that the gear is generated by an imaginary rack cutter. The mathematical model of circular-arc curvilinear-tooth gear can be derived based on the theory of gearing. The transverse gear chordal thickness measured at the middle section is larger than those of other sections.

2. The tooth undercutting condition is developed based on the mathematical model of the circular-arc curvilinear-tooth gear. According to the undercutting analysis results,

the occurrence of tooth undercutting at the middle sections of face width of the curvilinear-tooth gear is much easier than other sections. Compared with the concave tooth surfaces, convex tooth surfaces are mush easier to undercut. Tooth undercutting can be avoided by the design of gears with a larger number of teeth, pressure angle and radii of the circular-arc profile of the rack cutter.

3. Gear pairs with a higher contact ratio can be achieved by designing a smaller radius of the circular-edge of the cutter. The circular-arc curvilinear-tooth gear pair is insensitive to axial misalignments. However, it is sensitive to the center distance assembly error. The KE of a gear pair can be pre-design to a parabolic type by properly selecting the design parameters ΔR.

4. The bearing contact of a gear pair is localized near the middle region of the tooth flank by means of the curvilinear tooth trace, and the edge contact efficient be avoided. The instantaneous contact of tooth surfaces at a point is spread over an elliptical area. Besides, the shape of the contact ellipse can be adjusted by the radii R_{ab} of the disk-type cutter and the radii $R^{(i)}$ of circular-arc profile of the cutter. Length of the minor-axis of the contact ellipse can be increased by the design of a smaller radius $R^{(i)}$ of the circular-arc profile.

5. Gear pairs generated by cutters with smaller radii of the circular-arc profiles can efficiently enhance the gear strength because a larger contact area is induced. However, the cutter with a concave normal section is much easier to undercut the gear with a smaller radius of the circular-arc profile than a convex one. It is suggested that the gear with a higher number of teeth of the gear pair should be generated by a concave rack cutter.

7.2 Future Works

The mathematical model, undercutting condition and tooth contact analysis of the circular-arc curvilinear-tooth gear have been studied in this thesis. In the future, some future works can be studied are listed as follows:

1. The proposed theorems and computer simulated results can be verified by setting up suitable experiments by the following researchers.

2. When calculating TCA, the tooth surfaces are assumed to be rigid in the developed mathematical model. The effects of loads and elastic deformations of tooth surfaces are all neglected. The finite element analysis (FEA) may be implemented to attain more realistic TCA results.

3. The mathematical model is developed based on the consideration of an imaginary rack cutter with the circular-arc profile on its normal section and the rack cutter is moving along a circular trace. However, in practice manufacturing, the gears are usually generated CNC hobbing process. Therefore, the mathematical model of circular-arc curvilinear-tooth gear cut by a hob cutter may be developed in the future.

4. The tooth profile and trace of the circular-arc curvilinear-tooth gear are all in the form of circular-arc. It can be further extended to derive the mathematical model with a noncircular-arc curve, e.g. parabolic or elliptical curves.

References

[1] 王如鈺，齒輪原理概要，憬藝企業有限公司，台北，民國八十二年六月。

[2] Liu, S. T., "Curvilinear Cylindrical Gears," Gear Technology, pp. 8-12, 1988.

[3] 曾瑞堂，圓弧齒線圓柱型齒輪之特性研究，博士論文，交通大學，民國九十四年六月。

[4] 曾瑞堂，曲線齒圓柱型齒輪之齒面數學模式與接觸分析，碩士論文，交通大學，民國八十八年六月。

[5] Tsay, C. B., "Helical Gears with Involute Shaped Teeth: Geometry, Computer Simulation, Tooth Contact Analysis, and Stress Analysis," ASME Journal of Mechanisms, Transmissions and Automation in Design, Vol. 110, no. 4, pp. 484-491, 1988.

[6] Tseng, R. T. and Tsay, C. B., "Contact Characteristics of Cylindrical Gears with Curvilinear shaped teeth," Mechanism and Machine Theory, Vol. 39, pp. 905-919, 2004.

[7] Wildhaber, E., "Gears with Circular Tooth Profile Similar to the Novikov System," US Patent, no. 1,601,750, 1926.

[8] Novikov, M. L., USSR Patent, no.109,750, 1956.

[9] Linvin, F. L. and Tsay, C. B., "Helical Gears with Circular Arc Teeth: Simulation of Conditions of Meshing and Bearing Contact," ASME Journal of Mechanisms, Transmission, and Automation in Design, Vol. 107, pp. 556-564, 1985.

[10] Litvin, F. L. and Fuentes, A., Gear Geometry and Applied Theory, Cambridge University Press, UK, 1994.

[11] Litvin, F. L., Chen, N. X., Hsiao, C. L. and Handschuh, R. F., "Generation of Helical Gears with New Surfaces Topology by Application of CNC Machines," Gear Technology, pp. 30-33, 1994.

[12] Litvin, F. L. , Fan, Q., Vecchiato, D., Demenego, A., Handschuh, R. F. and Sep, T. M. "Computerized Generation and Simulation of Meshing of modified Spur and Helical Gears Manufactured by Shaving," Computer Method in Applied Mechanics and Engineering, Vol. 190, pp. 5037-5055, 2001.

[13] Litvin, F. L., Zhang, J., Handschuh, R. F., and Coy, J. J., "Topology of Modified Helical Gears," Surface Topography, pp. 41-58, 1989.

[14] Spitas, V., Costopoulos, T. and Spitas, C., "Increasing the Strength of Standard Involute Gear Teeth with Novel Circular Root Fillet Design," American Journal of Applied Sciences, Vol.2, no.6, pp.1058-1064, 2005.

[15] Anderson, N. E. and Loewenthal, S. H., "Efficiency of nonstandard and high contact ratio involute spur gears," ASME Journal of Mechanisms, Transmissions and Automation in Design, Vol. 108, pp. 119-126, 1986.

[16] Chen, Y. C. and Tsay, C. B. "Contact Ratios and Transmission Errors of a Helical Gear Set with Involute-Teeth Gear and Modified-Circular-Arc-Teeth Gear," JSME International Journal, Vol. 44, no.3, pp. 867-874, 2001.

[17] Litvin, F. L., Chen, N. X., Lu, J. and Handschuh, R. F., Computerized Design and Generation of Low-Noise Helical Gears with Modified Surface Topology, NASA Technical Memorandum, Minnesota, 1994.

[18] 邵家輝，圓弧齒輪，機械工業出版社，北京，民國八十三年。

[19] Chironis, N. P., <u>Gear Design and Application</u>, McGraw-Hill, New York, 1971.

[20] Litvin, F. L., <u>Theory of Gearing</u>, NASA Publication RP-1212, Washington D.X., 1989.

[21] Michalec, G. W., <u>Precision Gearing: Theory and Practice</u>, John Wiley & Sons, New York, 1966.

[22] Janninck, W. L., "Contact Surface Topology of Worm Gear Teeth," <u>Gear Technology</u>, March/April, pp. 31-47, 1988.

[23] Litvin, F. L., Chen, N. X. and Chen, J. S., "Computerized Determination of Curvature Relations and Contact Ellipse for Conjugate Surfaces," <u>Computer Methods in Applied Mechanics and Engineering</u>, Vol. 125, pp. 151-170, 1995.